The Dissertation Committee for Arjun Ram S P
certifies that this is the approved version of the following dissertation:

Onboard Control, Tracking and Navigation for Autonomous Systems

Committee:

Maruthi Akella, Supervisor

Renato Zanetti, Co-Supervisor

JP Clarke

Takashi Tanaka

Junmin Wang

Onboard Control, Tracking and Navigation for Autonomous Systems

by

Arjun Ram S P

DISSERTATION

Presented to the Faculty of the Graduate School of

The University of Texas at Austin

in Partial Fulfillment

of the Requirements

for the Degree of

DOCTOR OF PHILOSOPHY

THE UNIVERSITY OF TEXAS AT AUSTIN

May 2023

Acknowledgments

I would like to express my gratitude and appreciation to my advisors Dr. Maruthi Akella and Dr. Renato Zanetti for their constant support, motivation and guidance through the course of my graduate studies. It has been an honor to work with you and experience first hand the intellectual and professional prowess you both bring to research as well as the classroom. For the rest of my professional career, I aspire to reach your level of dedication and passion towards the work and at least a fraction of the impact and capability.

My sincere thanks to the faculty at UT Austin, especially Dr. Todd Humphreys, Dr. Takashi Tanaka, Dr. Junmin Wang, Dr. JP Clarke, Dr. Ufuk Topcu and Dr. Peter Stone whose classes and guidance I deeply enjoyed and impacted a lot of my choices for research as well as future pathways. I would also like to acknowledge Dr. Debashish Ghose at the Indian Institute of Science without whose support I wouldn't have been at UT or in the field of aerospace engineering.

My biggest blessings during my time at UT are the professional and personal connections I made here. I would like to thank Dr. Marcelino Almeida for being not just an excellent research collaborator but also a mentor and friend at CDUS as well as Pensa. I really appreciate Dr. Kirsten Tuggle, Dr. Rahul Moghe, Dr. Jhanani Selvakumar, Dr. Andrei Marchidan and Mr. Akhil

4

Shah for being wonderful friends and examples I could look up to throughout my PhD. Thank you to James, Enrico, Erika, Kristen, Mihir, Anahita and all my friends at ASE for putting up with me. I would also like to thank Athreya, Adithyan, Kartik and all my friends in Austin for the cherished memories in this city. Thank you Swetha for being a better companion and support than I could ever ask for and thank you Sanchit and Arvind for being my brothers through it all.

Finally I would like to express my love and gratitude to my family for being the foundation for everything my life leads up to. I can only dream of being as steadfast and courageous as my Ammachi. My career all leads back to my Appa talking electronics and tech to me as a child and he remains a constant pillar of calm and support I am deeply grateful for. All my accomplishments and checkpoints in life are naturally attributed to my Nema for molding the person that I am. I continue to look up to and aim to emulate her dedication, passion and achievements in all aspects of life. Always, thank you.

Onboard Control, Tracking and Navigation for Autonomous Systems

Publication No. _____

Arjun Ram S P, Ph.D.
The University of Texas at Austin, 2023

Supervisors: Maruthi Akella
                          Renato Zanetti

To operate effectively and safely, autonomous systems must be able to navigate complex environments, precisely control their attitude, accurately estimate their own states and make real-time decisions. A new adaptive controller is designed for attitude tracking control of rigid spacecraft with inertia uncertainties and full state feedback of attitude and angular rate. The controller preserves the proportional-derivative plus feedforward (PD+) structure but introduces time varying feedback gains, wherein the desired attitude state is represented by quaternions. Stable asymptotic tracking of the desired reference trajectories is guaranteed without any further restrictions upon the initial conditions, reference trajectories or any requirement for a priori availability of bounds upon the inertia matrix. The onboard estimation of the angular velocity of a spacecraft using Rate-integrating Gyroscopes (RIGs) is considered next. RIGs provide measurements of angular displacement which need to a

6

low pass filter or observer to obtain angular velocity of the system. A continuous time observer is proposed which estimates angular velocity using the RIG measurements and achieves exponential convergence, while asymptotic convergence is guaranteed for the adaptive inertia observer. Unlike conventional certainty equivalence methods, a novel adaptation update law is proposed with additional control knobs changing with the attitude states. The final part of the dissertation deals with the Simultaneous Localization and Mapping (SLAM) problem. Estimating the location of a robot along with the position of the surrounding features on a map can be done onboard recursively with a simple Extended Kalman Filter (EKF-SLAM), but has higher chances of divergence and inconsistency. The robocentric SLAM method transforms the map of features to a local reference frame centered at the robot's position, leading to reduced inconsistency due to lower linearization errors in the update function. Improvements to the robocentric SLAM methods are suggested in the form of addition of second order terms to the linear propagation step and elimination of the composition step by transforming the feature maps before every update step. These modifications provide better filter consistency and prevent divergence in cases which were previously not possible.

Table of Contents

List of Figures

10

Chapter 1

Introduction

The development of autonomous systems has transformed the way we live and work by revolutionizing many industries including transportation, search and rescue, and agriculture. Robotic systems are widely used in industrial applications to increase efficiency and speed of production, with robotic arms playing a major role in automating manufacturing on the factory floor. In the transportation sector, self-driving cars and delivery drones have seen tremendous research focus and are now at the brink of real-world commercial adoption. In the space domain too, with the increase in number of spacecraft and satellite servicing missions, efforts to automate processes like docking, rendezvous and close proximity operations are not just beneficial but also necessary. To operate effectively and safely, these systems must be able to navigate complex environments, avoid obstacles, and make decisions in real-time based on changing conditions. All of these autonomous systems including drones, spacecraft, robots, and self-driving vehicles require precise control over their attitude, navigation, and mapping.

Usual operations for any mobile autonomous system involves knowing where the system is, where it needs to be, and how to get there. For example,

an autonomous car would require a destination which can be provided by the passenger. It then needs to know where it is on a map with respect to the destination and this process of determining its location is called localization. A path planning algorithm has to calculate a route which can be followed to reach the destination. To follow the provided route, the vehicle needs a low level controller which keeps the vehicle on track to be able to reach the destination. This dissertation aims at providing solutions for the "where the system is" and "how to get there" parts of the pipeline in the form of an attitude tracking controller, an observer for estimating angular velocity and a novel algorithm for robotic localization and mapping. The knowledge of where the system needs to be is assumed to be known and provided by a different module or human operator.

Attitude control is the ability of a vehicle to maintain a specific orientation in 3-dimensional space. Attitude stabilization is the process of maintaining a vehicle's orientation in any reference frame at zero while attitude tracking is the process of following an orientation trajectory provided to the system. Different attitude representations are used to determine and control orientation of systems. The most common attitude kinematic representations are Euler angles, quaternions, rotation matrices, Rodrigues parameters and Modified Rodrigues parameters. Euler angles represent the orientation of an object as a combination of three rotations around the x, y, and z-axes, while quaternions represent the orientation with four parameters that obey a unit norm constraint and avoid issues of singularities that can occur with Euler

angles. They also have a more efficient computational representation compared to rotation matrices. Rotation matrices represent the orientation as a matrix that describes the transformation from the object's body frame to the reference frame. Each of these representations has its own advantages and disadvantages, depending on the specific application and the requirements of the system.

Nonlinear control theory provides tools and techniques to design controllers that can stabilize, track, and regulate the behavior of systems whose behavior cannot be modeled using linear differential equations. In this context, the study of nonlinear control theory is essential for engineers and researchers who wish to understand and design control systems for complex nonlinear systems. When a system's output converges to a steady state at an exponential rate, it is said to be exponentially stable which is an important result because it ensures not only stability, but also efficiency, robustness, and good performance in the presence of uncertainties and disturbances. Formally, for the states $\boldsymbol{x}$ of a control system described by $\dot{\boldsymbol{x}} = f(t, \boldsymbol{x})$, the equilibrium point $\boldsymbol{x} = 0$ is exponentially stable if there exist finite positive constants c,k, and λ such that for all $t \geq t_0$, we have

$$\|\boldsymbol{x}(t)\| \leq k\|\boldsymbol{x}(t_0)\| \exp^{-\lambda(t-t_0)}, \ \forall \|\boldsymbol{x}(t_0)\| < c \tag{1.1}$$

and globally exponentially stable if this condition is satisfied for any initial state $x(t_0)$. The result is said to be uniform exponentially stable (UES) if the preceding condition holds for any initial time $t_0 \in \Re$. If exponential stability

14

cannot be guaranteed for a system, the next best form of stability is asymptotic stability when the system state x is guaranteed to eventually converge to a desired steady state.

Lyapunov theory provides a powerful tool for analyzing the stability of nonlinear systems, which cannot be easily analyzed using traditional methods based on linearization. A Lyapunov function is a positive-definite function that assigns a scalar value to each state of the system, typically energy-like functions for the states. Lyapunov theory states that if the function is chosen such that its derivative along the system trajectories is negative-definite, the system is stable. For the case of systems with complex nonlinear dynamics, it may be difficult to design Lyapunov functions whose derivatives are strictly negative definite and LaSalle's invariance principle provides a criteria for proving asymptotic stability of an autonomous system using a function whose derivative is only negative semi-definite. Barbalat's lemma and its corollary can be used to show asymptotic stability of non-autonomous systems. More details about Lyapunov theory and nonlinear stability analysis are presented in the Appendix A.

The problem of controlling the attitude of systems like rigid-robots, spacecraft and aircraft tends to have highly nonlinear dynamics, making their control difficult to handle for simple linear PID (Proportional Integral Derivative) like controllers. However, in the attitude tracking case, adding a feed-forward term to handle the non-linearity has been effective in practical implementations and such attitude tracking controllers with the proportional

derivative structure along with feed-forward terms, called the "PD+" controller structure, have been extensively studied over the past several decades [5] and are widely used. This control law does not require knowledge of any system specific inertia parameters for the special case of set-point attitude stabilization (regulation) once the feedback gains are selected by the user (self-reduction property) and its simple structure enables its easy computation at any point of time on even small computers. If the kinematics are represented through the Modified Rodriguez parameters, the same PD+ controller was shown to provide uniformly exponential convergence for the tracking error states [6].

Adaptive control is a control strategy that allows a system to automatically adjust its control parameters in response to changing operating conditions. The goal of adaptive control is to improve the performance and robustness of the control system in the face of uncertainties, disturbances, and changes in the system dynamics. In chapter 2, the adaptive control problem for attitude tracking is revisited for rigid spacecraft with inertia uncertainties. A new adaptive controller is designed for this problem, that preserves the PD+ structure, wherein the desired attitude state is represented by quaternions and full-state feedback (attitude and angular rate) is assumed. Considering a system following Euler rotational dynamics, this new control law saliently preserves the self-reduction property, i.e., the controller reduces to simply having the linear PD feedback structure for the special case of set-point regulation with no further dependence upon the inertia matrix. Unlike the vast majority of prior results available in the literature for this adaptive control problem, a

major feature of the new 'PD+' law is the introduction of time-varying feedback gains along with an adaptive estimate for the inertia matrix, guaranteeing stable asymptotic tracking of the desired reference trajectories. No further restrictions are placed upon the initial conditions, reference trajectories or the requirement for a priori availability of bounds upon the inertia matrix.

Gyroscopes are used in aerospace applications as primary sensors for determining the attitude and velocity states of the system. Unlike traditional gyroscopes which measure angular velocity, Rate Integrating Gyroscopes (RIGs) measure integrated angular rates or angular displacement, requiring an observer or filter to provide full state feedback to the attitude controller. A numerical differentiator that approximates the derivative of a function at a point using a finite difference method is typically used to estimate this angular velocity. Such an approach does not utilize the knowledge of the dynamics of the system and hence cannot provide any guarantees on convergence of the estimates to the true value. In chapter 3, a nonlinear observer is presented which using only continuous-time measurements from an RIG, estimates the angular velocity of a rotating rigid body following Euler rotational dynamics. Torque applied to the system is assumed to be known. When the inertia matrix is accurately known, the provided observer achieves exponential convergence, while an asymptotically converging adaptive observer is designed for cases when the inertia is unknown. The non-adaptive observer is shown to be robust to bounded inaccuracies in the knowledge of inertia and external torque acting upon the system. For the adaptive observer, conventional certainty

17

equivalence methods require the angular rate states which are unavailable. To overcome this problem a novel update rule with additional control knobs is proposed which uses just the attitude states for inertia parameter adaptation.

The Kalman filter is optimal in the mean squared sense for estimating the states of a linear system with additive white Gaussian process and measurement noise. At each time step, the Kalman filter makes a prediction of the system's state based on the state model and then compares this prediction to the actual measurement from the sensors to update its estimate of the system's state. The Kalman filter provides estimates of the state and the error covariance which are best guesses of the system's state and uncertainty, given all available measurements. The Kalman filter assumes the system is linear which is not the case in most real world applications. The Extended Kalman Filter (EKF) is a variant of the Kalman Filter that addresses this limitation by linearizing the non-linear models using a first-order Taylor expansion around the current estimate. The linearized models are then used in the same way as in the standard Kalman filter. The EKF assumes that the errors in the state and measurement models are Gaussian and the Jacobian matrices are computable.

The problem of simultaneously determining the position of the robot while creating a map of it's environment(Simultaneous Localization and Mapping - SLAM) is considered in Chapter 4. Simultaneous Localization and Mapping (SLAM) using Extended Kalman Filters (EKF) provides some of the simplest and computationally faster implementations of SLAM and can be

used in many robotic systems for quick online navigation and mapping. This simplicity comes at the cost of increased chances of divergence and inconsistency of the filter. The robocentric approach was proposed in past literature to improve the EKF-SLAM consistency at the cost of a slightly higher computational load. At each time step, robocentric EKF-SLAM transforms the map features' coordinates to a frame centered at the robot's position. In its original implementation, robocentric EKF-SLAM reduces inconsistency and divergence but situations arise when they still occur. In this work we propose new steps to increase the robustness of robocentric EKF-SLAM by modifying the propagation step of the filter to include second order terms of the Taylor series expansion as well as transforming the feature states before each update step. These modifications demonstrate much better filter consistency with all data-sets tested, while not diverging even in a challenging counterexample case.

The remainder of the thesis is organized as follows and presents the main contributions of this dissertation:

- Chapter 2: An adaptive attitude tracking controller with dynamic feedback gains for systems with inertia uncertainties, preserving the self-reduction property and the 'PD+' controller structure.

- Chapter 3: A nonlinear observer for estimating angular velocity from the measurements of a Rate-Integrating Gyroscope (RIG).

- Chapter 4: A modified EKF-based robocentric SLAM algorithm that

provides a more consistent and robust method of estimating the position of a robot and mapping its surroundings.

Throughout this dissertation, uppercase letters are used to denote matrices and bold faced variables denote vectors. The 2-norm for vectors and the vector induced 2-norm for matrices are denoted by the $\|$ operator. For any symmetric matrix P, the notation $\lambda_{\min}(P)$ and $\lambda_{\max}(P)$ respectively denote the minimum and maximum eigenvalues.

Chapter 2

Adaptive Attitude Tracking Control Preserving the Self-Reduction Property

Attitude tracking control is frequently required for applications involving spaceflight vehicles, aircraft and rigid robots. Among the simplest controllers used for set-point regulation is the proportional-derivative (PD) feedback controller, which is combined with feedforward terms (the so called "PD+" structure) for reference trajectory tracking. The simple linear feedback structure of this controller makes it attractive from an implementation standpoint and has thus been extensively studied over the past several decades. For set-point regulation, the PD terms do not involve the inertia of the spacecraft (the so called self-reduction property), naturally providing a degree of robust stability in face of inertia uncertainties, but in the case of tracking a desired trajectory (like slew maneuvers), the feedforward terms in the PD+ controller require precise knowledge of the inertia matrix. In the context of on-orbit assembly, repair and refilling missions, this perfect knowledge of the inertia matrix is often not always available and therefore necessitates the use of adaptive controllers that can deal with model parameter uncertainties. For

---

The research presented in this chapter was performed by the authors and previously published in a peer reviewed journal [7]

such settings, an adaptive controller retains the overall PD+ structure but replaces the inertia matrix with its adaptively generated estimate (invoking the certainty equivalence principle). This inertia estimate is usually driven by an adaptive update law involving the tracking error states and eventually converges to the true value of the inertia in the case that the reference trajectory additionally satisfies certain persistent excitation conditions [8, Chapter 2].

Since the governing dynamics are nonlinear and time varying for the attitude tracking control problem, a key technical difficulty is the fact that the closed-loop stability for the control problem is established through energy-type Lyapunov functions that are not strict, i.e., their time derivatives are only negative semidefinite involving only the angular velocity error terms. In this setting, technical arguments involving LaSalle invariance (for stabilization or set-point regulation) and Barbalat's lemma (for trajectory tracking) are usually adopted for completing the closed-loop stability and convergence analysis. The nonstrict nature of the underlying Lyapunov-like functions that facilitate the stability analysis leads to the hurdle of the uniform detectability obstacle whenever PD-based adaptive controllers are used in conjunction with the certainty equivalence principle. The introduction of a strict Lyapunov-like function [1] in terms of the quaternion parameterization of the attitude helps preserve the PD-type feedback controller to ensure almost global closed-loop stability thereby successfully circumventing the detectability obstacle. However, construction of such strict Lyapunov functions usually requires an additional user-chosen parameter, along with extra restrictions imposed upon

the value of this parameter for ensuring closed-loop stability. This strictified Lyapunov analysis approach to adaptive attitude tracking control and some of its main limitations will be discussed in more detail in the following section.

Other adaptive control formulations in the literature sacrifice the elegant PD+ structure by introducing additional nonlinear feedback terms within the control law or by way of state augmentation through linear low-pass filters (higher-dimensional controller), notably [9] - [10]. Seo and Akella [9] pursue a non certainty equivalence approach to the adaptive control problem using a linear filter for the regressor matrix. Schaub, Akella and Junkins [11] present a nonlinear feedback control law while Egeland and Godhavn [12] use a passivity theory based approach on a linear parameterization of the equation of motion. Singh [13] describes a model reference adaptive control law while Ahmed, Coppola and Bernstein [10] design a nonlinear controller which does not require any knowledge of the inertia matrix. Another problem of interest is the attitude tracking controller without velocity measurements, an almost-global non-adaptive solution for which is provided by Tayebi [14], while Dawson et al. [15] provide a local adaptive controller for a system (high-gain action) with inertia uncertainties, both using quaternions for their attitude representation.

This work aims at developing a linear PD+ adaptive controller for the attitude tracking control problem, making no assumptions about availability of information upon the inertia in any form (unlike [1]), through the use of dynamic gains for the proportional and derivative feedback terms. The attitude kinematics are represented by quaternions and perfect measurement of

23

the full-state including the angular velocity is assumed. For the case when the inertia matrix is perfectly determined, it is a well-documented fact from the literature that the control law admits the classical PD+ structure [1],[16] - [17]. Moreover, if the kinematics are represented through the Modified Rodriguez parameters, the same PD+ controller was recently shown to provide uniformly exponential convergence for the tracking error states [6]. When there is uncertainty in the inertia matrix, this work replaces the inertia matrix within the control law with its adaptively generated estimate (certainty equivalence) [18, Chapter 9] and guarantees the Lyapunov-like function involving the tracking error states and the inertia estimation errors will monotonically decrease with time. There is no assurance that the inertia estimates converge to the true inertia matrix unless additional persistence of excitation conditions are imposed upon the reference trajectory. However, the tracking errors are shown to asymptotically converge to zero irrespective of whether the underlying reference trajectory is persistently exciting.

2.1   System Dynamics

Suppose the orientation of the body frame with respect to an inertial frame is represented by the quaternion $\boldsymbol{q}$ and let the desired reference orientation be denoted by the quaternion $\boldsymbol{q_r}$. We represent the error orientation also through the quaternion $\boldsymbol{s}$ such that the direction cosine matrix mapping the instantaneous rotational error between the body frame and the reference

frame is given by

$$C(s) = C(q)C^T(q_r) \tag{2.1}$$

The quaternion error kinematics for $s = \begin{bmatrix} s_0, s_v^T \end{bmatrix}^T$, are described by

$$\dot{s} = \frac{1}{2}E(s)\omega_e \tag{2.2}$$

$$E(s) = \begin{bmatrix} s_v & s_0\mathbb{I}_{3\times3} + s_v^* \end{bmatrix}^T \tag{2.3}$$

where $\mathbb{I}_{3\times3}$ is the size 3×3 identity matrix and s_v^* is the skew-symmetric matrix representing vector cross-product in three-dimensions such that $s_v^*\eta = s_v \times \eta$ for any three-dimensional vector η. The angular velocity error ω_e is the difference between the angular velocity of the body ω expressed in the body frame and the desired/reference velocity $\eta = C(s)\omega_r$ (mapped into the body frame). Thus,

$$\omega_e = \omega - \eta \tag{2.4}$$

Using Poisson differential equation for the rotational error kinematics

$$\dot{C}(s) = -\omega_e \times C(s) \tag{2.5}$$

and the Euler rotational dynamics equation,

$$J\dot{\omega} = -\omega^* J\omega + u \tag{2.6}$$

with $J = J^T$ being the inertia matrix with maximum and minimum eigenvalues $J_{\max}$ and $J_{\min}$ respectively, and u being the external torque vector (control

25

signal). Thus, the angular velocity error satisfies

$$
\begin{aligned}
\boldsymbol{J}\dot{\boldsymbol{\omega}}_e &= \boldsymbol{J}\dot{\boldsymbol{\omega}} - \boldsymbol{J}C(\boldsymbol{s})\dot{\boldsymbol{\omega}}_r - \boldsymbol{J}\dot{C}(\boldsymbol{s})\boldsymbol{\omega}_r \\
&= \boldsymbol{J}\dot{\boldsymbol{\omega}} - \boldsymbol{J}C(\boldsymbol{s})\dot{\boldsymbol{\omega}}_r + \boldsymbol{J}\boldsymbol{\omega}_e^* C(\boldsymbol{s})\boldsymbol{\omega}_r \\
&= -\boldsymbol{\omega}^*\boldsymbol{J}\boldsymbol{\omega} + \boldsymbol{u} - \boldsymbol{J}C(\boldsymbol{s})\dot{\boldsymbol{\omega}}_r + \boldsymbol{J}\boldsymbol{\omega}_e^* C(\boldsymbol{s})\boldsymbol{\omega}_r + \boldsymbol{J}\boldsymbol{\omega}_e^*\boldsymbol{\eta} \\
&= -(\boldsymbol{\omega}_e + \boldsymbol{\eta})^*\boldsymbol{J}(\boldsymbol{\omega}_e + \boldsymbol{\eta}) + \boldsymbol{u} + \boldsymbol{J}C(\boldsymbol{s})\dot{\boldsymbol{\omega}}_r - \boldsymbol{J}\boldsymbol{\eta}^*\boldsymbol{\omega}_e \\
&= -\boldsymbol{\omega}_e^*\boldsymbol{J}\boldsymbol{\omega}_e - \boldsymbol{\omega}_e^*\boldsymbol{J}\boldsymbol{\eta} - \boldsymbol{\eta}^*\boldsymbol{J}\boldsymbol{\omega}_e - \boldsymbol{\eta}^*\boldsymbol{J}\boldsymbol{\eta} - \boldsymbol{J}C(\boldsymbol{s})\dot{\boldsymbol{\omega}}_r - \boldsymbol{J}\boldsymbol{\eta}^*\boldsymbol{\omega}_e + \boldsymbol{u} \\
&= -\boldsymbol{\omega}_e^*\boldsymbol{J}\boldsymbol{\omega}_e - (\boldsymbol{\eta}^*\boldsymbol{J} + \boldsymbol{J}\boldsymbol{\eta}^*)\,\boldsymbol{\omega}_e - \boldsymbol{\omega}_e^*\boldsymbol{J}\boldsymbol{\eta} + [\boldsymbol{u} - (\boldsymbol{\eta}^*\boldsymbol{J}\boldsymbol{\eta} + \boldsymbol{J}C(\boldsymbol{s})\dot{\boldsymbol{\omega}}_r)]
\end{aligned}
$$
$$\tag{2.7}$$

Grouping the terms related to the input, let

$$
\boldsymbol{\Omega}\boldsymbol{\theta}^* = \boldsymbol{\eta}^*\boldsymbol{J}\boldsymbol{\eta} + \boldsymbol{J}C(\boldsymbol{s})\dot{\boldsymbol{\omega}}_r \tag{2.8}
$$

where $\boldsymbol{\theta}^* = \mathrm{Vec}(\boldsymbol{J})$, assumed to be unknown/uncertain for this problem. We note that $\mathrm{Vec}(\boldsymbol{J}) \in \mathbb{R}^6$ includes the unique elements of the symmetric inertia matrix $j \in \mathbb{R}^{3\times3}$. The regressor matrix $\boldsymbol{\Omega}$ is a bounded function of time, dependent upon the quantities $\boldsymbol{\eta}, \boldsymbol{s}$ and $\dot{\boldsymbol{\omega}}_r$. It can be readily recognized that the matrix expression $\boldsymbol{R} = (\boldsymbol{\eta}^*\boldsymbol{J} + \boldsymbol{J}\boldsymbol{\eta}^*)$ is skew-symmetric. Using these compacted notations Eq. (2.7) can be expressed as,

$$
\boldsymbol{J}\dot{\boldsymbol{\omega}}_e = -\boldsymbol{\omega}_e^*\boldsymbol{J}\boldsymbol{\omega}_e - \boldsymbol{\omega}_e^*\boldsymbol{J}\boldsymbol{\eta} - \boldsymbol{R}\boldsymbol{\omega}_e + \boldsymbol{u} - \boldsymbol{\Omega}\boldsymbol{\theta}^* \tag{2.9}
$$

Thus, if $\boldsymbol{\theta}^*$ is perfectly known, the PD+ control torque input used is defined by

$$
\boldsymbol{u} = -k_p\boldsymbol{s}_v - k_v\boldsymbol{\omega}_e + \boldsymbol{\Omega}\boldsymbol{\theta}^* \tag{2.10}
$$

where k_p, k_v (positive scalars) and $\boldsymbol{\theta}^*$ are respectively the proportional and rate feedback gains and the inertia matrix expressed in vectorized form.

2.2 Motivation

For the system dynamics described in the previous section, if $\boldsymbol{\omega_r}(t) \equiv 0 \forall t \geq 0$ and the task is to simply stabilize the attitude of the spacecraft to zero, the control input listed in Eq. 2.10 can be reduced to

$$\boldsymbol{u} = -k_p \boldsymbol{s_v} - k_v \boldsymbol{\omega_e} \tag{2.11}$$

Using a candidate Lyapunov-like function [1]

$$V_{00} = k_p[(s_0 - 1)^2 + \boldsymbol{s_v^T s_v}] + \frac{1}{2} \boldsymbol{\omega_e^T J \omega_e} \tag{2.12}$$

and differentiating with time, we get by substituting the control input from Eq.2.11

$$\dot{V}_{00} = k_p \boldsymbol{s_v^T \omega_e} + \boldsymbol{\omega_e^T J \dot{\omega}_e} = \boldsymbol{\omega_e^T}[u + k_p \boldsymbol{s_v}] = -k_v \|\boldsymbol{\omega_e}\|^2 \tag{2.13}$$

Since this derivative is non-positive, the value of the Lyapunov function V_{00} is bounded, implying that $\boldsymbol{s_v}$ and $\boldsymbol{\omega_e}$ are also bounded. Integrating both sides of Eq. 2.13, we can prove $\boldsymbol{\omega_e} \in L_2$ and using the corollary to the Barbalat's Lemma, prove that $\lim_{t \to \infty} \boldsymbol{\omega_e}(t) = 0$. Using the dynamics from the above section and the Barbalat's Lemma itself, $\boldsymbol{s_v}$ can also be shown to asymptotically converge to zero. This concludes our analysis of the "PD" controller for the attitude stabilization case.

Now in the case where there is a reference trajectory $\boldsymbol{\omega_r}$ to be tracked, consider the candidate Lyapunov-like function where $c > 0$ is a user chosen parameter [1]

$$V = (k_p + ck_v)[(s_0 - 1)^2 + \boldsymbol{s_v^T s_v}] + \frac{1}{2} \boldsymbol{\omega_e J \omega_e} + c \boldsymbol{s_v^T J \omega_e} \tag{2.14}$$

27

If the inertia matrix is accurately known, for the control input in Eq.2.10, the time derivative of Eq.2.14 satisfies the inequality

$$\dot{V} \leq -ck_p\|\boldsymbol{s_v}\|^2 - k_v\|\boldsymbol{\omega_e}\|^2 + cJ_{\max}\|\boldsymbol{\omega_e}\|^2 + 3cJ_{\max}\gamma_d\|\boldsymbol{s_v}\|\|\boldsymbol{\omega_e}\| \qquad (2.15)$$

where $\gamma_d = \|\boldsymbol{\omega_r}\|_\infty$ represents the infinity norm of the desired angular velocity, i.e. its maximum value, qualitatively speaking.

As can be seen from the above equations, for a small enough value of the parameter c, the Lyapunov candidate function in Eq.2.14 is non-negative and its derivative in Eq.2.15 is negative semi-definite. Using Barbalat's lemma, stable tracking along the reference trajectory can be demonstrated. The conditions on c can be rewritten in matrix form as the following two matrices being positive definite:

$$P = \frac{1}{2}\begin{bmatrix} 2(k_p + ck_v) & -cJ_{\max} \\ -cJ_{\max} & J_{\min} \end{bmatrix} > 0 \qquad (2.16)$$

$$Q = \frac{1}{2}\begin{bmatrix} 2ck_p & 3\gamma_d J_{\max}c \\ 3\gamma_d J_{\max}c & 2k_v - 4cJ_{\max} \end{bmatrix} > 0 \qquad (2.17)$$

It is to be noted here that in the known inertia case, the parameter c is only used in the Lyapunov analysis and is not implemented in the control input (Eq. 2.10) and is thus not necessary to be known. In the stability analysis for the non-adaptive case, c can even be chosen to be zero and would still not impact the overall closed-loop stability and convergence result. For the adaptive control case where the inertia matrix is not accurately known, using the certainty equivalence principle, the inertia term $\boldsymbol{\theta^*}$ in the control

input from Eq. 2.10 is replaced with its adaptively generated estimate $\hat{\boldsymbol{\theta}}$ and Eq.2.14 is modified to include an error in inertia ($\tilde{\boldsymbol{\theta}} \triangleq \hat{\boldsymbol{\theta}} - \boldsymbol{\theta}^*$) term:

$$V = (k_p + ck_v)[(s_0 - 1)^2 + \boldsymbol{s}_v^T \boldsymbol{s}_v] + \frac{1}{2}\boldsymbol{\omega}_e \boldsymbol{J}\boldsymbol{\omega}_e + c\boldsymbol{s}_v^T \boldsymbol{J}\boldsymbol{\omega}_e + \tilde{\boldsymbol{\theta}}^T \boldsymbol{\Gamma}^{-1}\tilde{\boldsymbol{\theta}} \quad (2.18)$$

where $\boldsymbol{\Gamma} = \boldsymbol{\Gamma}^T > 0$ is a user chosen learning rate matrix. Following standard techniques outlined in [1], the time derivative of the Lyapunov candidate function in Eq. 2.18 can be shown to satisfy the inequality in Eq.2.15 by using the update law

$$\dot{\hat{\boldsymbol{\theta}}} = -\boldsymbol{\Gamma}\boldsymbol{\Omega}^T \left(\boldsymbol{\omega}_e + c\boldsymbol{s}_v\right) \quad (2.19)$$

Thus even with uncertain inertia knowledge, for a small enough value of c the "PD+" control law with an inertia estimate following the adaptive update law from Eq. 2.19 can be shown to asymptotically track the reference trajectory following Barbalat's lemma. However, the parameter c now shows up explicitly as part of the update law, is implemented and thus needs to be some user chosen known positive constant satisfying the conditions in Eq. 2.17. As shown in matrices P and Q, the definition of "small enough" for c is however based on the values of $J_{\max}$, $J_{\min}$ and γ_d wherein $J_{\max}$ and $J_{\min}$ remain poorly determined when the inertia is unknown. Thus the update law in Eq. 2.19 depends upon poorly determined inertia bounds which is a risky endeavor from a closed-loop stability perspective. If the parameter c is chosen to be higher than the allowable upper bound for the particular values of inertia parameters, the controller could potentially cause closed loop instability. The option of choosing $c = 0$ also does not exist for the adaptive case since we run into the

29

uniform detectibility obstacle and this was the motivation behind introducing c in the first place within the update law in Eq. 2.19.

To further motivate the need for a new controller that mitigates this instability risk, Fig. 2.1 illustrates how this upper bound on parameter c changes as a function of the inertia parameters, reference trajectory and controller gains. To make the illustration simpler and reduce the number of variable design factors, we choose a "critically damped controller" with $k_p = \omega_n^2$ and $k_v = 2\omega_n$ respectively as the proportional and derivative feedback gains within Eq. 2.10, Fig. 2.1a shows the allowable upper bounds on c for different values of γ_d for a fixed inertia matrix. Fig. 2.1b does the same for different values of $J_{\max}$ and fixed $J_{\min}$ and reference trajectory. As can be seen in both figures, the bound for c increases with increasing values of the gains. On the other hand, qualitatively speaking, smaller spacecraft with smaller $J_{\max}$ and $J_{\min}$ inertia values can tolerate higher values for c. Similarly, higher values of γ_d, that is, more rapidly changing reference trajectories, have lower values of the bound for the c parameter. Thus, a randomly chosen, intuitively "small" value of $c = 0.1$ for example, may stabilize a small spacecraft with large values for the controller gains but it may fail for a spacecraft with larger inertia or for smaller controller gains. Similarly, the same value of c which works for a relatively slow changing trajectory may fail for a more aggressive reference trajectory.

An example of the effect of choosing a larger c value is shown in Fig. 2.2 where $c = 0.03$ stabilizes the closed loop system according to the sufficient

conditions in Eq. 2.17 but $c = 0.04$ does not for a simulation of the inertia of the Cassini spacecraft [19], with $J_{\max} = 8823\text{kg.m}^2$ and $J_{\min} = 4520\text{kg.m}^2$. The values of $k_p = 200$ and $k_v = 100$ were chosen such that the closed loop response without adaptation has a settling time of $200s$ for the norm of the angular rate errors to go below an error band of 0.1rad/s. This is consistent with the general practice of choosing controller gains to satisfy performance requirements before any adaptation algorithm is put in place. In this figure, we only plot the norm of the Lyapunov function from Eq. 2.18 to show the values of c at which the controller fails. For a smaller satellite, the safe values of c would be lower and instability would result at $c = 0.1$. This demonstrates the difficulty in choosing the value of this parameter given that it is so dependent on the system inertia and deeply impacts controller performance.

It should be emphasized that the conditions for stability on c based on matrices P and Q in Eq. 2.17 are sufficient but not necessary, which implies that the upper bounds on c discussed above can be often conservative and the actual value of c typically causing instability is usually higher than this bound. For example, for a "medium sized spacecraft" with inertia eigenvalues in the 10^3kg.m^2 range, the safe choice is in the range $c < 10^{-7}$, which is much smaller than the $c = 0.01$ value at which the simulation shown in Fig.2.2 presents convergence issues. What makes the controller design from [1] to be fragile, is the fact that the choice of this c parameter directly affects the convergence rate of the tracking errors, and thus conservatively choosing an arbitrarily small value would typically lead to sluggish closed-loop response. Since con-

31

trol designers would choose c values lower than the conservative upper bound for the particular system to ensure stability, performance of the controller is inherently compromised, illustrating a Hobson's choice for the designer. A salient feature of the controller presented in this chapter is that it does not require introduction of any preset parameter (such as c in [1]) or assumptions upon availability of inertia matrix eigenvalues, thereby eliminating the risks of compromised stability and performance.

(a) Changing reference trajectories   (b) Changing inertia matrix
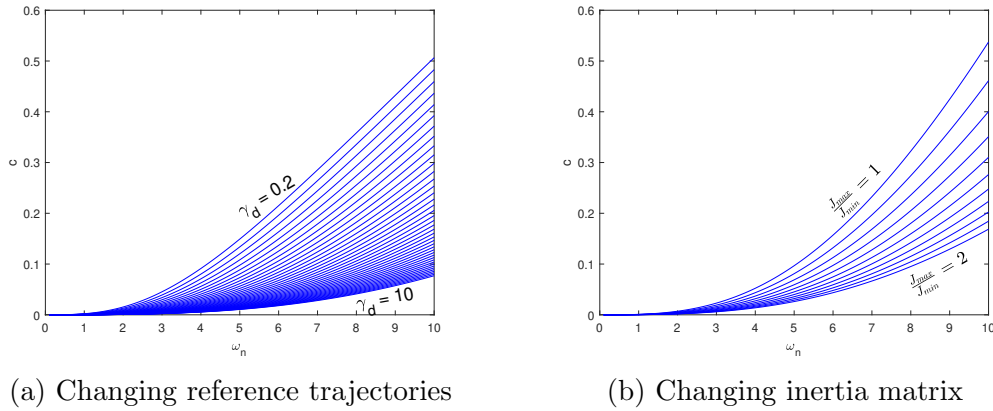
Figure 2.1: Upper bounds on the parameter c with changing controller gains

The major feature of this work is that, the so called "PD+" control law from Eq. 2.10 using fixed values of $k_p > 0$, $k_v > 0$ and the inertia estimate is modified to have dynamic gains for the proportional and derivative feedback terms:

$$u = -\hat{k}_p(t)\boldsymbol{s_v} - \hat{k}_v(t)\boldsymbol{\omega_e} + \boldsymbol{\Omega}\hat{\boldsymbol{\theta}} \tag{2.20}$$

It is important to emphasize that the basic "PD+" structure of the controller is retained and saliently, we will show that it naturally reduces to the
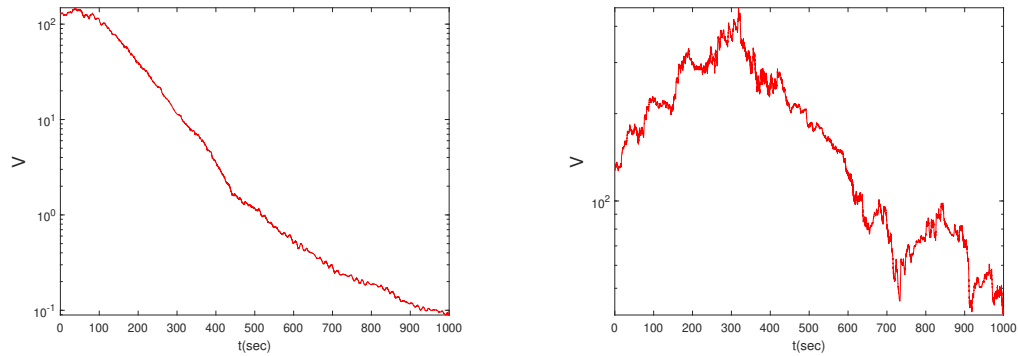
(a) Lyapunov function value from Eq. 2.18 for $c = 0.03$

(b) Lyapunov function value from Eq. 2.18 for $c = 0.04$

Figure 2.2: Norm of the Lyapunov function from [1] controller for different c values

pure PD controller in Eq. 2.11 for the set point regulation case, thus preserving the self-reduction property. A new Lyapunov-like function is designed for the stability analysis of the controller in Eq. 2.20, which provides us with update laws for the estimates of inertia parameters $\hat{\boldsymbol{\theta}}(t)$ as well as the time-varying proportional and rate-feedback gains (respectively denoted by scalars $\hat{k}_p$ and $\hat{k}_v$). These dynamic feedback gains allow us to design an adaptive controller that permits tracking the reference trajectory in a stable fashion without the requirement for any prior knowledge on the actual inertia of the system, as is the case for [1]. The modified Lyapunov-like function (to be introduced in the next section) blends the traditional energy-like terms from [1] along with certain judiciously designed cross-terms. The time derivative of this new Lyapunov-like function however has sign indefinite terms which are dominated by certain other negative terms, requiring that the value of $\hat{k}_p$ remains positive

33

for all times during the adaptation process. We thus implement a projection scheme for the proportional gain $\hat{k}_p$ signal, which ensures it stays above some user chosen (arbitrary) positive constant. It has to be emphasized that the value of this user chosen positive constant (lower bound for $\hat{k}_p$) does not affect the overall stability result but only impacts the transient properties and convergence rates for the resulting closed-loop solutions.

2.3 Controller Design

The controller design process for attitude tracking is started off with the classical Lyapunov function for attitude control with quaternion parameterization. For any positive constant k_p^* (used only for analysis purposes), the first Lyapunov-like function is slightly modified from Eq.2.12 based on the classical literature [1] as

$$V_0 = k_p^* \left[(s_0 - 1)^2 + \boldsymbol{s}_v^T \boldsymbol{s}_v \right] + \frac{1}{2} \boldsymbol{\omega}_e^T \boldsymbol{J} \boldsymbol{\omega}_e \qquad (2.21)$$

It should be noted that this analysis is particularly suited for the attitude tracking case and the attitude stabilization case has already been solved using the V_{00} analysis in the Motivation section. Next, a "cross-term" is introduced as follows

$$N = \boldsymbol{s}_v^T \boldsymbol{J} \boldsymbol{\omega}_e \qquad (2.22)$$

For a valid for Lyapunov analysis, using the torque input defined in Eq. 2.20, let us consider the conditions for the combination of these terms

above to be non-negative, using completion of squares:

$$V_0 + N = k_p^* \left[\boldsymbol{s}_v^T \boldsymbol{s}_v + (s_0 - 1)^2 \right] + \frac{1}{2} \boldsymbol{\omega}_e^T \boldsymbol{J} \boldsymbol{\omega}_e + \boldsymbol{s}_v^T \boldsymbol{J} \boldsymbol{\omega}_e$$

$$\geq k_p^* \| \boldsymbol{s}_v \|^2 + \frac{J_{\min}}{2} \| \boldsymbol{\omega}_e \|^2 - J_{\max} \| \boldsymbol{s}_v \| \| \boldsymbol{\omega}_e \|$$

$$\geq \frac{k_p^*}{2} \| \boldsymbol{s}_v \|^2 + \left[\frac{J_{\min}}{2} - \frac{J_{\max}^2}{2k_p^*} \right] \| \boldsymbol{\omega}_e \|^2$$

which will be non-negative if

$$k_p^* > \frac{J_{\max}^2}{J_{\min}} \tag{2.23}$$

Differentiating with respect to time the function in Eq. 2.21, followed by substituting Eq. 2.9 and the control law from Eq. 2.20 results in,

$$\dot{V}_0 = k_p^* \boldsymbol{s}_v^T \boldsymbol{\omega}_e + \boldsymbol{\omega}_e^T \boldsymbol{J} \dot{\boldsymbol{\omega}}_e$$

$$= \boldsymbol{\omega}_e^T \left[\boldsymbol{u} + k_p^* \boldsymbol{s}_v - \boldsymbol{\Omega} \boldsymbol{\theta}^* \right]$$

$$= -k_{vm} \| \boldsymbol{\omega}_e \|^2 + \boldsymbol{\omega}_e^T \left[\boldsymbol{u} + k_p^* \boldsymbol{s}_v + k_{vm} \boldsymbol{\omega}_e - \boldsymbol{\Omega} \boldsymbol{\theta}^* \right]$$

$$= -k_{vm} \| \boldsymbol{\omega}_e \|^2 - \tilde{k}_p \boldsymbol{\omega}_e^T \boldsymbol{s}_v - \tilde{k}_v \| \boldsymbol{\omega}_e \|^2 + \boldsymbol{\omega}_e^T \boldsymbol{\Omega} \tilde{\boldsymbol{\theta}} \tag{2.24}$$

where $k_{vm} > 0$ is a user chosen constant and

$$\tilde{k}_p = \hat{k}_p - k_p^* \tag{2.25}$$

$$\tilde{k}_v = \hat{k}_v - k_{vm} \tag{2.26}$$

while the time-derivative of the cross term N defined in Eq. 2.22 yields

$$
\begin{aligned}
\dot{N} &= \boldsymbol{\omega}_e^T \boldsymbol{J} \dot{\boldsymbol{s}}_v + \boldsymbol{s}_v^T \boldsymbol{J} \dot{\boldsymbol{\omega}}_e \\
&= \frac{1}{2} \boldsymbol{\omega}_e^T \boldsymbol{J} \left(s_0 \mathbb{I}_{3\times 3} + \boldsymbol{s}_v^* \right) \boldsymbol{\omega}_e + \boldsymbol{s}_v^T \left(-\boldsymbol{\omega}_e^* \boldsymbol{J} \boldsymbol{\omega}_e - \boldsymbol{\omega}_e^* \boldsymbol{J} \boldsymbol{\eta} - \boldsymbol{R}\boldsymbol{\omega}_e + \boldsymbol{u} - \boldsymbol{\Omega}\boldsymbol{\theta}^* \right) \\
&= \frac{1}{2} s_0 \boldsymbol{\omega}_e^T \boldsymbol{J} \boldsymbol{\omega}_e + \frac{1}{2} \boldsymbol{\omega}_e^T \boldsymbol{J} \boldsymbol{s}_v^* \boldsymbol{\omega}_e - \boldsymbol{s}_v^T \boldsymbol{\omega}_e^* \boldsymbol{J} \boldsymbol{\omega}_e - \boldsymbol{s}_v \boldsymbol{\omega}_e^* \boldsymbol{J} \boldsymbol{\eta} - \boldsymbol{s}_v^T \boldsymbol{R} \boldsymbol{\omega}_e \\
&\quad + \boldsymbol{s}_v^T \left(\boldsymbol{u} - \boldsymbol{\Omega}\boldsymbol{\theta}^* \right) \\
&= \frac{1}{2} s_0 \boldsymbol{\omega}_e^T \boldsymbol{J} \boldsymbol{\omega}_e - \frac{1}{2} \boldsymbol{\omega}_e^T \boldsymbol{J} \boldsymbol{s}_v^* \boldsymbol{\omega}_e - \boldsymbol{s}_v^T \boldsymbol{R} \boldsymbol{\omega}_e + \boldsymbol{s}_v \left(\boldsymbol{J}\boldsymbol{\eta} \right)^* \boldsymbol{\omega}_e + \boldsymbol{s}_v^T \left(\boldsymbol{u} - \boldsymbol{\Omega}\boldsymbol{\theta}^* \right) \\
&= \frac{1}{2} s_0 \boldsymbol{\omega}_e^T \boldsymbol{J} \boldsymbol{\omega}_e - \frac{1}{2} \boldsymbol{\omega}_e^T \boldsymbol{J} \boldsymbol{s}_v^* \boldsymbol{\omega}_e - \boldsymbol{s}_v^T \left[\boldsymbol{R} - \left(\boldsymbol{J}\boldsymbol{\eta} \right)^* \right] \boldsymbol{\omega}_e + \boldsymbol{s}_v^T \left(\boldsymbol{u} - \boldsymbol{\Omega}\boldsymbol{\theta}^* \right) \\
&\leq J_{\max} \| \boldsymbol{\omega}_e \|^2 + \rho \| \boldsymbol{s}_v \| \| \boldsymbol{\omega}_e \| - \hat{k}_p \boldsymbol{s}_v^T \boldsymbol{s}_v - \hat{k}_v \boldsymbol{s}_v^T \boldsymbol{\omega}_e + \boldsymbol{s}_v^T \boldsymbol{\Omega} \tilde{\boldsymbol{\theta}} \qquad (2.27)
\end{aligned}
$$

where ρ represents an upper bound for the norm of the bounded function $\boldsymbol{R} - \left(\boldsymbol{J}\boldsymbol{\eta} \right)^*$, i.e., $\sup_{t \geq 0} \| \boldsymbol{R} - \left(\boldsymbol{J}\boldsymbol{\eta} \right)^* \| \leq \rho < \infty$.

Since $\hat{k}_p$ multiplies the quadratic term in s_v in Eq. 2.27, it needs to stay positive at all times for purposes of the ongoing stability analysis. Thus, an update law will be introduced in the sequel through projection techniques for the dynamic gain $\hat{k}_p(t)$ such that $\hat{k}_p(t) \geq k_{pm} > 0$ for all $t \geq 0$, where k_{pm} is any user chosen (arbitrary) constant. Using this lower-bound for $\hat{k}_p(t)$ in Eq. 2.27 and completing squares, we have

$$
\dot{N} \leq -\frac{k_{pm}}{2} \| \boldsymbol{s}_v \|^2 - \hat{k}_v \boldsymbol{s}_v^T \boldsymbol{\omega}_e + \left(J_{\max} + \frac{\rho^2}{2 k_{pm}} \right) \| \boldsymbol{\omega}_e \|^2 + \boldsymbol{s}_v^T \boldsymbol{\Omega} \tilde{\boldsymbol{\theta}} \qquad (2.28)
$$

Combining the initial Lyapunov function V_0 with the cross term N and a quadratic measure of the error in inertia estimate $\tilde{\boldsymbol{\theta}} = \hat{\boldsymbol{\theta}} - \boldsymbol{\theta}^*$, for a adaptive inertia learning rate of $\boldsymbol{\Gamma} = \boldsymbol{\Gamma}^T > 0$ (user chosen) we arrive at the second

Lyapunov-like function

$$V = V_0 + N + \frac{1}{2}\tilde{\boldsymbol{\theta}}^T \boldsymbol{\Gamma}^{-1} \tilde{\boldsymbol{\theta}} \tag{2.29}$$

Differentiating Eq. 2.29, and combining Eq. 2.24 and Eq. 2.27,

$$\dot{V} \leq -\frac{k_{pm}}{2}\|\boldsymbol{s_v}\|^2 - k_{vm}\|\boldsymbol{\omega_e}\|^2 - \left[\hat{k}_v - \left(k_{vm} + J_{\max} + \frac{\rho^2}{2k_{pm}}\right)\right]\|\boldsymbol{\omega_e}\|^2$$
$$- \left(\hat{k}_p + \hat{k}_v - k_p^*\right)\boldsymbol{s_v}^T\boldsymbol{\omega_e} + \tilde{\boldsymbol{\theta}}^T\boldsymbol{\Gamma}^{-1}\left[\dot{\hat{\boldsymbol{\theta}}} + \boldsymbol{\Gamma}\boldsymbol{\Omega}^T\left(\boldsymbol{\omega_e} + \boldsymbol{s_v}\right)\right] \tag{2.30}$$

The $\tilde{\boldsymbol{\theta}}$ terms above can be eliminated by choosing

$$\dot{\hat{\boldsymbol{\theta}}} = -\boldsymbol{\Gamma}\boldsymbol{\Omega}^T\left(\boldsymbol{\omega_e} + \boldsymbol{s_v}\right) \tag{2.31}$$

which leaves

$$\dot{V} \leq -\frac{k_{pm}}{2}\|\boldsymbol{s_v}\|^2 - k_{vm}\|\boldsymbol{\omega_e}\|^2 - \left(\hat{k}_v - k_v^*\right)\|\boldsymbol{\omega_e}\|^2$$
$$- \left(\hat{k}_p + \hat{k}_v - k_p^*\right)\boldsymbol{s_v}^T\boldsymbol{\omega_e}$$
$$\leq -\frac{k_{pm}}{2}\|\boldsymbol{s_v}\|^2 - k_{vm}\|\boldsymbol{\omega_e}\|^2 - \left(\hat{k}_v - k_v^*\right)(\|\boldsymbol{\omega_e}\|^2 + \boldsymbol{s_v}^T\boldsymbol{\omega_e})$$
$$- \left(\hat{k}_p + k_v^* - k_p^*\right)\boldsymbol{s_v}^T\boldsymbol{\omega_e} \tag{2.32}$$

where in we introduce for convenience of notation

$$k_v^* = k_{vm} + J_{\max} + \frac{\rho^2}{2k_{pm}} \tag{2.33}$$

As stated already, the parameter k_p^* is not required for controller implementation but is chosen to satisfy the condition

$$k_p^* > \max\left(\frac{J_{\max}^2}{J_{\min}}, k_{pm} + k_v^*\right) \tag{2.34}$$

37

To lower bound the proportional gain $\hat{k}_p$ by the constant k_{pm}, a projection scheme is used through reparameterization via another variable $\hat{\phi}$ as given by

$$\hat{k}_p = k_{pm} + e^{\hat{\phi}} \tag{2.35}$$

The constant k_v^* from Eq. 2.33 is reparameterized too using a constant ϕ^*,

$$k_p^* - k_v^* = k_{pm} + e^{\phi^*} \tag{2.36}$$

Combining Eq. 2.35 and Eq. 2.36 yields,

$$\hat{k}_p + k_v^* - k_p^* = e^{\phi^*} \left[e^{(\hat{\phi} - \phi^*)} - 1 \right] \tag{2.37}$$

Using this projection scheme, the final Lyapunov-like function is defined as

$$\tilde{V} = V + \frac{1}{2\gamma_1}(\hat{k}_v - k_v^*)^2 + \frac{e^{\phi^*}}{\gamma_2}\left[e^{(\hat{\phi} - \phi^*)} - (\hat{\phi} - \phi^*) \right] \tag{2.38}$$

$$\dot{\tilde{V}} = \dot{V} + \frac{1}{\gamma_1}(\hat{k}_v - k_v^*)\dot{\hat{k}}_v + \frac{e^{\phi^*}}{\gamma_2}\left[\dot{\hat{\phi}}e^{(\hat{\phi} - \phi^*)} - \dot{\hat{\phi}} \right]$$

$$\leq -\frac{k_{pm}}{2}\|\boldsymbol{s_v}\|^2 - k_{vm}\|\boldsymbol{\omega_e}\|^2 + (\hat{k}_v - k_v^*)\left(\frac{\dot{\hat{k}}_v}{\gamma_1} - \|\boldsymbol{\omega_e}\|^2 - \boldsymbol{s_v}^T\boldsymbol{\omega_e} \right)$$

$$+ e^{\phi^*}\left[e^{(\hat{\phi} - \phi^*)} - 1 \right]\left[\frac{\dot{\hat{\phi}}}{\gamma_2} - \boldsymbol{s_v}^T\boldsymbol{\omega_e} \right] \tag{2.39}$$

In its simple form, the feedback gains are dynamically updated even for the attitude stabilization special case, where the reference trajectory is zero. Since we know that the inertia estimate does not update for the stabilization

case, it would be convenient if our control input just reduced to the traditional PD controller with constant gains. To achieve this, we scale the parameters $\bar{\gamma}_1 > 0$ and $\bar{\gamma}_2 > 0$, which are the user chosen learning rates for the estimates of the inertia matrix and feedback gains respectively, by the maximum norm of the desired/reference velocity, $\gamma_d = \|\boldsymbol{\omega_r}\|_\infty$:

$$\gamma_1 = \gamma_d \bar{\gamma}_1 \tag{2.40}$$

$$\gamma_2 = \gamma_d \bar{\gamma}_2 \tag{2.41}$$

This scaling ensures that the gains do not change when the desired velocity is just zero, hence preserving the self reduction property. It is important to note that the preceding analysis is meant only for the reference trajectory tracking case when $\gamma_d \neq 0$ and hence involving the reciprocals of γ_1 and γ_2 within Eq. 2.38 is a valid operation. The analysis for the attitude stabilization case does not require progressing beyond Eq.2.12 while this γ_d scaling ensures there is no design switch necessary for the control inputs for the two cases. Thus, choosing the update equations to be

$$\dot{\hat{\boldsymbol{\theta}}} = -\boldsymbol{\Gamma}\boldsymbol{\Omega}^T \left(\boldsymbol{\omega_e} + \boldsymbol{s_v}\right) \tag{2.42}$$

$$\dot{\hat{k}}_v = \gamma_1 \|\boldsymbol{\omega_e}\|^2 + \gamma_1 \boldsymbol{s_v}^T \boldsymbol{\omega_e} \tag{2.43}$$

$$\dot{\hat{k}}_p = \gamma_2 \left(\hat{k}_p - k_{pm}\right) \boldsymbol{s_v}^T \boldsymbol{\omega_e} \tag{2.44}$$

results in the derivative of the Lyapunov function being negative semi-definite

$$\dot{\tilde{V}} \leq -\frac{k_{pm}}{2}\|\boldsymbol{s_v}\|^2 - k_{vm}\|\boldsymbol{\omega_e}\|^2 \tag{2.45}$$

39

Since the Lyapunov function in Eq. 2.39 is lower bounded and its derivative is negative semi-definite, $\tilde{V} \in L_\infty$, which implies $\boldsymbol{s_v} \in L_\infty$, $\boldsymbol{\omega_e} \in L_\infty$ and $\tilde{\boldsymbol{\theta}} \in L_\infty$. Since $\dot{\boldsymbol{\omega}}_e$ and $\dot{\boldsymbol{s}}_v$ are functions of these bounded variables, they are bounded as well ($\dot{\boldsymbol{\omega}}_e \in L_\infty$ and $\dot{\boldsymbol{s}}_v \in L_\infty$). Moreover, since $\tilde{V}$ is monotonic (non-increasing) and lower bounded, we have the existence of the limit

$$\lim_{t \to \infty} \tilde{V}(t) \triangleq \tilde{V}_\infty \tag{2.46}$$

Thus, integrating both sides of Eq. 2.45, we can show that $\boldsymbol{s_v} \in L_2$ and $\boldsymbol{\omega_e} \in L_2$. Finally, using the corollary to the Barbalat's lemma [18], we have,

$$\lim_{t \to \infty} [\boldsymbol{s_v}(t), \boldsymbol{\omega_e}(t)] = 0 \tag{2.47}$$

We note that Eq. 2.44 was obtained by substituting $\dot{\hat{\phi}} = \gamma_2 \boldsymbol{s}_v^T \boldsymbol{\omega_e}$ into Eq. 2.35. It is to be noted that $\hat{\phi}$ was used as part of the Lyapunov analysis and helps ensuring the $k_p > k_{pm}$ condition, but does not show up as part of the implementation. Moreover, no projection scheme is imposed upon the angular rate gain $\hat{k}_v(t)$, leading to the rare yet distinct possibility that the cross term in Eq. 2.43 be negative and dominate the first term, driving $\hat{k}_v(t)$ to negative values in the transient. This is an interesting attribute of the proposed controller and does not affect any of the stability results provided.

It needs to be emphasized that the update laws and the control input do not require any additional knowledge of parameters that rely upon the inertia matrix. All the constants that are part of the adaptive controller implementation are user chosen (arbitrary) and closed-loop stability is guaranteed.

The only impact of the user chosen values will be on the rate of convergence (closed-loop performance) which can be tuned through judicious numerical experiments. On the other hand in cases like Wen and Delgado [1], which use constant feedback gains $\bar{k}_p$ and $\bar{k}_v$ unlike our dynamically changing gains, the adaptation law for the inertia estimate involves an extra parameter c. As discussed already in the motivation section, for any given spacecraft, bounds on c can be violated by changing the reference trajectory which also means that a chosen set of controller parameters cannot be uniformly engaged for certain reference trajectories even after having passed many test runs.

The controller formulation presented here applies only to rigid spacecraft where the inertia $\boldsymbol{J}$ is not accurately known but is still constant over time. In the case of non-rigid spacecraft, while the inertia is still bounded, there might be a non-negligible rate of change of the inertia $\dot{\boldsymbol{\theta}}$, which will need to be factored into the Lyapunov analysis through appropriate robustness modifications from adaptive control [20, Chapter 9]. If the rate of change of inertia is known and bounded, additional conditions can be placed on the minimum value of k_{pm} and k_{vm} based on the upper bound $\dot{\theta}_{\max} = \max(\|\dot{\boldsymbol{\theta}}\|)$ to dominate the terms involving the rate of inertia change, as well as adding $\dot{\boldsymbol{\theta}}$ to the adaptation in Eq. 2.31. A more detailed analysis of the applicability of the proposed controller to non-rigid spacecraft falls outside the scope of this work and can be considered for future studies.

2.4 Simulation Results

The proposed adaptive controller was simulated using the inertia matrix and initial error conditions from [9] corresponding to a persistently exciting reference trajectory. The resulting closed-loop solutions of the error states and control torque are shown in Fig. 2.3 and Fig. 2.4. For these simulations, the unknown inertia matrix is represented by

$$\boldsymbol{\theta}^* = [20, 1.2, 0.9, 17, 1.4, 15]^T = \text{Vec}(\boldsymbol{J}) \tag{2.48}$$

and the initial error in the state

$$\boldsymbol{s}(0) = [\sqrt{1 - 3 \times 0.1826^2}, 0.1826, 0.1826, 0.1826]^T \tag{2.49}$$

The body is initially at rest and the reference angular velocity profile is

$$\boldsymbol{\omega_r}(t) = [0.1 * \cos 2t + 0.1, 0.5 \cos t, 0.1 * \sin t + 0.1]^T \tag{2.50}$$

The initial values chosen for the feedback gains were $\hat{k}_p(0) = 50$ and $\hat{k}_v(0) = 20$, while the proportional gain was lower bounded through the projection scheme at $k_{pm} = 5$. The learning rates were chosen as $\boldsymbol{\Gamma} = 10\mathbb{I}_{6\times6}$, $\gamma_1 = 5$ and $\gamma_2 = 10$. Fig. 2.3 uses an initial estimate of the inertia with an uncertainty of 5% and Fig. 2.4 has an uncertainty of 25%, which has an impact on the time taken for the inertia estimates to converge to the true value as seen in the time axis of Fig. 2.3e and Fig. 2.4e. Fig. 2.3f and Fig. 2.4f show the norm of the control torque values, which are well within the range of values reported from the controller in [9] that uses a completely different

42

adaptive controller construction based upon state-augmentation approaches. The attitude and angular rate states converge to track the reference trajectory as shown in Figs. 2.3c,2.4c,2.3d,2.4d using the dynamic proportional and derivative gains in Figs. 2.3a,2.4a,2.3b,2.4b.
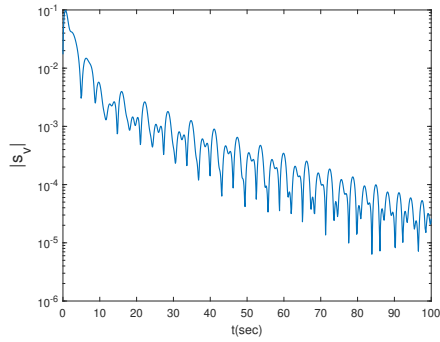
As demonstrated by the example numerical simulations, the proposed adaptive control law drives the system states to track the reference trajectory. This was achieved without requiring any additional information concerning the inertia matrix (such as an upper bound upon its norm) which is a novel result. This performance is compared with the performance of the controller in Wen and Delgado [1] in Fig. 2.5 for an initial inertia guess with 5% uncertainty of the real inertia of the Cassini Spacecraft [19]. The values of the proportional and differential gains for the proposed controller were initialized at $k_p = 50$ and $k_v = 30$ but are free to change according to our update laws in Eq. (2.44) and Eq. (2.43), while the values for Wen and Delgado were chosen to stay constant at $\bar{k}_p = 50$ and $\bar{k}_v = 45$ for a fair comparison, since our dynamic value of k_v settled at around 45. The update law parameter c was chosen to be 1, which satisfied the condition of positive definiteness of $\boldsymbol{P}$ and $\boldsymbol{Q}$ matrices from Eq. (2.17). As can be seen from Figs. 2.5a,2.5b, the error states in both the cases are comparable while the torque too was in a similar range. The inertia estimates in Fig.2.5c also converge to the true (unknown) value in a similar time frame. These values will vary with the choice of controller parameters like the gains and the constant c, but the performance was observed to be similar. The transient for the proposed controller is seen to be slower than
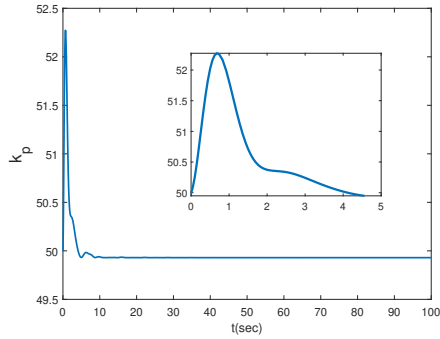
(a) Proportional gain
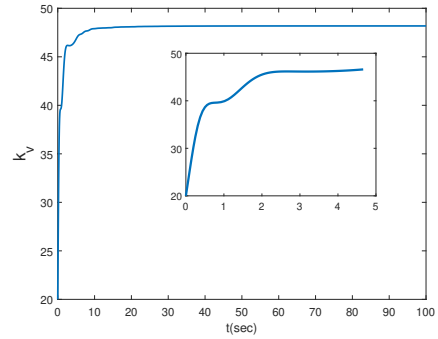
(b) Derivative feedback gain

(c) Quaternion vector norm

(d) Angular velocity error norm

(e) Norm of inertia estimate

(f) Norm of the control torque

Figure 2.3: Closed-loop error trajectories resulting from application of the proposed adaptive controller for a 5% error in the initial inertia estimate, $k_p(0) = 50$ and $k_v(0) = 30$
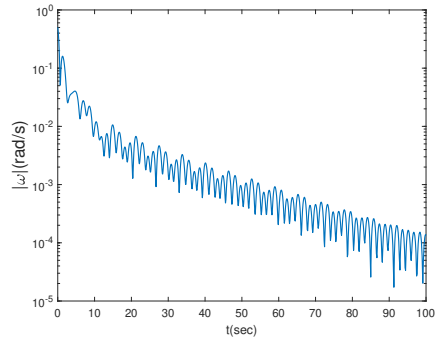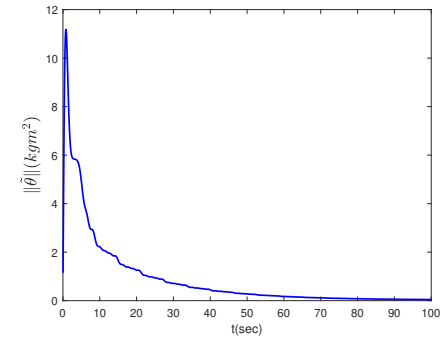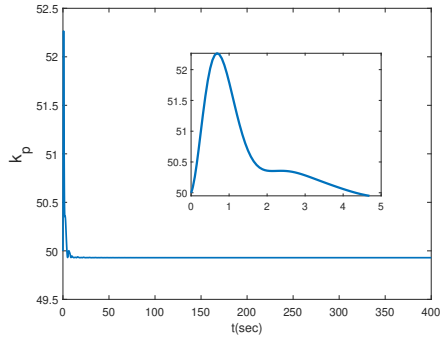
(a) Proportional gain

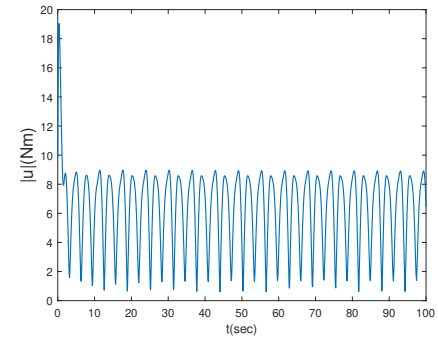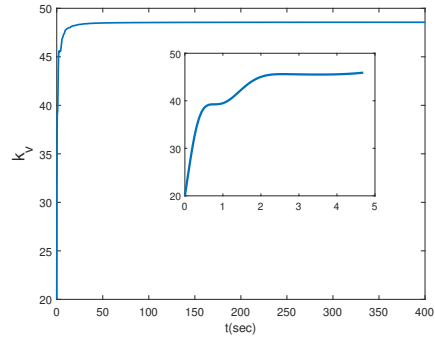(b) Derivative feedback gain
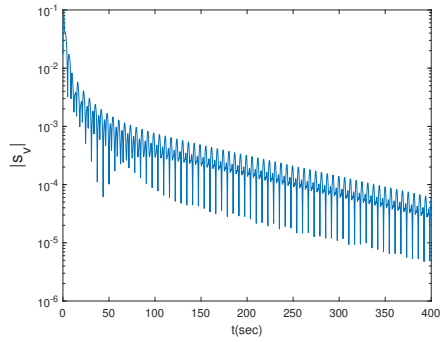
(c) Quaternion vector norms
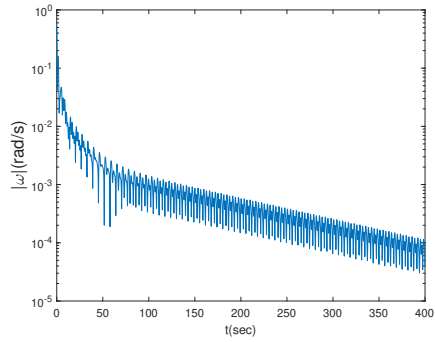
(d) Angular velocity error norm
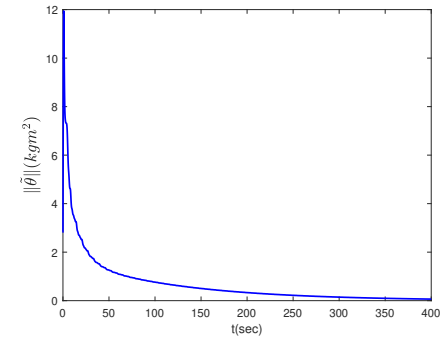
(e) Norm of inertia estimate
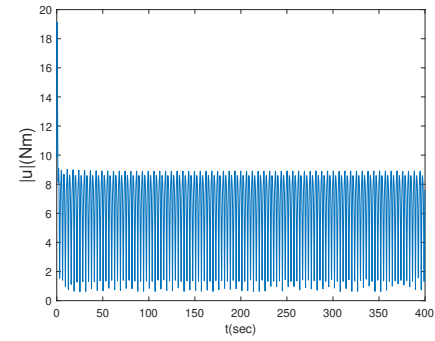
(f) Norm of the control torque

Figure 2.4: Closed-loop error trajectories resulting from application of the proposed adaptive controller for a 25% error in the initial inertia estimate, $k_p(0) = 50$ and $k_v(0) = 30$
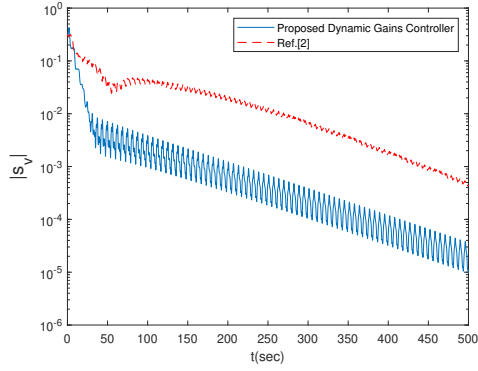
(a) Quaternion vector norm
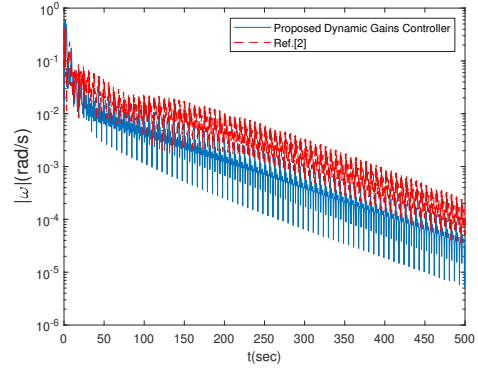
(b) Angular velocity error norm
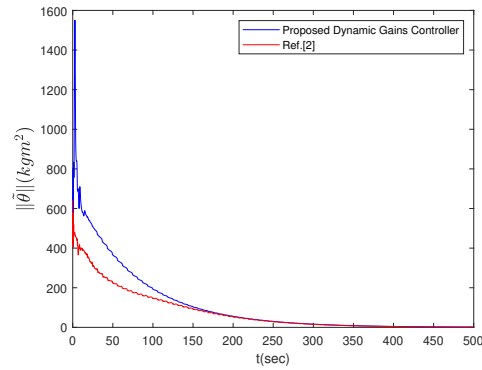
(c) Norm of inertia estimate

Figure 2.5: Comparison of the performance of the proposed controller ($k_p(0) = 500$, $k_v(0) = 300$) against Wen and Delgado [1] ($\bar{k}_p = 500$, $\bar{k}_v = 450$, $c = 0.01$)

[1] in this simulation but this can be improved by increasing the value of the learning rate $\mathbf{\Gamma}$.

2.5 Conclusions

A novel method for attitude tracking control for rigid spacecraft with inertia uncertainties was developed, which assumes no knowledge on the inertia matrix or its bounds. This was achieved using dynamic feedback gains while retaining the simple classical proportional differential control structure with feed-forward terms (PD+), a previously unknown result for the linear PD+ control law, made possible by a novel Lyapunov-like analysis and a projection scheme to lower limit the evolution of the proportional feedback gain. The proposed controller preserves the self-reduction property and achieves performance comparable to existing methods without requiring any additional information about the eigenvalues (bounds) upon the inertia matrix. Future work will focus on applying this novel idea of dynamic feedback gains for a wider class of system dynamics.

Chapter 3

Angular Velocity Estimation Using Rate-Integrating Gyro Measurements

Inertial navigation is a critical component of aerospace control systems as it is responsible for the calculation of position, velocity and orientation using measurements from Inertial Measurement Units (IMUs). These systems are usually comprised of accelerometers and gyroscopes and integrate forward in time the initial state of the vehicle by replacing dynamic models with IMU measurements. Inertial navigation systems have been used since the 1950s and were part of the Apollo missions on the Saturn V rockets, as well as the command module and the lunar module. In a strapdown inertial navigation system [22], the IMU is rigidly mounted on the vehicle. Strapdown gyroscopes have been used for many applications including spacecraft attitude estimation [23], underwater vehicle navigation [24], manned navigation systems [25] and robotic navigation [26].

One approach to attitude determination is to integrate Euler's equation using models of the torques applied to the vehicle. Alternatively, inertial navigation bypasses the need for these models by measuring angular velocity directly (referred to as model replacement mode [27]). This methodology is preferred when IMU information is more accurate than the available models of rotational dynamics and torques. Moreover, model replacement is computationally simpler and hence ideal for real-time onboard applications.

Rate Integrating Gyroscopes (RIGs) do not directly measure the angular rate but rather accumulate angular displacements by integrating the feedback required to null internal gyroscope motions. They provide measurements of the integrated rate and thus provide a direct measurement of neither the attitude state nor the angular velocity. They are preferred in spacecraft applications compared to conventional rate gyroscopes for their low noise due to degenerate mode operation and exceptional scale factor stability [28]. Modern RIGs use micro-electromechanical system devices [29].

Attitude controllers for aerospace systems typically require full state feedback, where the state consists of the attitude and angular rate signals. However, since rate integrating gyroscopes do not provide angular rate measurements, state feedback controllers require an observer to reconstruct the full state using the RIG measurements. Kalman filters have been used in the literature to estimate this full state [30][31], but require accurate characterization of the noise and do not provide any convergence guarantees. For gyroscopes systems that measure angular velocity directly, nonlinear observers for attitude

and gyro bias with exponential stability exist [32][33]. In many practical RIG applications the angular velocity is obtained from a numerical differentiator followed by a low pass filter to remove high frequency noise on the derivative of the RIG measurements. This method does not provide guarantees that the state provided by the differentiator converges to the true angular rates. Moreover in this context, the low pass filter is applied on the derivative of the measurements we receive from the RIG, which highly amplifies the noise in the measurements. This poses an extra challenging situation in distinguishing the signal from the noise as it passes through the low pass filter.

This work focuses on designing observers which use continuous measurements from an RIG and provides estimates for the angular rate states. We consider a rigid body governed by Euler rotational dynamics, the torque applied to the system is assumed to be known and the angular rotational rate is assumed to satisfy a known upper bound. We present two nonlinear observer designs, for the known inertia and adaptive cases. The observer dynamics are linear in the measurement term and involve a user chosen parameter that controls the convergence rate. The estimates are guaranteed to converge to the true values of the state exponentially fast when the inertia is known and at least asymptotically when adapting for inertia. The angular velocity estimates provided by this so called high gain observer can be used in controllers for stabilizing the system or tracking desired reference trajectories. To the best of our knowledge, no prior work exists in the literature on continuous time observers for RIG systems. In contrast to the results provided by a nu-

merical differentiator, this exponential convergence guarantee, or asymptotic convergence when adaptation is used for inertia uncertainties, is the primary advantage of using our observer over existing methods. RIGs are used for high precision applications because they provide the entire history of the angular velocity as its integrated value. The alternative of sampling the angular velocity at discrete times is typically less accurate as information on how the angular velocity varies in-between samples is lost. While we use continuous time RIG measurements here, discretizing the output of a continuous observer such as the one presented in this work will help in using this observer with discrete time computer systems, while preserving the theoretical guarantees presented for the observer and the inherent advantages of using RIGs [34].

Dabroom and Khalil [35] present different methods for converting continuous time high gain observers to a discrete time implementation and the bilinear transformation method was shown to have the lowest transient and steady state error when compared to other discretization methods. High gain observers used along with the bi-linear transformation were also shown to deal with measurement noises better than numerical differentiation methods. When dealing with measurement noise, which is commonly the case with IMUs, the parameters of the discretization method can be tuned according to the signal to noise ratio of the sensor, making high gain observers better than numerical differentiators at reducing state estimation errors [35]. The discrete time sampled data from the continuous output of high gain observers was also shown to be effective in closed loop performance when used as part of a control system

51

[36]. Thus, high gain observers like the one proposed in this chapter, especially when used with a well tuned discretization method, can provide guaranteed convergence of the estimates to the true states and also handle sensor measurement noise, especially low frequency time varying biases, better than typical numerical methods. An in-depth study of discretization methods and their effects are outside the scope of this work but interesting avenues for future research.

When IMUs are used in space applications, in the context of on-orbit assembly, repair and refilling missions, perfect knowledge of the inertia matrix is often not always available and therefore necessitates the use of adaptive observers that can deal with model parameter uncertainties. We present an adaptive nonlinear observer design, which provides estimates of the angular rate states while adapting for the inertia terms. Unlike the certainty equivalence adaptive methods, the design of this observer, inspired by the Immersion and Invariance (I & I) control method [37], includes two extra adaptation parameters which help compensate for the dynamics of the unmeasured terms. In the adaptive case, the rate of change of the torque applied is also assumed to be known as it is required in the parameter adaptation equations.

While the RIG measurements can be used directly to determine the attitude state, the proposed observer also generates an estimate of the attitude as part of its state for use within its update equations. These estimates can be discarded but need to be kept bounded. A Lyapunov-like analysis is used to prove that the attitude and angular velocity state estimates converge

to the true values as long as the initial states are within a Region Of Attraction (ROA), hence the result is semi-global. With adaptation, the inertia terms can be estimated to the true value asymptotically if persistence of excitation conditions are met. Further, the non-adaptive observer is shown to have exponential convergence, to be robust to uncertainties in the inertia matrix and the external torque, and its estimates converge to the true states within a residual set as long as the errors in inertia and torque are bounded. These results are demonstrated in numerical simulations.

Extending the observer to adapt for inertia uncertainties using conventional adaptive observer methods is not straightforward since the available measurements from the RIG are only of the angular displacement while the inertia matrix is only part of the dynamics involving the angular velocity. Methods inspired by Cho and Rajamani [38] require the measurement outputs to have a strictly positive definite transfer function to the unknown inertia parameters, which is not the case in this system as will be discussed in the sequel. Moreover, the measurement here is the integrated angular rate vector and hence Marino and Tomei's [39] method of linearizing the system on the basis of output injection and filtered transformations cannot be used, since it requires the output to be a real valued scalar or linear with respect to the unknown parameters. Observers for multi-output systems which are affine in the unmeasured states [40] can also not be used since the dynamics are not linear in the angular velocity states.

The formulation of two nonlinear observers, one for accurately known

inertia and the second with adaptation for inertia uncertainties, which use continuous time measurements of the integrated rate from an RIG and provide angular rate estimates which converge to the true values exponentially and asymptotically respectively, are the main contributions of this work.

3.1 Known Inertia

3.1.1 Dynamics

Consider Euler rotational dynamics for a system with inertia matrix $J = J^T > 0$ subject to bounded external torque $\boldsymbol{\tau}$ given by

$$J\dot{\boldsymbol{\omega}} = -\boldsymbol{\omega}^* J \boldsymbol{\omega} + \boldsymbol{\tau} \tag{3.1}$$

wherein $\boldsymbol{\omega}(t) \in \mathbb{R}^3$ has components in the body-fixed frame of reference. The skew-symmetric matrix $\boldsymbol{\omega}^*$ represents the vector cross product. We also assume:

- J is perfectly known

- $\boldsymbol{\tau}$ is perfectly determined

- $\boldsymbol{\omega} \in \mathbb{L}\infty$ is a bounded signal and we know $\omega_m \triangleq \sup_{t \geq 0} \|\boldsymbol{\omega}(t)\|$

The assumption that an upper bound ω_m is known is reasonable since any spacecraft is physically designed to only be able to rotate or tumble below a certain angular rate. The bound can be chosen beyond the design limits of the spacecraft.

3.1.2 Measurements

We have an RIG providing attitude measurements $\boldsymbol{\sigma}(t) \in \mathbb{R}^3$ which are the incremental accumulated values of the angular rate $\boldsymbol{\omega}$ such that:

$$\frac{d\boldsymbol{\sigma}}{dt} = \boldsymbol{\omega}(t) \tag{3.2}$$

where $\boldsymbol{\sigma}(t)$ is assumed to be measured perfectly.

3.1.3 Objective

Using perfect measurements of $\boldsymbol{\sigma}(t)$, the goal is to generate an estimate $\hat{\boldsymbol{\omega}}(t)$ of the true angular rate $\boldsymbol{\omega}(t)$ such that

$$\lim_{t \to \infty} \|\hat{\boldsymbol{\omega}}(t) - \boldsymbol{\omega}(t)\| = 0 \tag{3.3}$$

keeping all signals bounded.

3.1.4 Observer Design

The following observer design is proposed for estimating the angular rate:

$$\dot{\hat{\boldsymbol{\sigma}}} = \hat{\boldsymbol{\omega}} - k(\hat{\boldsymbol{\sigma}} - \boldsymbol{\sigma}) \quad \text{for some } k > 0 \tag{3.4}$$

$$J\dot{\hat{\boldsymbol{\omega}}} = -\hat{\boldsymbol{\omega}}^* J\hat{\boldsymbol{\omega}} + \boldsymbol{\tau} - k^2 J(\hat{\boldsymbol{\sigma}} - \boldsymbol{\sigma}) \tag{3.5}$$

We define the estimation errors

$$\boldsymbol{\sigma_e} = \hat{\boldsymbol{\sigma}} - \boldsymbol{\sigma} \tag{3.6}$$

$$\boldsymbol{\omega_e} = \hat{\boldsymbol{\omega}} - \boldsymbol{\omega} \tag{3.7}$$

55

Using these definitions in (3.4)-(3.5) gives

$$\dot{\boldsymbol{\sigma}}_e = \boldsymbol{\omega}_e - k\boldsymbol{\sigma}_e \tag{3.8}$$

$$J\dot{\boldsymbol{\omega}}_e = -(\hat{\boldsymbol{\omega}}^* J\hat{\boldsymbol{\omega}} - \boldsymbol{\omega}^* J\boldsymbol{\omega}) - k^2 J\boldsymbol{\sigma}_e \tag{3.9}$$

Expanding the terms within the parenthesis on the right-hand side of (3.9) gives

$$\hat{\boldsymbol{\omega}}^* J\hat{\boldsymbol{\omega}} - \boldsymbol{\omega}^* J\boldsymbol{\omega} = \boldsymbol{\omega}_e^* J\boldsymbol{\omega} + \boldsymbol{\omega}^* J\boldsymbol{\omega}_e + \boldsymbol{\omega}_e^* J\boldsymbol{\omega}_e \tag{3.10}$$

If we define $\boldsymbol{\Psi} \triangleq -[\boldsymbol{\omega}^* J\boldsymbol{\omega}_e + \boldsymbol{\omega}_e^* J\boldsymbol{\omega} + \boldsymbol{\omega}_e^* J\boldsymbol{\omega}_e]$, Eq. 3.9 can be rewritten as

$$\dot{\boldsymbol{\omega}}_e = -k^2 \boldsymbol{\sigma}_e + J^{-1}\boldsymbol{\Psi} \tag{3.11}$$

If we define the error states to be $\boldsymbol{\sigma}_e$ and $\boldsymbol{\omega}_e/k$, using (3.4) and (3.11), we have the dynamics for the error states as:

$$\begin{bmatrix} \dot{\boldsymbol{\sigma}}_e \\ \frac{\dot{\boldsymbol{\omega}}_e}{k} \end{bmatrix} = k \begin{bmatrix} -\mathbb{I}_{3\times3} & \mathbb{I}_{3\times3} \\ -\mathbb{I}_{3\times3} & \mathbb{O}_{3\times3} \end{bmatrix} \begin{bmatrix} \boldsymbol{\sigma}_e \\ \frac{\boldsymbol{\omega}_e}{k} \end{bmatrix} + \begin{bmatrix} \mathbb{O}_{3\times1} \\ \frac{J^{-1}}{k}\boldsymbol{\Psi} \end{bmatrix} \tag{3.12}$$

Renaming the states as

$$\begin{matrix} \boldsymbol{z}_1 = \boldsymbol{\sigma}_e \\ \boldsymbol{z}_2 = \frac{\boldsymbol{\omega}_e}{k} \end{matrix} \quad \Leftrightarrow \quad \boldsymbol{z} \triangleq \begin{bmatrix} \boldsymbol{z}_1 \\ \boldsymbol{z}_2 \end{bmatrix} \in \mathbb{R}^6 \tag{3.13}$$

allows us to express (3.12) as

$$\dot{\boldsymbol{z}} = k \begin{bmatrix} -\mathbb{I}_{3\times3} & \mathbb{I}_{3\times3} \\ -\mathbb{I}_{3\times3} & \mathbb{O}_{3\times3} \end{bmatrix} \boldsymbol{z} + \begin{bmatrix} \mathbb{O}_{3\times1} \\ \frac{J^{-1}}{k}\boldsymbol{\Psi} \end{bmatrix} \tag{3.14}$$

Since the inertia matrix is known, we can use its maximum and minimum eigenvalues to express

$$J_M = \lambda_{\max}(J) = \|J\| \tag{3.15}$$

$$J_m = \lambda_{\min}(J) = \frac{1}{\|J^{-1}\|} \tag{3.16}$$

Define

$$\alpha \triangleq (J_M / J_m) \tag{3.17}$$

Revisiting the $\boldsymbol{\Psi}$ term introduced after Eq. 3.10, we have

$$\boldsymbol{\Psi} = -\left(\boldsymbol{\omega}^* J \boldsymbol{\omega_e} + \boldsymbol{\omega_e^*} J \boldsymbol{\omega} + \boldsymbol{\omega_e^*} J \boldsymbol{\omega_e}\right) \tag{3.18}$$

$$-J^{-1}\boldsymbol{\Psi} = J^{-1}\left(\boldsymbol{\omega}^* J \boldsymbol{\omega_e} + \boldsymbol{\omega_e^*} J \boldsymbol{\omega}\right) + J^{-1}\boldsymbol{\omega_e^*} J \boldsymbol{\omega_e} \tag{3.19}$$

Consider the norm of the first term

$$\left\| J^{-1}\left(\boldsymbol{\omega}^* J \boldsymbol{\omega_e} + \boldsymbol{\omega_e^*} J \boldsymbol{\omega}\right) \right\| \leq \frac{2J_M}{J_m}\omega_m\|\boldsymbol{\omega_e}\| = 2\alpha\omega_m\|\boldsymbol{\omega_e}\| \tag{3.20}$$

Next,

$$\|J^{-1}\boldsymbol{\omega_e^*} J \boldsymbol{\omega_e}\| \leq \frac{1}{J_m}\sqrt{J_M(J_M - J_m)}\|\boldsymbol{\omega_e}\|^2 = k\sqrt{\alpha(\alpha-1)}\|\boldsymbol{z_2}\|^2 \tag{3.21}$$

Thus, making use of the bounds calculated in Eq. 3.20 and 3.21 and substituting them in Eq. 3.19 results in

$$\|J^{-1}\Psi\| \leq 2\alpha\omega_m\|\boldsymbol{\omega_e}\| + \sqrt{\alpha(\alpha-1)}\|\boldsymbol{\omega_e}\|^2 \tag{3.22}$$

which can be rewritten as

$$\|\frac{J^{-1}\Psi}{k}\| \leq 2\alpha\omega_m\|z_2\| + k\sqrt{\alpha(\alpha-1)}\|z_2\|^2 \tag{3.23}$$

3.1.5 Convergence Analysis

For stability and convergence analysis, consider a Lyapunov-like candidate function

$$
V = \frac{1}{k} \left[\boldsymbol{z}_1^T \boldsymbol{z}_1 + \frac{3}{2} \boldsymbol{z}_2^T \boldsymbol{z}_2 - \boldsymbol{z}_1^T \boldsymbol{z}_2 \right] = \begin{bmatrix} \boldsymbol{z}_1 & \boldsymbol{z}_2 \end{bmatrix} \underbrace{\frac{1}{k} \begin{bmatrix} \mathbb{I}_{3\times3} & -\frac{1}{2}\mathbb{I}_{3\times3} \\ -\frac{1}{2}\mathbb{I}_{3\times3} & \frac{3}{2}\mathbb{I}_{3\times3} \end{bmatrix}}_{P\in\mathbb{R}^{6\times6}} \begin{bmatrix} \boldsymbol{z}_1 \\ \boldsymbol{z}_2 \end{bmatrix}
$$

$$
= \begin{bmatrix} \boldsymbol{z}_1 & \boldsymbol{z}_2 \end{bmatrix} \left(\underbrace{\frac{1}{k} \begin{bmatrix} 1 & -\frac{1}{2} \\ -\frac{1}{2} & \frac{3}{2} \end{bmatrix}}_{R\in\mathbb{R}^{2\times2}} \otimes \mathbb{I}_{3\times3} \right) \begin{bmatrix} \boldsymbol{z}_1 \\ \boldsymbol{z}_2 \end{bmatrix}
$$

$$(3.24)$$

where $\otimes$ denotes the Kronecker product.

We know the maximum and minimum eigenvalues of P and R are equal: $\lambda_{\min}(P) = \lambda_{\min}(R)$ and $\|P\| = \lambda_{\max}(P) = \lambda_{\max}(R)$ which gives us

$$
\lambda_{\min}(P) = \frac{5 - \sqrt{5}}{4k} = c_1 \tag{3.25}
$$

and

$$
\lambda_{\max}(P) = \frac{5 + \sqrt{5}}{4k} = c_2 \tag{3.26}
$$

Thus, V defined in Eq. (3.24) satisfies

$$
c_1 \|\boldsymbol{z}\|^2 \leq V = \boldsymbol{z}^T P \boldsymbol{z} \leq c_2 \|\boldsymbol{z}\|^2 \tag{3.27}
$$

Next, taking the time derivative of V in Eq. (3.24), followed by substi-

tuting Eq. 3.14 and Eq. 3.19 results in

$$
\begin{aligned}
\dot{V} &= \frac{2}{k}\boldsymbol{z}_1^T\dot{\boldsymbol{z}}_1 + \frac{3}{k}\boldsymbol{z}_2^T\dot{\boldsymbol{z}}_2 - \frac{1}{k}\boldsymbol{z}_1^T\dot{\boldsymbol{z}}_2 - \frac{1}{k}\boldsymbol{z}_2^T\dot{\boldsymbol{z}}_1 \\
&= -\boldsymbol{z}_1^T\boldsymbol{z}_1 - \boldsymbol{z}_2^T\boldsymbol{z}_2 + \frac{3}{k}\boldsymbol{z}_2^T\frac{J^{-1}\boldsymbol{\Psi}}{k} - \frac{1}{k}\boldsymbol{z}_1^T\frac{J^{-1}\boldsymbol{\Psi}}{k} \\
&\leq -\|\boldsymbol{z}\|^2 + \frac{3}{k}\|\boldsymbol{z}_2\|\|\frac{J^{-1}\boldsymbol{\Psi}}{k}\| + \frac{1}{k}\|\boldsymbol{z}_1\|\|\frac{J^{-1}\boldsymbol{\Psi}}{k}\| \\
&\leq -\|\boldsymbol{z}\|^2 + \frac{4}{k}\|\boldsymbol{z}\|\|\frac{J^{-1}\boldsymbol{\Psi}}{k}\|
\end{aligned}
\tag{3.28}
$$

Next, using (3.20) and (3.21), we have

$$
\begin{aligned}
\dot{V} &\leq -\|\boldsymbol{z}\|^2 + \frac{4}{k}\|\boldsymbol{z}\|\left[2\alpha\omega_m\|\boldsymbol{z}\| + k\sqrt{\alpha(\alpha-1)}\|\boldsymbol{z}\|^2\right] \\
&= -\left(1 - \frac{8\alpha\omega_m}{k}\right)\|\boldsymbol{z}\|^2 + 4\sqrt{\alpha(\alpha-1)}\|\boldsymbol{z}\|^3
\end{aligned}
\tag{3.29}
$$

To ensure the coefficient of the $\|\boldsymbol{z}\|^2$ term is negative, we select k such that $1 - (8\alpha\omega_m)/k > 0$, i.e.,

$$
k > 8\alpha\omega_m
\tag{3.30}
$$

Thus, we have

$$
\begin{aligned}
\dot{V} &\leq -\left(1 - \frac{8\alpha\omega_m}{k}\right)\|\boldsymbol{z}\|^2 + 4\beta\|\boldsymbol{z}\|^3 \\
\dot{V} &\leq -\|\boldsymbol{z}\|^2\left[\left(1 - \frac{8\alpha\omega_m}{k}\right) - 4\beta\|\boldsymbol{z}\|\right] \\
&\triangleq -W(\boldsymbol{z})
\end{aligned}
\tag{3.31}
$$

where we introduce the notation $\beta = \sqrt{\alpha(\alpha-1)}$

Define a scalar function $\rho(k)$:

$$
\rho(k) \triangleq \frac{1}{4\beta}\left(1 - \frac{8\alpha\omega_m}{k}\right)\sqrt{\frac{c_1}{c_2}}
\tag{3.32}
$$

59

which after substituting the values of c_1 and c_2 respectively from (3.25) and (3.26) becomes

$$\rho(k) = \frac{1}{4\beta}\left(1 - \frac{8\alpha\omega_m}{k}\right)\sqrt{\frac{5 - \sqrt{5}}{5 + \sqrt{5}}} \tag{3.33}$$

Suppose we restrict initial conditions $\boldsymbol{z}(t_0)$ at time $t_0 = 0$, such that $\|\boldsymbol{z}(t_0)\| \leq \rho(k)$, then using Eq. 3.31,

$$
\begin{aligned}
W(\boldsymbol{z}(0)) &= \|\boldsymbol{z}(0)\|^2\left[\left(1 - \frac{8\alpha\omega_m}{k}\right) - 4\beta\|\boldsymbol{z}(0)\|\right] \\
&= 4\beta\|\boldsymbol{z}(0)\|^2\left[\frac{1}{4\beta}\left(1 - \frac{8\alpha\omega_m}{k}\right) - \|\boldsymbol{z}(0)\|\right] \\
&\geq 4\beta\|\boldsymbol{z}(0)\|^2\left[\rho(k)\sqrt{\frac{c_2}{c_1}} - \rho(k)\right] \\
&\geq 0
\end{aligned} \tag{3.34}
$$

since $c_2 > c_1$.

By definition of $W(\boldsymbol{z})$ in Eq. 3.31, we know that $\dot{V}(t) \leq 0$ whenever $W(\boldsymbol{z}(t)) \geq 0$. Thus, having a region of attraction $\|\boldsymbol{z}(0)\| \leq \rho(k)$ ensures $\dot{V}(t) \leq 0$ for all $t \geq 0$, that is, $V(t)$ is non-increasing with time. For more details on ROA, the reader is referred to Khalil [41], Chapter 8. Substituting this in (3.27) leads to

$$c_1\|\boldsymbol{z}(t)\|^2 \leq V(t) \leq V(0) \leq c_2\|\boldsymbol{z}(0)\|^2 \tag{3.35}$$

Thus,

$$\|\boldsymbol{z}(t)\| \leq \sqrt{\frac{c_2}{c_1}}\|\boldsymbol{z}(0)\| \tag{3.36}$$

Also, using the definition of $W(\boldsymbol{z})$ from (3.31),

$$W(\boldsymbol{z}(t)) = \|\boldsymbol{z}(t)\|^2 \left[\left(1 - \frac{8\alpha\omega_m}{k} \right) - 4\beta\|\boldsymbol{z}(t)\| \right]$$

$$\geq \|\boldsymbol{z}(t)\|^2 \left[\left(1 - \frac{8\alpha\omega_m}{k} \right) - 4\beta\sqrt{\frac{c_2}{c_1}}\|\boldsymbol{z}(0)\| \right]$$

Defining c_3 to be the terms inside the square brackets,

$$c_3 = \left(1 - \frac{8\alpha\omega_m}{k} \right) - 4\beta\sqrt{\frac{c_2}{c_1}}\|\boldsymbol{z}(0)\| \tag{3.37}$$

we have

$$-W(\boldsymbol{z}(t)) \leq -c_3\|\boldsymbol{z}(t)\|^2 \tag{3.38}$$

Thus we have $\dot{V}(t) \leq -W(\boldsymbol{z}(t)) \leq -c_3\|\boldsymbol{z}(t)\|^2$ or,

$$\dot{V}(t) \leq -\frac{c_3}{c_2}V(t)$$

$$V(t) \leq \exp\left(\frac{-c_3 t}{c_2} \right) V(0) \tag{3.39}$$

Using this result alongside the inequality from (3.27) results in

$$\|\boldsymbol{z}(t)\| \leq \sqrt{\frac{c_2}{c_1}} \exp\left(\frac{-c_3 t}{2c_2} \right) \|\boldsymbol{z}(0)\| \tag{3.40}$$

which proves exponential stability but is a local result for $\|\boldsymbol{z}(0)\| \leq \rho(k)$.

3.1.6 Discussion

For choosing the value of k, from Eq. 3.30 we have a lower bound $8\alpha\omega_m$. From (3.25) and (3.26) we know, as $k \to \infty$, both $c_1 \to 0$ and $c_2 \to 0$.

However, the ratio

$$\sqrt{\frac{c_1}{c_2}} = \sqrt{\frac{5 - \sqrt{5}}{5 + \sqrt{5}}} \tag{3.41}$$

is independent of k. Hence, the upper bound on the initial value of $\|\boldsymbol{z}(0)\|$ given by Eq.3.32, in the limit becomes

$$\lim_{k \to \infty} \rho(k) = \rho^* = \frac{1}{4\beta}\sqrt{\frac{c_1}{c_2}} = \frac{1}{4\beta}\sqrt{\frac{5 - \sqrt{5}}{5 + \sqrt{5}}} \tag{3.42}$$

Thus, the initial condition on the norm of the error states is upper bounded by ρ^* and also lower bounded due to the non-zero positive lower bound on k.

Note that local stability implies specifically our initial condition $\boldsymbol{z}(0) \in \mathbb{M}$ where

$$\mathbb{M} = \left\{ \boldsymbol{z} \in \mathbb{R}^6 \quad | \quad \|\boldsymbol{\sigma_e}(0)\|^2 + \frac{\|\boldsymbol{\omega_e}(0)\|^2}{k^2} \leq \rho^2(k) \right\} \tag{3.43}$$

which is the region of attraction. $\boldsymbol{\sigma_e}(0)$ is usually not a restriction because, we can always select $\hat{\boldsymbol{\sigma}}(0) = \boldsymbol{\sigma}(0) \Leftrightarrow \boldsymbol{\sigma_e}(0) = 0$

On the other hand, $\boldsymbol{\omega_e}(0)$ can be arbitrarily large. However, we can always choose large enough k such that irrespective of $\boldsymbol{\omega_e}(t)$, $\boldsymbol{z}(0) \in \mathbb{M}$. In this context, it is crucial that irrespective of how much we increase k, the largest region of attraction ρ^* in Eq. 3.42 above is a finite constant. Hence, the result is semi-global.

3.1.7   Effect of measurement noise

In the presence of measurement noise, let us consider the measurement to evolve as

$$\dot{\boldsymbol{\sigma}}(t) = \boldsymbol{\omega}(t) + \boldsymbol{n}(t)$$

where $\boldsymbol{n}(t)$ is a zero mean white random process, known as angular random walk (ARW), with power spectral density $\boldsymbol{S}$ which has units of rad^2/s. With the addition of measurement noise, the error dynamics of Eq.3.12 become

$$\begin{bmatrix} \dot{\boldsymbol{\sigma}}_e \\ \dot{\boldsymbol{\omega}}_e \end{bmatrix} = \begin{bmatrix} -k\mathbb{I}_{3\times3} & \mathbb{I}_{3\times3} \\ -k^2\mathbb{I}_{3\times3} & \mathbb{O}_{3\times3} \end{bmatrix} \begin{bmatrix} \boldsymbol{\sigma}_e \\ \boldsymbol{\omega}_e \end{bmatrix} + \begin{bmatrix} \mathbb{O}_{3\times1} \\ J^{-1}\boldsymbol{\Psi} \end{bmatrix} + \begin{bmatrix} \boldsymbol{n} \\ \mathbb{O}_{3\times1} \end{bmatrix} \tag{3.44}$$

To analyze the error evolution, we will linearize the above equation about $\boldsymbol{\sigma}_e(t)$ to obtain

$$\begin{bmatrix} \dot{\boldsymbol{\sigma}}_e \\ \dot{\boldsymbol{\omega}}_e \end{bmatrix} \cong \begin{bmatrix} -k\mathbb{I}_{3\times3} & \mathbb{I}_{3\times3} \\ -k^2\mathbb{I}_{3\times3} & \boldsymbol{J}^{-1}\left[(\boldsymbol{J}\hat{\boldsymbol{\omega}}(t))^* - \hat{\boldsymbol{\omega}}(t)^*\boldsymbol{J}\right] \end{bmatrix} \begin{bmatrix} \boldsymbol{\sigma}_e \\ \boldsymbol{\omega}_e \end{bmatrix} + \begin{bmatrix} \boldsymbol{n} \\ \mathbb{O}_{3\times1} \end{bmatrix} \tag{3.45}$$

Let us start by considering the case when $\hat{\boldsymbol{\omega}}(t)$ is constant, so that

$$\begin{bmatrix} \dot{\boldsymbol{\sigma}}_e \\ \dot{\boldsymbol{\omega}}_e \end{bmatrix} \cong \begin{bmatrix} -k\mathbb{I}_{3\times3} & \mathbb{I}_{3\times3} \\ -k^2\mathbb{I}_{3\times3} & \boldsymbol{C} \end{bmatrix} \begin{bmatrix} \boldsymbol{\sigma}_e \\ \boldsymbol{\omega}_e \end{bmatrix} + \begin{bmatrix} \boldsymbol{n} \\ \mathbb{O}_{3\times1} \end{bmatrix} = \boldsymbol{A}\begin{bmatrix} \boldsymbol{\sigma}_e \\ \boldsymbol{\omega}_e \end{bmatrix} + \begin{bmatrix} \boldsymbol{n} \\ \mathbb{O}_{3\times1} \end{bmatrix} \tag{3.46}$$

where $\boldsymbol{C} \in \mathbb{R}_{3\times3}$ is a constant matrix since we have assumed $\hat{\boldsymbol{\omega}}$ to be constant. The corresponding estimation error covariance evolves as

$$\dot{\boldsymbol{P}}(t) = \boldsymbol{A}\boldsymbol{P}(t) + \boldsymbol{P}(t)\boldsymbol{A}^T + \boldsymbol{Q} \tag{3.47}$$

where

$$\boldsymbol{P} = \begin{bmatrix} \boldsymbol{P}_{\sigma\sigma} & \boldsymbol{P}_{\sigma\omega} \\ \boldsymbol{P}_{\omega\sigma} & \boldsymbol{P}_{\omega\omega} \end{bmatrix} \tag{3.48}$$

and

$$Q = \begin{bmatrix} S & 0 \\ 0 & 0 \end{bmatrix} \tag{3.49}$$

The steady state estimation error covariance is given by $\dot{P}(t) = \mathbb{O}_{6\times 6}$ resulting

in

$$\mathbb{O}_{3\times 3} = -2k P_{\sigma\sigma} + P_{\sigma\omega} + P_{\omega\sigma} + S \tag{3.50}$$

$$\mathbb{O}_{3\times 3} = -k P_{\sigma\omega} + C P_{\sigma\omega} + P_{\omega\omega} - k^2 P_{\sigma\sigma} \tag{3.51}$$

$$\mathbb{O}_{3\times 3} = -k^2 P_{\sigma\omega} - k^2 P_{\omega\sigma} + 2C P_{\omega\omega} \tag{3.52}$$

Considering $P_{\sigma\omega} = P_{\omega\sigma}$ and solving the above system of equations,

$$P_{\omega\sigma} = \frac{k}{2} C(C - k\mathbb{I}_{3\times 3})^{-2} S \tag{3.53}$$

$$P_{\sigma\sigma} = \frac{C}{2}(C - k\mathbb{I}_{3\times 3})^{-2} S + \frac{S}{2k} \tag{3.54}$$

$$P_{\omega\omega} = \frac{k^3}{2}(C - k\mathbb{I}_{3\times 3})^{-2} S \tag{3.55}$$

To gain valuable insights on the estimation performance of the observer, let us consider the case when $\hat{\omega}$ is negligible. The steady state covariances in this case become

$$P_{\omega\sigma} = \mathbb{O}_{3\times 3} \qquad P_{\sigma\sigma} = \frac{1}{2k} S \qquad P_{\omega\omega} = \frac{k}{2} S$$

So the steady-state estimation error covariance of the angular velocity observer is $P_{\omega\omega} = kS/2$. The parameter k should be chosen as a compromise between fast response (large values) and noise attenuation (small values).

Let us consider the alternative to using our proposed observer, which is to use a numerical differentiator on the RIG measurements and then apply

a low pass filter to obtain angular velocity estimates. For a sampling time period of Δt and measurements $\boldsymbol{\sigma}(t)$ at time t, a crude differentiator can be defined as:

$$\boldsymbol{\omega}_{nd}(t_k) = \frac{\boldsymbol{\sigma}(t_k) - \boldsymbol{\sigma}(t_{k-1})}{\Delta t} \tag{3.56}$$

Using the mean value theorem, $\boldsymbol{\sigma}(t_k)$ can be approximated as

$$\boldsymbol{\sigma}(t_k) = \boldsymbol{\sigma}(t_{k-1}) + \boldsymbol{\omega}(t_{k-1}^*)\Delta t + \Delta\boldsymbol{n} \tag{3.57}$$

where $t_{k-1} \leq t_{k-1}^* \leq t_k$ and $\Delta\boldsymbol{n}$ is the integrated ARW over the sampling time Δt and has covariance matrix $\boldsymbol{S}\Delta t$.

Substituting (3.57) into (3.56)

$$\boldsymbol{\omega}_{nd}(t_k) = \boldsymbol{\omega}(t_{k-1}^*) + \boldsymbol{w}(t_{k-1}) \tag{3.58}$$

The numerical differentiation introduces a delay $\Delta t_{k-1}^* = t_k - t_{k-1}^*$ and a noise $\boldsymbol{w}(t_{k-1}) = \Delta n/\Delta t$. The noise has covariance matrix given by $\boldsymbol{S}/\Delta t$, which means small discretization steps result in very noisy estimates.

The noisy estimates obtained from numerical differentiation can be improved with a low pass filter:

$$\boldsymbol{\omega}_{lp}(t_k) = k_{lp}\boldsymbol{\omega}_{lp}(t_{k-1}) + (1 - k_{lp})\boldsymbol{\omega}_{nd}(t_k) \tag{3.59}$$

The error dynamics of $\boldsymbol{\omega}_{elp}(t_k) = \boldsymbol{\omega}(t_k) - \boldsymbol{\omega}_{lp}(t_k)$ is given by

$$\begin{aligned}
\boldsymbol{\omega}_{elp}(t_k) &= \boldsymbol{\omega}(t_k) - k_{lp}\boldsymbol{\omega}_{lp}(t_{k-1}) - (1 - k_{lp})\boldsymbol{\omega}_{nd}(t_k) \\
&= \boldsymbol{\omega}(t_k) - k_{lp}\boldsymbol{\omega}_{lp}(t_{k-1}) - (1 - k_{lp})\big(\boldsymbol{\omega}(t_{k-1}^*) + \boldsymbol{w}(t_{k-1})\big) \\
&= \big(\boldsymbol{\omega}(t_k) - \boldsymbol{\omega}(t_{k-1}^*)\big) + k_{lp}\big(\boldsymbol{\omega}(t_{k-1}^*) - \boldsymbol{\omega}_{lp}(t_{k-1})\big) - (1 - k_{lp})\boldsymbol{w}(t_{k-1})
\end{aligned} \tag{3.60}$$

Adding and subtracting $k_{lp}\boldsymbol{\omega} t_{k-1}$ we obtain, after some reshuffling

$$\boldsymbol{\omega}_{elp}(t_k) = \big(\boldsymbol{\omega}(t_k) - \boldsymbol{\omega}(t_{k-1}^*)\big) + k_{lp}\big(\boldsymbol{\omega}(t_{k-1}^*) - \boldsymbol{\omega}(t_{k-1})\big)$$
$$+ k_{lp}\boldsymbol{\omega}_{elp}(t_{k-1}) - (1 - k_{lp})\boldsymbol{w}(t_{k-1}) \tag{3.61}$$

The term $\big(\boldsymbol{\omega}(t_k) - \boldsymbol{\omega}(t_{k-1}^*)\big)$ is the latency introduced by numerical differenti-ation while the term $k_{lp}\big(\boldsymbol{\omega}(t_{k-1}^*) - \boldsymbol{\omega}(t_{k-1})\big)$ is additional latency added by the filtering process. For the filter to be stable it is required that $0 \le k_{lp} < 1$. Once again if we consider a static system and ignore the latencies, the noise-induced steady-state estimation error is given by:

$$\boldsymbol{P}_{\omega_{lp}} = \frac{(1 - k_{lp})^2}{1 - k_{lp}^2}\boldsymbol{S}/\Delta t = \frac{1 - k_{lp}}{1 + k_{lp}}\boldsymbol{S}/\Delta t \tag{3.62}$$

In a static system as assumed above, where the latency is not considered, the low pass filter can be averaged over time to have no noise in the output. However, in any dynamic system with non-zero velocity, a value of k_{lp} very close to one will reduce the noise but will add the most latency and also have a slow error decay response. Conversely, a value of k_{lp} close to zero represents no filtering at all and will have no noise attenuation. The sampling time period Δt tends to be small and thus the steady state value of the noise response is inflated by faster sampling of the RIG measurements. The response of our observer in Eq. 3.56 on the other hand is not impacted by the sampling rate and will thus have a better noise response for the same values of latency. A practical discussion of the effect of noise is presented in the simulations section.

3.1.8 Convergence Rate

In (3.40), $(-c_3/2c_2)$ is the rate of convergence. Note that

$$c_3 = \left(1 - \frac{8\alpha\omega_m}{k}\right) - 4\beta\sqrt{\frac{c_2}{c_1}}\|\boldsymbol{z}(0)\| \tag{3.63}$$

Thus, as $k \to \infty$, $c_3 \to c_3^*$ where

$$c_3^* = 1 - 4\beta\sqrt{\frac{5 + \sqrt{5}}{5 - \sqrt{5}}}\|\boldsymbol{z}(0)\| \tag{3.64}$$

which is independent of k. Also recall that $c_2 \to 0$ as $k \to \infty$. Thus, the rate of convergence $(c_3/2c_2) \to \infty$ as $k \to \infty$. Thus selecting large k implies faster convergence.

3.2 Robustness Analysis

We consider the robustness properties of the non-adaptive observer from Eqs. 3.4 and 3.5 in two different scenarios:

- The external torque $\boldsymbol{\tau}$ is unavailable but is bounded and an upper bound is known i.e., $\boldsymbol{\tau} \in \mathbb{L}_\infty$ and there exists some finite $\tau_M = \sup_{t \geq 0}\|\boldsymbol{\tau}(t)\|$. Can the observer be ensured to converge to a residual set?

- The inertia matrix J is inaccurately modelled as $\bar{J} = \bar{J}^T > 0$ (nominal inertia) and thus, there is an inertia error $(J - \bar{J})$? Can the observer errors be bounded in this setting?

We provide positive answers to both these cases in the sequel.

67

3.2.1 Unknown Torque

We assume some bounded unknown external torque $\boldsymbol{\tau}$ acting upon the spacecraft. The observer from Eq. 3.4 and Eq.3.5 is modified to:

$$\dot{\hat{\boldsymbol{\sigma}}} = \hat{\boldsymbol{\omega}} - k(\hat{\boldsymbol{\sigma}} - \boldsymbol{\sigma}) \tag{3.65}$$

$$J\dot{\hat{\boldsymbol{\omega}}} = -\hat{\boldsymbol{\omega}}^* J\hat{\boldsymbol{\omega}} - k^2 J(\hat{\boldsymbol{\sigma}} - \boldsymbol{\sigma}) \tag{3.66}$$

This leads to the error dynamics Eq.3.12 being modified to

$$\dot{\boldsymbol{\sigma}}_e = -k\boldsymbol{\sigma}_e + k\left(\frac{\boldsymbol{\omega}_e}{k}\right) \tag{3.67}$$

$$\frac{\dot{\boldsymbol{\omega}}_e}{k} = -k\boldsymbol{\sigma}_e + \frac{J^{-1}}{k}\boldsymbol{\Psi} - \frac{J^{-1}}{k}\boldsymbol{\tau} \tag{3.68}$$

leading to

$$\dot{\boldsymbol{z}} = k\begin{bmatrix} -\mathbb{I} & \mathbb{I} \\ -\mathbb{I} & 0 \end{bmatrix}\boldsymbol{z} + \begin{bmatrix} 0 \\ \frac{J^{-1}}{k}\boldsymbol{\Psi} \end{bmatrix} + \begin{bmatrix} 0 \\ -\frac{J^{-1}}{k}\boldsymbol{\tau} \end{bmatrix} \tag{3.69}$$

where the last term is defined as the disturbance

$$\boldsymbol{d} \triangleq \begin{bmatrix} 0 \\ -\frac{J^{-1}}{k}\boldsymbol{\tau} \end{bmatrix} \tag{3.70}$$

For the case with known torque ($\boldsymbol{d} = 0$), we already have from Eq. 3.38, a Lyapunov function such that

$$c_1\|\boldsymbol{z}\|^2 \leq V(\boldsymbol{z}) \leq c_2\|\boldsymbol{z}\|^2 \tag{3.71}$$

$$\dot{V} \triangleq \left(\frac{\partial V}{\partial z}\right)^T \dot{\boldsymbol{z}} \leq -c_3\|\boldsymbol{z}\|^2 \tag{3.72}$$

where the constants c_1, c_2, and c_3 are defined in Eqs.3.25, 3.26 and 3.37 respectively. Also recall from Eq.3.24

$$V(\boldsymbol{z}) = \frac{1}{k}\left(\boldsymbol{z}_1^T\boldsymbol{z}_1 + \frac{3}{2}\boldsymbol{z}_2^T\boldsymbol{z}_2 - \boldsymbol{z}_1^T\boldsymbol{z}_2\right) = \boldsymbol{z}^T P\boldsymbol{z} \tag{3.73}$$

68

Thus, $\frac{\partial V}{\partial z} = 2P\boldsymbol{z}$

$$\Leftrightarrow \|\frac{\partial V}{\partial z}\| \leq 2\lambda_{\max}(P)\|\boldsymbol{z}\| = 2c_2\|\boldsymbol{z}\| \tag{3.74}$$

since $\|P\| = \lambda_{\max}(P) = c_2 = (5 + \sqrt{5})/4k$.

From Eq.3.70,

$$\|\boldsymbol{d}\| \leq \frac{\tau_m}{kJ_m} \tag{3.75}$$

Based on the value of $\rho(k)$, let us select some $\zeta \in (0, 1)$ which will make the following inequality true:

$$\frac{\tau_m}{kJ_m} < \frac{c_3}{2c_2}\sqrt{\frac{c_1}{c_2}}\zeta\rho(k) \tag{3.76}$$

this implies that there exists k sufficiently large such that

$$\tau_m < \frac{c_3}{2c_2}\sqrt{\frac{c_1}{c_2}}\zeta kJ_m\rho(k) \tag{3.77}$$

Then using Lemma 9.2 from Khalil [41], for all $\|\boldsymbol{z}(0)\| < \sqrt{c_1/c_2}\rho(k)$, we have

$$\|\boldsymbol{z}(t)\| \leq \sqrt{\frac{c_2}{c_1}}\exp\left(-\gamma(t)\right)\|\boldsymbol{z}(0)\| \quad \forall\, 0 \leq t \leq T \tag{3.78}$$

and

$$\|\boldsymbol{z}(t)\| \leq b \text{ for } t \geq T \tag{3.79}$$

which is a residual set and a uniform ultimate bound for some finite $T > 0$, where

$$\gamma = \frac{(1 - \zeta)c_3}{2c_2} \tag{3.80}$$

and

$$b = \frac{2c_2}{c_3}\sqrt{\frac{c_2}{c_1}}\frac{\tau_m}{J_m k\zeta} \tag{3.81}$$

69

note that $b \to 0$ as $k \to \infty$. The choice of ζ affects both the rate of convergence as well as the size of the residual set b. If the objective is to have a smaller residual set, $\zeta \in (0, 1)$ can be chosen to be the largest value that still satisfies Eq.3.76.

3.2.2 Inaccurate Inertia Model

If the inertia matrix J is poorly modeled, a nominal inertia $\bar{\boldsymbol{J}}$ is adopted with maximum and minimum eigenvalues $\bar{J}_M$ and $\bar{J}_m$ respectively. We once again modify the observer from Eq.3.4 and Eq.3.5 to be:

$$\dot{\hat{\boldsymbol{\sigma}}} = \hat{\boldsymbol{\omega}} - k(\hat{\boldsymbol{\sigma}} - \boldsymbol{\sigma}) \tag{3.82}$$

$$\dot{\hat{\boldsymbol{\omega}}} = -k^2(\hat{\boldsymbol{\sigma}} - \boldsymbol{\sigma}) - \bar{J}^{-1}\hat{\boldsymbol{\omega}}^*\bar{J}\hat{\boldsymbol{\omega}} + \bar{J}^{-1}\boldsymbol{\tau} \tag{3.83}$$

such that the disturbance term in Eq. 3.70 can be modified as follows

$$\bar{\boldsymbol{d}} = \begin{bmatrix} 0 \\ -\frac{1}{k}(\bar{J}^{-1}\boldsymbol{\omega}^*\bar{J}\boldsymbol{\omega} - J^{-1}\boldsymbol{\omega}^*J\boldsymbol{\omega}) + (\bar{J}^{-1} - J^{-1})\boldsymbol{\tau}) \end{bmatrix} \tag{3.84}$$

The nominal system, i.e., with $\bar{\boldsymbol{d}} = 0$, provides us with the same behavior as the unknown torque case above, hence (3.78) and (3.79) hold with the convergence rate in (3.80). However, the modified ratio of eigenvalues of the inertia matrix, α is replaced by $\bar{\alpha} = \bar{J}_M/\bar{J}_m$ and the residual set to which the norm of the states converges to is now:

$$b = \frac{2c_2}{c_3}\sqrt{\frac{c_2}{c_1}}\frac{1}{J_m\bar{J}_m k\zeta}\left[\tau_m(\bar{J}_m + J_m) + \omega_m^2(J_M\bar{J}_m + \bar{J}_M J_m)\right] \tag{3.85}$$

This proves that the proposed observer is robust to inaccuracies in the inertia matrix and unknown external torques, with the angular velocity estimates always converging to a local residual region surrounding the true value of the state. However, this still only guarantees convergence to a residual set, which will be compared to the performance of the adaptive controller in the simulations section.

3.3   Adaptive Observer

In scenarios when the knowledge of the inertia is poorly characterized such that the robust performance of the non-adaptive observer is still unsatisfactory, we propose an adaptive observer which adapts for the inertia terms. The construction of this observer is described in this section.

3.3.1   Dynamics and Measurement

Rearranging the dynamics in Eq.3.1,

$$\dot{\boldsymbol{\omega}} = -J^{-1}\boldsymbol{\omega}^*J\boldsymbol{\omega} + J^{-1}\boldsymbol{\tau}$$

$$= \Lambda(\boldsymbol{\omega})\boldsymbol{\theta}^* + W(\boldsymbol{\tau})\boldsymbol{\phi}^* \tag{3.86}$$

where $\Lambda : \mathbb{R}^3 \to \mathbb{R}^{3\times 18}$ and $W : \mathbb{R}^3 \to \mathbb{R}^{3\times 6}$ are regressor matrices which are purely functions of the angular rate and torque respectively, $\boldsymbol{\theta}^* \in \mathbb{R}^{18\times 1}$ and $\boldsymbol{\phi}^* \in \mathbb{R}^{6\times 1}$ are vectorized versions of functions of the inertia matrix J terms. The separation of variables to obtain these regressor matrices is detailed in Appendix B. Apart from the same assumptions on $\boldsymbol{\omega}$ and $\boldsymbol{\tau}$ as for the non-

adaptive observer, we additionally assume $\dot{\boldsymbol{\tau}}$ is perfectly determined. Moreover we assume that some bounds on the maximum and minimum eigenvalues of the inertia matrix are known, which can be highly conservative if the characteristics of J are highly undefined. The measurements available are the same as the known inertia case, following Eq.3.2.

3.3.2 Objective

The goal is to generate an estimate $\hat{\boldsymbol{\omega}}(t)$ of the true angular rate $\boldsymbol{\omega}(t)$ such that

$$\lim_{t \to \infty} \|\hat{\boldsymbol{\omega}}(t) - \boldsymbol{\omega}(t)\| = 0 \tag{3.87}$$

without knowledge of the terms of the inertia matrix J and hence without $\boldsymbol{\theta}^*$ and $\boldsymbol{\phi}^*$, keeping all signals bounded.

3.3.3 Observer Design

The following observer design is proposed for estimating the angular rate:

$$\dot{\hat{\boldsymbol{\sigma}}} = \hat{\boldsymbol{\omega}} - k(\hat{\boldsymbol{\sigma}} - \boldsymbol{\sigma}) \quad \text{for some } k > 0 \tag{3.88}$$

$$\dot{\hat{\boldsymbol{\omega}}} = \Lambda(\hat{\boldsymbol{\omega}})(\hat{\boldsymbol{\theta}} + \boldsymbol{\beta}_\theta) + W(\boldsymbol{\tau})(\hat{\boldsymbol{\phi}} + \boldsymbol{\beta}_\phi) - k^2(\hat{\boldsymbol{\sigma}} - \boldsymbol{\sigma}) \tag{3.89}$$

where $\hat{\boldsymbol{\theta}}$, $\hat{\boldsymbol{\phi}}$, $\boldsymbol{\beta}_\theta$ and $\boldsymbol{\beta}_\phi$ will be defined later. This observer is unique due to the availability of an extra design parameter choice in the form of $\boldsymbol{\beta}_\theta$ and $\boldsymbol{\beta}_\phi$, similar to Immersion and Invariance (I & I) methods [37]. However unlike the I & I method, in this paper, we do not need to enforce the manifold attractivity

condition. As mentioned in the introduction, the linearized transfer function from the measurement $\boldsymbol{\sigma}$ to the unknown parameters $\boldsymbol{\theta}^*$ and $\boldsymbol{\phi}^*$ has two poles at the origin, implying that the transfer function is not strictly positive definite, leaving our problem incompatible with the method suggested by Cho and Rajamani [38].

Using the same definition of $\boldsymbol{z} = [\boldsymbol{z}_1, \boldsymbol{z}_2]^T$ from Eq.3.13, gives us the error dynamics:

$$\dot{\boldsymbol{z}} = k \begin{bmatrix} -\mathbb{I}_{3\times3} & \mathbb{I}_{3\times3} \\ -\mathbb{I}_{3\times3} & \mathbb{O}_{3\times3} \end{bmatrix} \boldsymbol{z} + \frac{1}{k} \begin{bmatrix} \mathbb{O}_{3\times1} \\ \Lambda(\hat{\boldsymbol{\omega}})(\hat{\boldsymbol{\theta}} + \boldsymbol{\beta_\theta}) - \Lambda(\boldsymbol{\omega})\boldsymbol{\theta}^* + W(\boldsymbol{\tau})(\hat{\boldsymbol{\phi}} + \boldsymbol{\beta_\phi} - \boldsymbol{\phi}^*) \end{bmatrix} \tag{3.90}$$

The quantity $(\hat{\boldsymbol{\phi}} + \boldsymbol{\beta_\phi} - \boldsymbol{\phi}^*)$ takes the physical meaning of the parameter estimation error. Consider the Lyapunov-like candidate function

$$V = \frac{1}{k} \left[\boldsymbol{z}_1^T \boldsymbol{z}_1 + \frac{3}{2} \boldsymbol{z}_2^T \boldsymbol{z}_2 - \boldsymbol{z}_1^T \boldsymbol{z}_2 \right] + \frac{1}{2\gamma_1 k^2} \|\hat{\boldsymbol{\theta}} + \boldsymbol{\beta_\theta} - \boldsymbol{\theta}^*\|^2 + \frac{1}{2\gamma_2 k^2} \|\hat{\boldsymbol{\phi}} + \boldsymbol{\beta_\phi} - \boldsymbol{\phi}^*\|^2 \tag{3.91}$$

For the inertia terms, let us define error states

$$\boldsymbol{z}_\theta = \frac{\hat{\boldsymbol{\theta}} + \boldsymbol{\beta_\theta} - \boldsymbol{\theta}^*}{k} \tag{3.92}$$

$$\boldsymbol{z}_\phi = \frac{\hat{\boldsymbol{\phi}} + \boldsymbol{\beta_\phi} - \boldsymbol{\phi}^*}{k} \tag{3.93}$$

and combine these with $\boldsymbol{z}$ to form the concatenated state

$$\boldsymbol{Z} = \begin{bmatrix} \boldsymbol{\sigma}_e^T & \dfrac{\boldsymbol{\omega}_e^T}{k} & \boldsymbol{z}_\theta^T & \boldsymbol{z}_\phi^T \end{bmatrix}^T = \begin{bmatrix} \boldsymbol{z}^T & \boldsymbol{z}_\theta^T & \boldsymbol{z}_\phi^T \end{bmatrix}^T \tag{3.94}$$

Using the constants c_1 and c_2 from Eqs. 3.25 and 3.26 respectively, we

73

can bound the function in Eq.3.91 at any time t as follows:

$$c_1 \|z(t)\|^2 \leq V(t) \leq c_2 \|z(t)\|^2 + \frac{1}{\gamma_1} \|z_\theta(t)\|^2 + \frac{1}{\gamma_2} \|z_\phi(t)\|^2 \tag{3.95}$$

The derivative of Eq.3.91 can be simplified to

$$
\begin{aligned}
\dot{V} = & -\|z_1\|^2 - \|z_2\|^2 + \frac{1}{k^2}(3z_2 - z_1)^T \left[\Lambda(\hat{\omega}) - \Lambda(\omega) \right] \boldsymbol{\theta}^* \\
& + \frac{1}{k^2}(3z_2 - z_1)^T \left[\Lambda(\hat{\omega})(\hat{\boldsymbol{\theta}} + \boldsymbol{\beta}_\theta - \boldsymbol{\theta}^*) + W(\boldsymbol{\tau})(\hat{\boldsymbol{\phi}} + \boldsymbol{\beta}_\phi - \boldsymbol{\phi}^*) \right] \\
& + \frac{1}{\gamma_1 k^2}(\hat{\boldsymbol{\theta}} + \boldsymbol{\beta}_\theta - \boldsymbol{\theta}^*)^T (\dot{\hat{\boldsymbol{\theta}}} + \dot{\boldsymbol{\beta}}_\theta) + \frac{1}{\gamma_2 k^2}(\hat{\boldsymbol{\phi}} + \boldsymbol{\beta}_\phi - \boldsymbol{\phi}^*)^T (\dot{\hat{\boldsymbol{\phi}}} + \dot{\boldsymbol{\beta}}_\phi) \tag{3.96}
\end{aligned}
$$

The first three terms of this equation do not involve the inertia estimate error and can follow the same procedure as the non-adaptive case. Thus, if we manage to make the adaptation terms equal zero, we can use the Barbalat's lemma [41] to prove asymptotic convergence to zero of the error states. However, if we did not have the choice of the control knobs $\boldsymbol{\beta}_\theta \in \mathbb{R}^{18 \times 1}$ and $\boldsymbol{\beta}_\phi \in \mathbb{R}^{6 \times 1}$, the update law $\dot{\hat{\boldsymbol{\theta}}}$ would have to involve z_2 which is not an available error state, only z_1 is available. This is what necessitates the inclusion of these control knobs we shall now define as:

$$\boldsymbol{\beta}_\theta = \frac{-3\gamma_1}{k} \Lambda(\hat{\omega})^T z_1 \tag{3.97}$$

$$\boldsymbol{\beta}_\phi = \frac{-3\gamma_2}{k} W(\boldsymbol{\tau})^T z_1 \tag{3.98}$$

The derivatives of these terms are:

$$\dot{\boldsymbol{\beta}}_\theta = 3\gamma_1 \Lambda(\hat{\omega})^T z_1 - 3\gamma_1 k^2 \Lambda(\hat{\omega})^T z_2 - \frac{3\gamma_1}{k} \left(\frac{\partial \Lambda}{\partial \hat{\omega}} \dot{\hat{\omega}} \right)^T z_1 \tag{3.99}$$

$$\dot{\boldsymbol{\beta}}_\phi = 3\gamma_2 W(\boldsymbol{\tau})^T \boldsymbol{z}_1 - 3\gamma_2 W(\boldsymbol{\tau})^T \boldsymbol{z}_2 - \frac{3\gamma_1}{k}\left(\frac{\partial W}{\partial \tau}\dot{\boldsymbol{\tau}}\right)^T \boldsymbol{z}_1 \qquad (3.100)$$

The details of the partial derivatives are discussed in Appendix B.

Substituting these derivatives back into Eq.3.96, the $\boldsymbol{z}_2$ term cancels out and for the rest of the inertia error terms, with learning rates γ_1 and γ_2, we choose the following update rules:

$$\dot{\boldsymbol{\theta}} = \frac{3\gamma_1}{k}\left(\frac{\partial \Lambda}{\partial \hat{\omega}}\dot{\hat{\boldsymbol{\omega}}}\right)^T \boldsymbol{z}_1 - 2\gamma_1 \Lambda^T(\hat{\boldsymbol{\omega}})\boldsymbol{z}_1 \qquad (3.101)$$

and

$$\dot{\boldsymbol{\phi}} = \frac{3\gamma_2}{k}\left(\frac{\partial W}{\partial \tau}\dot{\boldsymbol{\tau}}\right)^T \boldsymbol{z}_1 - 2\gamma_2 W^T(\boldsymbol{\tau})\boldsymbol{z}_1 \qquad (3.102)$$

Thus with these choices for the inertia estimate terms, we finally have

$$\dot{V} = -\|\boldsymbol{z}_1\|^2 - \|\boldsymbol{z}_2\|^2 + \frac{1}{k^2}(3\boldsymbol{z}_2 - \boldsymbol{z}_1)^T\left(\Lambda(\hat{\boldsymbol{\omega}}) - \Lambda(\boldsymbol{\omega})\right)\boldsymbol{\theta}^* \qquad (3.103)$$

We know that $\Lambda(\boldsymbol{\omega})\boldsymbol{\theta}^*$ is just a different representation of $J^{-1}\boldsymbol{\omega}^* J\boldsymbol{\omega}$. Thus we can bound the last term in the equation above using Eq. 3.23:

$$\frac{1}{k}\left(\Lambda(\hat{\boldsymbol{\omega}}) - \Lambda(\boldsymbol{\omega})\right)\boldsymbol{\theta}^* \le \left(2\alpha\omega_m\|\boldsymbol{z}_2\| + k\beta\|\boldsymbol{z}_2\|^2\right) \qquad (3.104)$$

Going back to Eq. 3.103,

$$\begin{aligned}
\dot{V} &\le -\|\boldsymbol{z}\|^2 + \frac{1}{k}\left(3\|\boldsymbol{z}_2\| + \|\boldsymbol{z}_1\|\right)\left(2\alpha\omega_m\|\boldsymbol{z}_2\| + k\beta\|\boldsymbol{z}_2\|^2\right) \\
&\le -\|\boldsymbol{z}\|^2 + \frac{4}{k}\|\boldsymbol{z}\|^2\left(2\alpha\omega_m + k\beta\|\boldsymbol{z}\|\right) \\
&= -\left(1 - \frac{8\alpha\omega_m}{k}\right)\|\boldsymbol{z}\|^2 + 4\beta\|\boldsymbol{z}\|^3 \qquad (3.105)
\end{aligned}$$

where similar to the non-adaptive case, $\alpha = \frac{J_M}{J_m}$ is the ratio of the nominal maximum and minimum eigenvalues J_M and J_m of J and $\beta = \sqrt{\alpha(\alpha - 1)}$. To ensure the first term is negative, we can choose k such that

$$k > 8\omega_m \alpha = 8\omega_m \frac{J_M}{J_m} \tag{3.106}$$

Since $\boldsymbol{\theta}^*$ is not known in this case, a conservative upper bound on the largest eigenvalue J_M and lower bound on the smallest eigenvalue J_m of the inertia matrix can be used.

Now if we manage to restrict the initial conditions for the states that will make $\dot{V}(t) \leq 0$ for all time $t \geq 0$, we can then have a non-increasing V, that is, $V(t) \leq V(0), \quad \forall t > 0$. If this condition is met, using Eq.3.95, we have

$$c_1 \|\boldsymbol{z}(t)\|^2 \leq V(t) \leq V(0) \leq c_2 \|\boldsymbol{z}(0)\|^2 + \frac{1}{2\gamma_1}\|\boldsymbol{z}_\theta(0)\|^2 + \frac{1}{2\gamma_2}\|\boldsymbol{z}_\phi(0)\|^2$$

which leads to $\quad \|\boldsymbol{z}(t)\|^2 \leq \frac{c_2}{c_1}\|\boldsymbol{z}(0)\|^2 + \frac{1}{2c_1\gamma_1}\|\boldsymbol{z}_\theta(0)\|^2 + \frac{1}{2c_1\gamma_2}\|\boldsymbol{z}_\phi(0)\|^2$

$$\tag{3.107}$$

Let us define a new constant

$$\mu_0^2 \triangleq \max\left[\frac{c_2}{c_1}, \frac{1}{2c_1\gamma_1}, \frac{1}{2c_1\gamma_2}\right] \tag{3.108}$$

which always satisfies $\mu_0 > 1$ since $c_2 > c_1$.

Thus whenever $\dot{V}(t) \leq 0$, we have

$$\|\boldsymbol{z}(t)\|^2 \leq \mu_0^2 \left(\|\boldsymbol{z}(0)\|^2 + \|\boldsymbol{z}_\theta(0)\|^2 + \|\boldsymbol{z}_\phi(0)\|^2\right)$$

leading to $\quad\quad\quad \|\boldsymbol{z}(t)\| \leq \mu_0 \|\boldsymbol{Z}(0)\| \tag{3.109}$

76

We can modify Eq.3.105 to

$$\dot{V} \leq -\left(1 - \frac{8\alpha\omega_m}{k}\right)\|\boldsymbol{z}\|^2 + 4\beta\|\boldsymbol{z}\|^2\mu_0\|\boldsymbol{Z}(0)\|$$

$$= -4\beta\mu_0\|\boldsymbol{z}\|^2\left[\frac{1}{4\mu_0\beta}\left(1 - \frac{8\alpha\omega_m}{k}\right) - \|\boldsymbol{Z}(0)\|\right] \qquad (3.110)$$

For an initial condition

$$\|\boldsymbol{Z}(0)\| \leq \frac{1}{4\mu_0\beta}\left(1 - \frac{8\alpha\omega_m}{k}\right) \triangleq \rho_a(k) \qquad (3.111)$$

we have

$$\dot{V} \leq -4\mu_0\mu_1\beta\|\boldsymbol{z}\|^2 \leq 0 \qquad (3.112)$$

Eq.3.111 defines $\rho_a(k)$ as a condition on the initial error state which differs from Eq.3.32 by a scaling constant μ_0, instead of just $\sqrt{c_2/c_1}$, but $\rho_a(k) > 0$ is still positive due to Eq.3.106, and

$$\mu_1 = \frac{1}{4\mu_0\beta}\left(1 - \frac{8\alpha\omega_m}{k}\right) - \|\boldsymbol{Z}(0)\| > 0 \qquad (3.113)$$

It is to be noted that unlike the non-adaptive case, this upper bound is now on the full state $\boldsymbol{Z}(0)$ and not just on $\boldsymbol{z}(0)$, the implications of which will be discussed later.

Similar to the non-adaptive scenario, if we select $\boldsymbol{Z}(t_0)$ at time $t_0 = 0$ without loss of generality such that $\|\boldsymbol{Z}(0)\| \leq \rho_a(k)$ we can ensure $\dot{V}(t) \leq 0$, $\forall t \geq 0$. For a small enough initial $\|\boldsymbol{Z}(0)\|$, V is non-increasing and thus $\lim_{t\to\infty} V(t) = V_\infty$ exists, implying $V \in \mathbb{L}_\infty$ and $\boldsymbol{z} \in \mathbb{L}_\infty$. Since V is bounded, the terms $\left(\hat{\boldsymbol{\theta}} + \boldsymbol{\beta}_\theta - \boldsymbol{\theta}^*\right)$ and $\left(\hat{\boldsymbol{\phi}} + \boldsymbol{\beta}_\phi - \boldsymbol{\phi}^*\right)$ are also bounded, leaving the

derivative of z to also be bounded using Eq. 3.111, i.e., $\dot{z} \in \mathbb{L}_\infty$. Integrating Eq.3.112 on both sides,

$$\int_0^\infty \dot{V} dt \leq \int_0^\infty -4\beta\mu_0\mu_1 \|z\|^2 dt$$

$$V_\infty - V(0) \leq -4\beta\mu_0\mu_1 \int_0^\infty \|z\|^2 dt$$

$$\int_0^\infty \|z\|^2 dt \leq \frac{V(0) - V_\infty}{4\beta\mu_0\mu_1} \tag{3.114}$$

which implies $z \in \mathbb{L}_2$. Using the corollary to the Barbalat's lemma, since $z \in \mathbb{L}_2 \cap \mathbb{L}_\infty$ and $\dot{z} \in \mathbb{L}_\infty$, we have $\lim_{t\to\infty} z(t) = 0$, so the observer errors in attitude and angular rate asymptotically converge to zero for the following region of attraction $\boldsymbol{Z}(0) \in \mathbb{M}_a$ where

$$\mathbb{M}_a = \left\{ \boldsymbol{Z} \in \mathbb{R}^{30} \middle| \|\boldsymbol{\sigma_e}(0)\|^2 + \frac{\|\boldsymbol{\omega_e}(0)\|^2}{k^2} \right.$$
$$\left. + \frac{\|\hat{\boldsymbol{\theta}}(0) + \boldsymbol{\beta_\theta}(0) - \boldsymbol{\theta}^*\|^2}{k^2} + \frac{\|\hat{\boldsymbol{\phi}}(0) + \boldsymbol{\beta_\phi}(0) - \boldsymbol{\phi}^*\|^2}{k^2} \leq \rho_a^2(k) \right\} \tag{3.115}$$

The errors in the estimates of the inertia terms z_θ and z_ϕ will also converge to zero subject to adequate persistence of excitation.

3.3.4   Discussion

The size of the region of attraction ρ_a for the initial state $\|\boldsymbol{Z}(0)\|$ which guarantees asymptotic convergence of the error state $\|z\|$ to zero, is impacted by the value of the user chosen parameter k, the trajectory followed by the system, the knowledge we have of α the ratio of the maximum and minimum eigenvalues of the inertia matrix and by the fact that we are adapting for an unknown inertia matrix.

78

3.3.4.1 Choosing k

The discussion from the non-adaptive section holds, that we have the option to choose the attitude error state $\boldsymbol{\sigma}_e(0)$ to be zero initially by selecting $\hat{\boldsymbol{\sigma}}(0) = \boldsymbol{\sigma}(0)$ but $\boldsymbol{\omega}_e(0)$, $(\hat{\boldsymbol{\theta}}(0) + \boldsymbol{\beta}_\theta(0) - \boldsymbol{\theta}^*)$ and $(\hat{\boldsymbol{\phi}} + \boldsymbol{\beta}_\phi - \boldsymbol{\phi}^*)$ can be arbitrarily large. Selecting k large enough can accommodate for these large values since higher k still leads to lower $\boldsymbol{z}_2$, $\boldsymbol{z}_\theta$ and $\boldsymbol{z}_\Phi$. However, higher values of k should also be accompanied by higher values of γ_1 and γ_2 since large k reduces $c_1 = (5 - \sqrt{5})/4k$ and increases μ_0 in Eq. 3.108 at low learning rates. Large values of μ_0 can in turn reduce $\rho_a(k)$ from Eq. 3.111 and make the region of attraction smaller.

3.3.4.2 The cost of adaptation

It is important to note that by choosing to adapt for the unknown inertia matrix terms, we do sacrifice on the size of the initial region of attraction. Eq. 3.111 is different from the non-adaptive case Eq. 3.32 since the adaptive ROA is for the norm of the full state including the inertia error terms along with the attitude and velocity states. For the sake of this discussion, let us consider that the initial attitude error state $\boldsymbol{z}_1$ is zero, that is, $\hat{\boldsymbol{\sigma}}(0) = \boldsymbol{\sigma}(0)$. This would make $\boldsymbol{\beta}_\theta(0) = \boldsymbol{\beta}_\phi(0) = 0$. If there are good estimates available of the largest and smallest eigenvalues of the inertia matrix, those estimates can be used for the initial estimates $\hat{\boldsymbol{\theta}}$ and $\hat{\boldsymbol{\phi}}$. However, if no good estimates are available, the initial estimates can just be set to zero, $\hat{\boldsymbol{\theta}}(0) = 0$ and $\hat{\boldsymbol{\phi}}(0) = 0$. If we consider this to be the worst case scenario for the initial guess of the

inertia parameters, we have $\boldsymbol{z}_\theta(0) = \boldsymbol{\theta}^*/k$ and $\boldsymbol{z}_\phi(0) = \boldsymbol{\phi}^*/k$ and the condition on the initial errors for convergence is

$$\frac{\|\boldsymbol{\omega}_e(0)\|^2}{k^2} + \frac{\|\boldsymbol{\theta}^*\|^2}{k^2} + \frac{\|\boldsymbol{\phi}^*\|^2}{k^2} \leq \rho_a^2(k)$$

$$\|\boldsymbol{\omega}_e(0)\|^2 + \|\boldsymbol{\theta}^*\|^2 + \|\boldsymbol{\phi}^*\|^2 \leq \frac{k^2}{16\beta^2\mu_0^2}\left(1 - \frac{8\alpha\omega_m}{k}\right)^2 \tag{3.116}$$

$$\|\boldsymbol{\omega}_e(0)\|^2 \leq \frac{k^2}{16\beta^2\mu_0^2}\left(1 - \frac{8\alpha\omega_m}{k}\right)^2 - \|\boldsymbol{\theta}^*\|^2 - \|\boldsymbol{\phi}^*\|^2$$

$$\tag{3.117}$$

If a better estimate of the inertia terms is available and an upper bound on their errors is known, those upper bounds can be used in place of $\|\boldsymbol{\theta}^*\|$ and $\|\boldsymbol{\phi}^*\|$ in the above equations. The condition above is clearly smaller than the region of attraction for $\|\boldsymbol{\omega}_e(0)\|$ in the non-adaptive scenario, which is the price to pay for adaptation, along with sacrificing exponential convergence for asymptotic convergence. However, we can choose k large enough to accommodate for any values of the initial rate error, since as k grows, the right hand side of Eq. 3.116 increases. The value of μ_0 is constant at $\sqrt{c_2/c_1}$ for small values of k, but for larger values of k and small learning rates γ_1 and γ_2, the maximum function in Eq. 3.108 switches to the second or third parameter. For the sake of this discussion, let us consider a case when $\gamma_1 < \gamma_2$ and $\mu_0^2 = 1/2c_1\gamma_1$. In this case, Eq. 3.116 becomes

$$\|\boldsymbol{\omega}_e(0)\|^2 + \|\boldsymbol{\theta}^*\|^2 + \|\boldsymbol{\phi}^*\|^2 \le \frac{2c_1\gamma_1 k^2}{16\beta^2}\left(1 - \frac{8\alpha\omega_m}{k}\right)^2$$

$$\|\boldsymbol{\omega}_e(0)\|^2 + \|\boldsymbol{\theta}^*\|^2 + \|\boldsymbol{\phi}^*\|^2 \le \frac{2(5-\sqrt{5})\gamma_1 k^2}{64k\beta^2}\left(1 - \frac{8\alpha\omega_m}{k}\right)^2$$

$$\|\boldsymbol{\omega}_e(0)\|^2 + \|\boldsymbol{\theta}^*\|^2 + \|\boldsymbol{\phi}^*\|^2 \le \frac{(5-\sqrt{5})\gamma_1}{32k\beta^2}\left(k - 8\alpha\omega_m\right)^2 \qquad (3.118)$$

Clearly this inequality can be satisfied for any value of the initial errors in rate and inertia terms by choosing a sufficiently large k and thus guarantee the convergence results for the attitude and velocity states.

3.3.4.3   Semi-global result

The upper bound on $\|\boldsymbol{Z}(0)\|$ in Eq.3.111 in the limit is still finite:

$$\lim_{k\to\infty} \rho_a(k) = \frac{1}{4\beta\mu_0} \qquad (3.119)$$

This indicates that the result is once again semi-global since irrespective of the choice of k, Eq. 3.119 gives the upper bound on the size of the region of attraction for the full initial state $\|\boldsymbol{Z}(0)\|$. This upper bound is impacted by our choice of α (since $\beta = \sqrt{\alpha(\alpha-1)}$), which also directly impacts the lower bound on our choice of $k > 8\alpha\omega_m$. In the adaptive case when the true value of α is unknown, this demonstrates how being overly conservative and choosing large values of α makes our region of attraction smaller for the initial state. On the other hand if α is chosen smaller than the true value, the lower bound on k from Eq. 3.106 could in turn be too small, leading to choices of k that are too small to provide convergence of the observer to the true states.

3.3.4.4 Persistence of Excitation

The estimates $\hat{\boldsymbol{\theta}} + \boldsymbol{\beta_\theta}$ and $\hat{\boldsymbol{\phi}} + \boldsymbol{\beta_\phi}$ will converge to the true values of $\boldsymbol{\theta}^*$ and $\boldsymbol{\phi}^*$ when we have an applied torque that is rich enough or persistently exciting (PE). It is important to note that we still require the angular velocity to be bounded. Moreover, while a PE torque helps with the estimation of the inertia parameters, it is not required for the RIG observer estimates of the attitude and angular velocity to converge to their true values, which is guaranteed for any known and bounded torque with initial states satisfying Eq. 3.111. There are also no PE requirements on any of the non-adaptive results.

3.3.4.5 Zero torque case

A special case to be noted is when there is no torque acting on the system. If $\boldsymbol{\tau}$ is identically zero, we can avoid adapting for $\boldsymbol{\phi}$ since $W(\boldsymbol{\tau}) = 0$ in Eq.3.89 and can thus leave out the $\boldsymbol{z}_\phi$ term from the Lyapunov function in Eq.3.91. This also implies that $\tilde{\phi} = 0$ and we can have a bigger region of attraction for the attitude and rate states in Eq.3.116 using the same Lyapunov analysis as above without any of the terms involving $\boldsymbol{z}_\phi$ and $\rho_a(k)$, the ROA for the full state, does not change:

$$\|\boldsymbol{z}(0)\|^2 \leq \rho_a^2(k) - \|\boldsymbol{z}_\theta(0)\|^2 \tag{3.120}$$

which in the case when the inertia terms and attitude error are initialized to zero, $\hat{\boldsymbol{\theta}}(0) = 0$ and $\hat{\boldsymbol{\sigma}}(0) = \boldsymbol{\sigma}(0)$, becomes

$$\|\boldsymbol{\omega}_e(0)\|^2 \leq k^2 \rho_a^2(k) - \|\boldsymbol{\theta}^*\|^2 \tag{3.121}$$

If the system is tumbling through a persistently exciting trajectory, the estimates of $\boldsymbol{\theta}$ can still converge to the true value and the inertia terms be recovered from the estimate even in this zero torque scenario.

3.4 Simulations

We perform numerical simulations for a spacecraft with an inertia matrix:

$$J = \begin{bmatrix} 200 & 12 & 9 \\ 12 & 170 & 14 \\ 9 & 14 & 150 \end{bmatrix} \text{kg/m}^2 \tag{3.122}$$

starting from $\boldsymbol{s}(0) = [0, 0, 0]^T$rad and $\boldsymbol{\omega}(0) = [0.1, 0.05, 0]^T$rad/sec.

Two different external torques are used:

$$\boldsymbol{\tau_1} = \begin{bmatrix} 0.1\sin(t) \\ 0.2\cos(2t) \\ 0.3\cos(3t) \end{bmatrix} \text{Nm} \tag{3.123}$$

and

$$\boldsymbol{\tau_2} = \begin{bmatrix} 0.1\cos(2t) + 0.2 \\ 0.5\cos(2t) + 0.4 \\ 0.1\sin(2t) + 0.2 \end{bmatrix} \text{Nm} \tag{3.124}$$

For the case when the inertia and torque are known accurately, all the states estimates are initialized to be zero and the error in velocity is shown in Fig. 3.1 for J, $\boldsymbol{\tau_1}$ and $k = 20$. The estimate can clearly be seen to converge
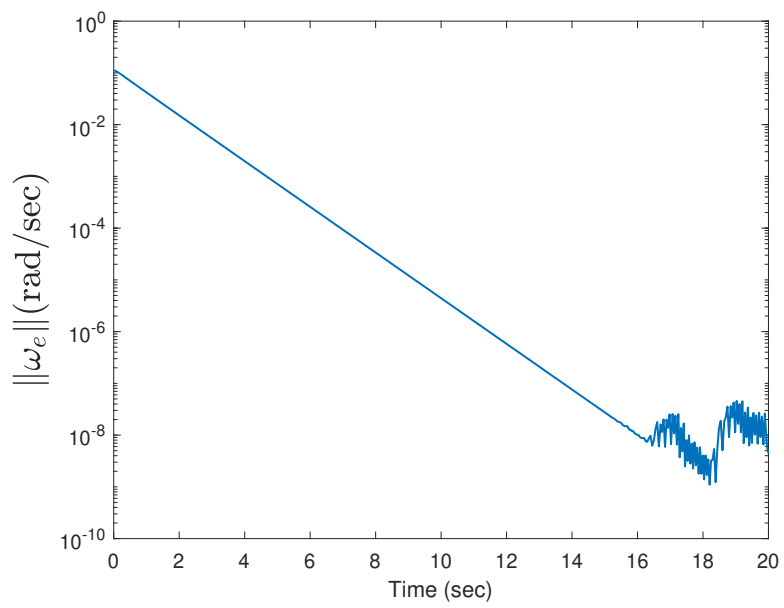
Figure 3.1: Angular velocity estimation error norm for non-adaptive known torque and inertia
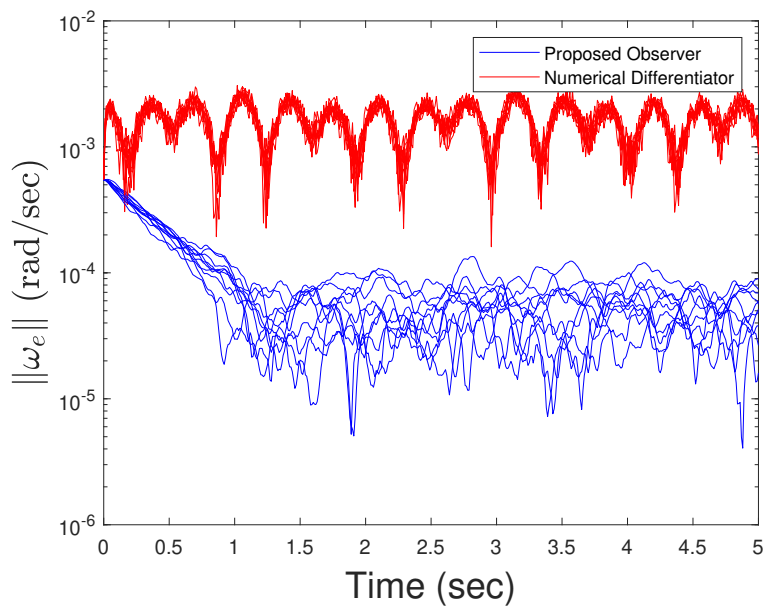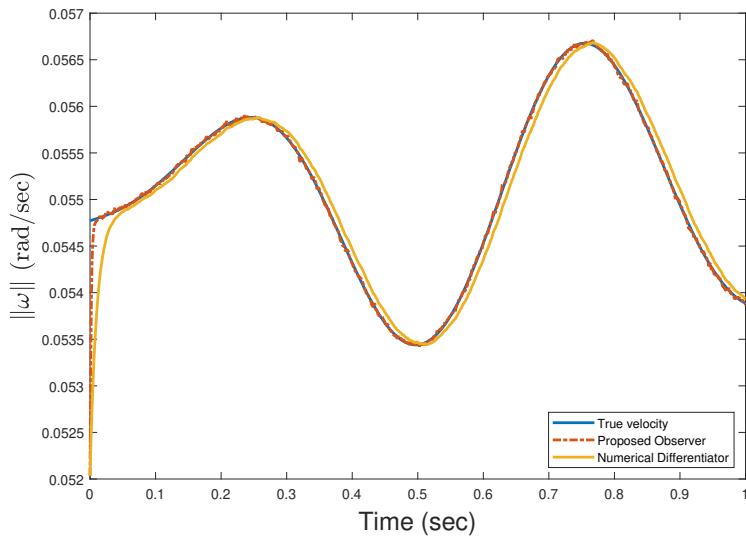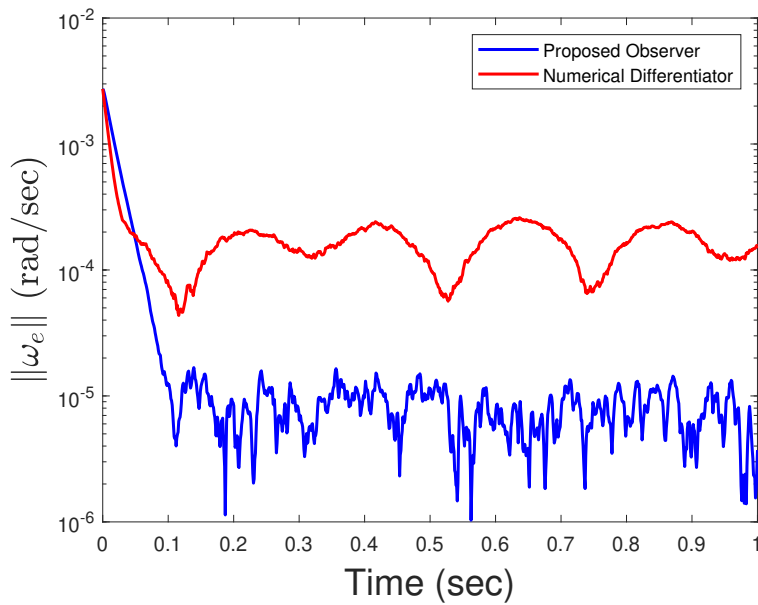
Figure 3.2: Angular velocity estimation error norm for 10 Monte Carlo runs comparing the numerical differentiator and the proposed non-adaptive observer

(a) Tracking of the angular velocity norm by the two methods

(b) Angular velocity estimation error norm

Figure 3.3: Comparison of the latency properties of the numerical differentiator with the proposed non-adaptive observer

to the real values of the angular velocity and the errors go to zero, within the tolerance limits of the simulator integration method. If we consider $\omega_m = 0.5$, the region of attraction in this case would be $\|\boldsymbol{z}(0)\| \leq 0.14$ which was true for our simulation, $\|\boldsymbol{z}(0)\| = \|\boldsymbol{\omega_e}(0)\| = 0.11\text{rad/sec}$.

The impacts of noise are more complicated to understand when the system is not at rest since the value of the angular velocity states affects the steady state noise value. Figs. 3.2 shows 10 Monte Carlo runs comparing the effects of measurement noise on our proposed observer and a numerical differentiator followed by a low pass filter, where the noise response of our observer can clearly seen to be orders of magnitude better. Zero mean noise affects the RIG measurements with an angular random walk of $0.15 \deg / \sqrt{hr}$ (spectral density $S = 10^{-9}\mathbb{I}_{3\times3} rad^2/s$) at a sampling time period of $\delta t = 10^{-3}s$ ($1000Hz$ frequency) for the same inertia and torque as Fig. 3.1 above. $k_{lp} = 0.9$ was chosen for Eq.3.59 since it presented the best experimental results while $k = 20$ was chosen for our observer. Fig. 3.3 shows how the latency for the proposed observer is lower than the numerical differentiator for the same level of noise response. A torque of three times higher frequency as Eq.3.123 was applied to the system with $k_{lp} = 0.99$ and $k = 1000$ so that the noise response was of a similar level when tested on a system moving at constant velocity. The numerical differentiator output waveform in Fig.3.3a visibly lags the true value while our observer has a much lower latency. The velocity estimation error is shown in Fig. 3.3b but the error in the numerical differentiator could not be reduced below this level due to the latency in the output contributing

to the error. Higher errors due to latency will arise as the system moves at a higher velocity.

For demonstrating the robustness properties of the observer, we use the system with inertia J from Eq.3.122 with the non-adaptive observer using an inertia estimate of

$$\bar{J} = \begin{bmatrix} 170 & 22 & 19 \\ 22 & 180 & 24 \\ 19 & 24 & 160 \end{bmatrix} \text{kg/m}^2 \qquad (3.125)$$

which represents approximately 5% error in the inertia parameter model. The torque input from Eq. 3.123 was applied to the system but is unknown to the observer. For the chosen value of $k = 500$, the system satisfied Eq.3.76 with a high value of $\zeta = 0.99$. The angular velocity and norm of the error states are shown in Fig. 3.4, where once again, the estimate error norm remains bounded, demonstrating the robustness of the observer to inertia and torque inaccuracies.

To demonstrate the working of the adaptive observer, we use the same inertia matrix J above with $\boldsymbol{\tau_2}$. Fig.3.5a shows the norm of the angular velocity error for an initial inertia guess of $\bar{J}$ above acted upon by τ_1, while Fig.3.5b shows the same results for an initial inertia error of 20% of J with τ_2. Both the simulations were run with $k = 300$, $\gamma_1 = 10^5$ and $\gamma_2 = 10^5$. Fig.3.6 compares the norm of the full error state for the non-adaptive and adaptive observers. If we consider the parameter estimation error to be represented by

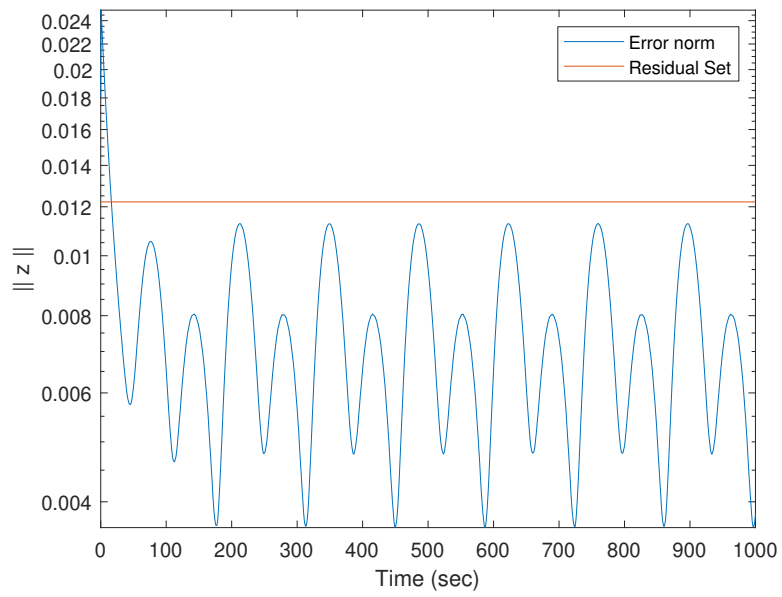$$\tilde{\phi} = \|\hat{\boldsymbol{\phi}} + \boldsymbol{\beta_\phi} - \boldsymbol{\phi}^*\| \qquad (3.126)$$

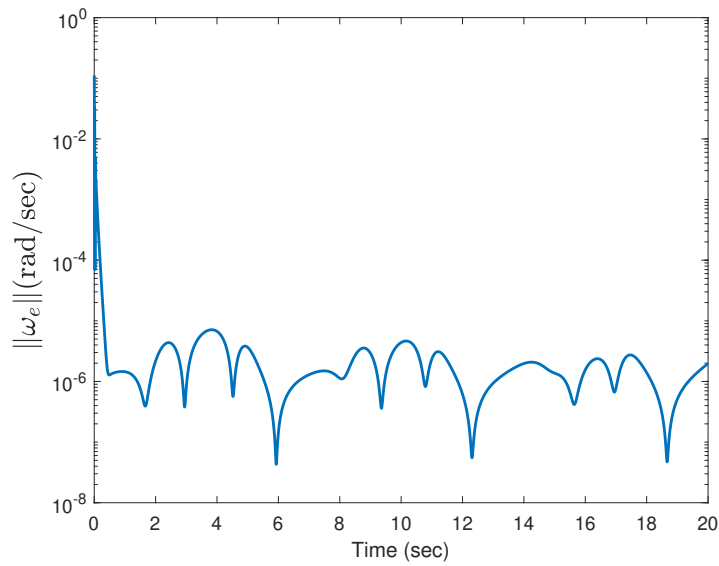Figure 3.4: Simulation of the non-adaptive inaccurate inertia and unknown torque case

For J with a persistently exciting torque $\boldsymbol{\tau_2}$, Fig. 3.7 shows that $\tilde{\phi}$ converges to zero. This demonstrates the convergence of the estimate $\hat{\boldsymbol{\phi}} + \boldsymbol{\beta_\phi}$ to the true value of $\boldsymbol{\phi}^*$, representing the terms in the inverse of the inertia matrix. The inertia matrix can be retrieved from the estimate $\hat{\boldsymbol{\phi}} + \boldsymbol{\beta_\phi}$ if required. The plots for the error in estimating $\boldsymbol{\theta}^*$ follow a trend similar to Fig. 3.7 and have been left out for brevity. All the time scales for the plots were chosen for the sake of easier visualization and clarity.

3.5 Conclusions

A novel observer was designed for estimating the angular rate states from the continuous measurements of a Rate Integrating Gyroscope (RIG), along with an adaptation modification when the inertia of the system is not accurately characterized. The construction involves a high-gain element. Such high gain observers have been shown in the literature to perform better than numerical differentiators in terms of convergence properties as well as their response to measurement noise. The observer dynamics are linear in the measurement term and involve a single user chosen parameter which controls the convergence rate of the estimate and the region of attraction for the initial value of the state. The non-adaptive observer exhibits robustness to an inaccurately modeled inertia matrix as well as unknown torque inputs to the system.
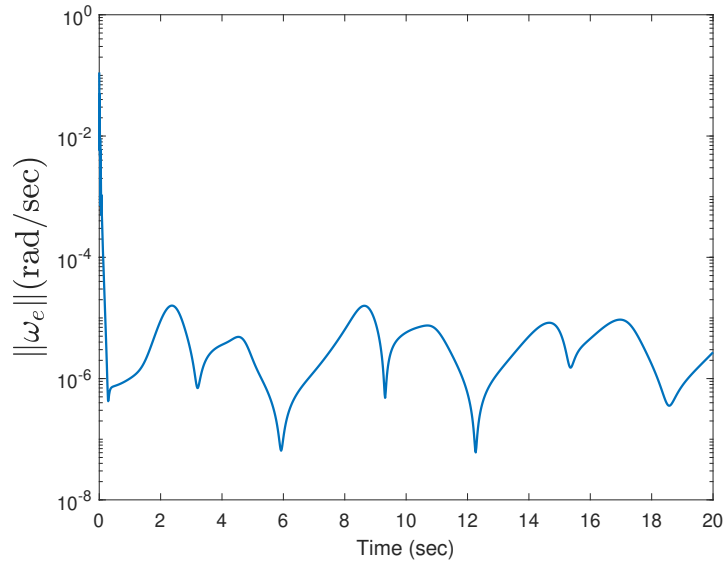
(a) Adaptive angular velocity estimation error norm for τ_1 and $\bar{J}$

(b) Adaptive angular velocity estimation error norm for τ_2 and an initial guess of $0.8 * J$

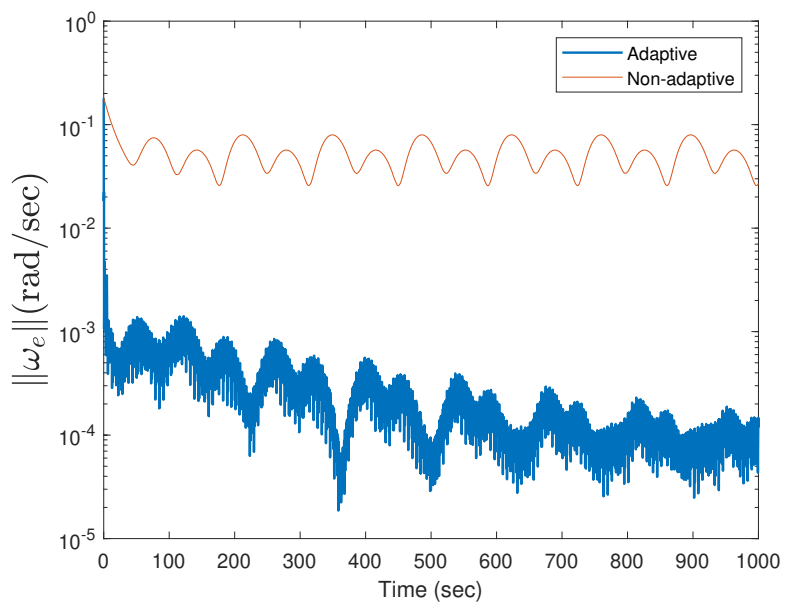Figure 3.5: Simulations for adaptive inertia and known torque

Figure 3.6: Comparison of the norm of full error states - Adaptive vs non adaptive
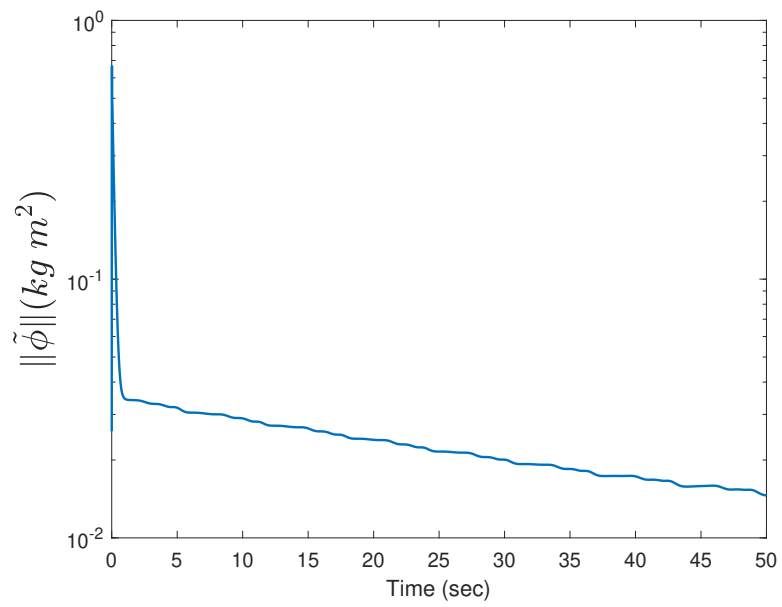
Figure 3.7: Norm of the parameter estimation error for ϕ

Chapter 4

Robocentric SLAM

The future of planetary exploration relies on autonomous rovers which can navigate themselves in unknown environments [42]. The problem of Simultaneous Localization and Mapping (SLAM) for robotic systems has been extensively studied for spatial exploration [43][44][45]. The idea of using a robotic agent that combines the problem of building a map of a new space along with locating the agent in the map being built is ideal for a rover exploring a planet. The robot performing the exploration task is usually equipped with some form of sensor, often visual, that helps the robot observe its surroundings as well as some form of odometry that helps the robot measure its own motion. Map building is often done in the form of features extracted from sensor measurements of the surroundings, stored along with their locations in a known frame of reference. Knowledge of the position of the rover at the time of observation is required to place new features on the map or refine their estimated position. The interlink between robot and feature positions leads to correlations between their estimates; having both the position of the rover and features in the filter's state accounts for these correlations and helps reduce

---

errors in both. Planning of the rover's path by the motion controller requires the rovers current location relative to the environment. The SLAM objective is to provide the motion controller with the position of the rover and the map of features as needed.

The nonlinear SLAM problem is usually formulated as either a recursive filter or via sparse optimization. Keyframe-based Bundle Adjustment (BA) techniques [46][47] aggregate measurements at different times and use a numerical optimizer to compute the SLAM solution. Alternatively, recursive implementations only process the latest measurement and are typically based on either the Extended Kalman Filter (EKF) or the particle filter. Particle filters (unlike the EKF) are nonlinear estimators, and their implementations for SLAM applications, such as FAST-SLAM [48], have their own strengths and limitations in terms of complexity and consistency. In this chapter we focus on the EKF-SLAM approach and represent the state and the uncertainty with an estimated mean and a covariance matrix. EKF-SLAM employs linearization to apply the Kalman filter algorithm to the nonlinear propagation and measurement functions. Linearization can affect the consistency of the filter as situations arise when the linear approximation of the function is not sufficiently accurate. This is particularly problematic because the SLAM system is inherently nonlinear and unobservable, a combination known to cause divergence in the EKF. This phenomenon led to extensive work to study the consistency of the EKF-SLAM showing that the algorithm is eventually bound to be inconsistent [49][50][51][2]. Divergence of the SLAM algorithm can be

detrimental to any exploration task since it can lead to loss of localization feedback for controlling the rover as well as map feature locations becoming inconsistent since they are interlinked with the position.

The SLAM linearization approximation introduces apparent observability to the unobservable subspace [52]. As a result, the covariance estimates of the EKF undergo reduction in directions of the state-space where no information is actually available, making the filter more confident than it should, thus creating inconsistency and even divergence. A classic example to demonstrate the divergence problems of EKF-SLAM is given in Ref.[2], where a stationary robot with no process noise, observing a single stationary feature, eventually diverges. A relative measurement between the robot and the features (for example a LIDAR returning range and bearing angles) is the only sensor available, and hence the absolute positions in the global frame are not observable, and neither is the global heading angle.

A source of inconsistency is given by the linearization of the rover's heading error which affects the rotation transformation of the odometry; small errors in heading can lead to large errors in position. In the robocentric approach [50][3], the global position of the robot is kept as a state in the EKF together with position of the features relative to it. The robocentric features positions are fully observable and the measurement model can be linearized more accurately providing much better consistency characteristics for the EKF algorithm. Ref.[3], in order to reduce the complexity of the propagation step, does not propagate the change in robocentric position of the features due to

the robot's motion; rather, it appends all odometry values starting from the latest measurement update step as components of the state vector. When a new measurement is available from the LIDAR, the global robot position is updated followed by the features positions, while the odometry states are discarded. The robocentric mapping idea presented in Ref.[3] has much better consistency properties as compared to the traditional EKF because the odometry states have small uncertainty as they get reset often, but some of the underlying observability issues are still present. Ref.[53] modifies this approach for visual-inertial odometry and reduces the computational complexity by not mapping the features and thus reducing the size of the state-space, an approach similar to Ref.[54] but including the robocentric idea. The robocentric approach is readily applicable and an excellent choice of SLAM for relative navigation problems where the objective is to navigate a robot to one or more of the features being observed.

In this work, we propose two key modifications to the robocentric mapping idea. First, the odometry measurements are used to propagate both the robot's position and the robocentric features' positions, with all relevant correlation terms accounted for. Second, we include second order terms of the Taylor series expansion of the heading error during the propagation step to greatly improving the consistency of the filter over time. The only minor disadvantage to this method is the increased computational complexity in roto-translating the map features positions during the propagation step whereas they are stationary in the classic EKF-SLAM formulation. In the counter ex-

97

ample proposed by Julier and Uhlmann [2], with a stationary robot and no process noise, our proposed algorithm never diverges, but neither does the original robocentric approach [3]. However, when we make a slight modification to the counter example in Ref.[2] and add process noise to the propagation step, the algorithm in Ref.[3] diverges, while the method proposed in this chapter does not. Moreover, the proposed algorithm is more consistent than existing methods in the presented simulated scenarios involving a moving robot observing features using a Lidar. The effectiveness of the method is tested in a 2D simulation as well as in experiments on a ground rover and compared against Ref.[3].

The contributions of this chapter are: analysis of the observability of the states of the EKF in the global and robocentric frame for a better understanding of how the transformation impacts the filter, and introduction of the above-mentioned modifications to the existing robocentric SLAM algorithm to improve its consistency and robustness.

4.1   EKF-SLAM Algorithm

Consider a rover navigating in a 2D environment, equipped with odometry and a LIDAR. The path taken by the rover is assumed prescribed and the localization and mapping module does not receive feedback inputs from the motion controller. We assume a feature detection technique identifies and extracts points of interest in the measurement data from the LIDAR. The data used by EKF-SLAM are the range and angle measurements from the

rover to these features. The odometer is providing measurements of linear translational and rotational velocity, which can be integrated over time to obtain the distance moved and change in heading of the robot since the last odometer reading. We also assume Gaussian random noise with known covariance matrices Q and R corrupting the odometry and LIDAR measurements respectively.

4.1.1 Classical EKF-SLAM

Standard SLAM applications use the position of the robot

$$\boldsymbol{r}_r^G = \left[x_r^G, y_r^G, \theta_G^R\right]^T$$

and the landmark features

$$\boldsymbol{r}_{f_i}^G = [x_{f_i}^G, y_{f_i}^G]^T$$

where $i = 1, 2, ...$ uniquely identify the features. The superscript G indicates the quantity is expressed in a fixed global frame of reference $\{G\}$ and the quantity θ_G^R is the angle from the global to a robot-fixed robot-centered frame $\{R\}$. Since the center and orientation of the global reference frame is unobservable, it is typically chosen to be the initial location of the robot setting the initial uncertainty to zero, which was shown to produce better filter consistency than choosing any other fixed global frame with non-zero initial uncertainty in the robot position [3]. The state estimates at any time t_k are given by

$$\hat{\boldsymbol{x}}_k^G = \left[\hat{\boldsymbol{r}}_r^G(k)^T, \hat{\boldsymbol{r}}_{f_1}^G(k)^T, \hat{\boldsymbol{r}}_{f_2}^G(k)^T...\right]^T$$

The propagation step for the classical EKF-SLAM algorithm adds the odometry $\boldsymbol{u}_k^R = [\delta x_k^R, \delta y_k^R, \delta\theta_k^R]^T$ to the robot position states. The odometry measurement is obtained in a robocentric frame of reference $\{R\}$.

$$
\begin{bmatrix} \bar{x}_r^G(k+1) \\ \bar{y}_r^G(k+1) \\ \bar{\theta}^G(k+1) \end{bmatrix} = \begin{bmatrix} \hat{x}_r^G(k) \\ \hat{y}_r^G(k) \\ \hat{\theta}^G(k) \end{bmatrix} + \begin{bmatrix} T\big(\hat{\theta}_G^R(k)\big)^T & 0 \\ & & 0 \\ 0 & 0 & 1 \end{bmatrix} \boldsymbol{u}_k^R \tag{4.1}
$$

where

$$
T(\alpha) = \begin{bmatrix} \cos\alpha & \sin\alpha \\ -\sin\alpha & \cos\alpha \end{bmatrix}
$$

so that $T\big(\hat{\theta}_G^R(k)\big)$ is the Direction Cosines Matrix to change coordinates from the global frame to the robocentric frame. The features' positions remain the same across the time propagation phase of the filter.

P^G is the covariance of the state $\boldsymbol{x}_k^G$ given by:

$$
P^G = \begin{bmatrix} P_{rr}^G & P_{rf}^G \\ P_{fr}^G & P_{ff}^G \end{bmatrix}
$$

where we have divided the state covariance into the cross covariance of the robot position and feature positions and their auto-covariances. The propagation of the covariance is given by

$$
\bar{P}_{rr}^G(k+1) = \left[\frac{\partial \bar{r}_r^G(k+1)}{\partial \hat{r}_r^G(k)}\right]^T \hat{P}_{rr}^G(k) \left[\frac{\partial \bar{r}_r^G(k+1)}{\partial \hat{r}_r^G(k)}\right]
$$

$$
+ \left[\frac{\partial \bar{r}_r^G(k+1)}{\partial u}\right]^T Q \left[\frac{\partial \bar{r}_r^G(k+1)}{\partial u}\right] \tag{4.2}
$$

$$
\bar{P}_{rf}^G(k+1) = \left[\frac{\partial \bar{r}_r^G(k+1)}{\partial \hat{r}_r^G(k)}\right]^T \hat{P}_{rf}^G(k) \tag{4.3}
$$

$$
\bar{P}_{ff}^G(k+1) = \hat{P}_{ff}^G(k) \tag{4.4}
$$

The noisy measurement from the LIDAR at true robot position $[x_r^G, y_r^G, \theta_G^R]^T$ to the n-th landmark feature at true global position $[x_{f,n}^G, y_{f,n}^G]^T$ in the global frame is given by

$$\tilde{\boldsymbol{z}}_n = \boldsymbol{z}_n + \begin{bmatrix} w_r \\ w_\phi \end{bmatrix} \tag{4.5}$$

where $[w_r, w_\phi]$ are the noise corrupting the range and bearing respectively, with covariance matrix R, and

$$z_n = \begin{bmatrix} r_n \\ \phi_n \end{bmatrix} = \begin{bmatrix} \sqrt{(x_{f,n}^G - x_r^G)^2 + (y_{f,n}^G - y_r^G)^2} \\ \tan^{-1}\left((y_{f,n}^G - y_r^G)/(x_{f,n}^G - x_r^G)\right) - \theta_G^R \end{bmatrix} \tag{4.6}$$

The filter's predicted measurement is given by

$$\bar{\boldsymbol{z}}_n = \begin{bmatrix} \bar{r}_n \\ \bar{\phi}_n \end{bmatrix} = \begin{bmatrix} \sqrt{(\bar{x}_{f,n}^G - \bar{x}_r^G)^2 + (\bar{y}_{f,n}^G - \bar{y}_r^G)^2} \\ \tan^{-1}\left((\bar{y}_{f,n}^G - \bar{y}_r^G)/(\bar{x}_{f,n}^G - \bar{x}_r^G)\right) - \bar{\theta}_G^R \end{bmatrix} \tag{4.7}$$

The Jacobian of the measurement equation is

$$H_n^G = \begin{bmatrix} H_{r,n}^G & H_{f_1,n}^G & H_{f_2,n}^G & \cdots \end{bmatrix} \tag{4.8}$$

where

$$H_{r,n}^G = \frac{\partial \boldsymbol{z}_n}{\partial \boldsymbol{r}_r^G} \tag{4.9}$$

and

$$H_{f_j,n}^G = \begin{cases} \frac{\partial \boldsymbol{z}_n}{\partial \boldsymbol{r}_{f_j}^G} & \text{if } n = j \\ \mathbf{0} & \text{if } n \neq j \end{cases} \tag{4.10}$$

The measurement residual is given by

$$\boldsymbol{y}_n = \tilde{\boldsymbol{z}}_n - \bar{\boldsymbol{z}}_n \tag{4.11}$$

and the innovation covariance matrix is

$$S = H_n^G \bar{P}^G (H_n^G)^T + R \tag{4.12}$$

101

The Kalman gain is given by

$$K = \bar{P}^G (H_n^G)^T S^{-1} \tag{4.13}$$

The updated state and covariance matrix are

$$\hat{\boldsymbol{x}} = \bar{\boldsymbol{x}} + K \boldsymbol{y}_n \tag{4.14}$$

$$\hat{P} = \bar{P} - K H_n \bar{P} \tag{4.15}$$

4.1.2 Robocentric EKF-SLAM

To handle the well-documented inconsistencies in the above described classic EKF-SLAM, Ref.[3] proposes the use of a robocentric frame of reference in which the features locations are stored with respect to a moving frame attached to the robot. Often times the relative position of the robot with respect to specific features and locations is all that is needed to accomplish mission objectives; for example obstacle avoidance, rendezvous with another robot, searching for a specific feature, or close proximity operations for in-orbit satellite repair. In those scenarios the global position of neither the robot nor features is of importance. Thus, in these applications, robocentric SLAM algorithms provide a more stable method to calculate the needed information. The state vector of the robocentric EKF includes the position of the robot in the global frame $\{G\}$ (which can also be removed when purely relative information is needed) $\boldsymbol{r}_r^G = \left[x_r^G, y_r^G, \theta_G^R\right]^T$, and the positions of the features $\boldsymbol{r}_{f_i}^R = [x_{f_i}^R,\ y_{f,i}^R]^T$ expressed in the robocentric frame $\{R\}$. The state estimate

at any time t_k is given by

$$\hat{\boldsymbol{x}}_k^R = \left[\hat{\boldsymbol{r}}_r^G(k)^T, \hat{\boldsymbol{r}}_{f_1}^R(k)^T, \hat{\boldsymbol{r}}_{f_2}^R(k)^T...\right]^T \tag{4.16}$$

The global position of the features can be retrieved as needed.

In Ref.[3] the odometry data are added to the state vector during the time propagation step, increasing the state dimension. The measurement update step uses this augmented state to correct for the global position of the robot, the robot-relative positions of the features, and the odometry measurement added to the state. A third filter step is then introduced, the composition step, which transforms the feature positions to the current robocentric frame using the updated odometry data and then discards the odometry components of the state estimate.

In the classic EKF-SLAM approach, the global positions of the robot and of the features are individually not observable, but their difference is. Therefore neither uncertainty collapses but relative measurements build correlation between the two. The filter updates the different state components based on the relative uncertainty between the robot's position and the feature's. If the robot's position was known exactly, for example, its estimate would not change when a LIDAR measurement is processed but only the estimate of the feature's position would change. Larger uncertainty also results in the measurement Jacobian being potentially evaluated at an estimated state value far from the truth.

Ref.[3] effectively introduces a new global frame after each measure-

ment update, so that the odometry states and the features are individually unobservable, but their difference is. This method performs better than the classic EKF-SLAM in terms of consistency because the uncertainty associated with the odometry states is much smaller than the typical uncertainty associated with the robot's position, hence the filter "knows" where to apply the measurement update. Yet, under challenging scenarios (for example a long measurement drop-off or very noisy odometry) the original robocentric EKF-SLAM can still diverge. The stationary robot observing a stationary feature counter example [2] is an example where EKF-SLAM diverges and switching to a robocentric frame helps with filter consistency. However, if process noise is added to this same example scenario, the robocentric approach in Ref.[3] does diverge after extended periods of time. To mitigate this behavior, we introduce a new robocentric EKF-SLAM formulation.

4.2 Modified Robocentric EKF-SLAM

In the proposed algorithm, we recommend the use of the robocentric frame but eliminate the process of appending the odometry data to the state. Instead, we use odometry in the time propagation step to move the estimated position of the robot and at the same time transform the estimated feature positions to the new robocentric frame, removing the need for the composition step of Refs.[3] [53]. The propagation and update steps are described next.

4.2.1 Propagation

Like before, the true position of the robot is $\boldsymbol{r}_r^G = \begin{bmatrix} x_r^G, y_r^G, \theta_G^R \end{bmatrix}^T$ and the odometry measurement is modeled as

$$\boldsymbol{u}_k^R = \begin{bmatrix} T\big(\theta_G^R(k)\big) \begin{bmatrix} x_r^G(k+1) - x_r^G(k) \\ y_r^G(k+1) - y_r^G(k) \end{bmatrix} \\ \theta_G^R(k+1) - \theta_G^R(k) \end{bmatrix} + \boldsymbol{v}_k \tag{4.17}$$

the heading angle θ_G^R is counted positive from G to R so that $T\big(\theta_G^R(k)\big)$ is the DCM to transform coordinates from G to R. The odometry noise $\boldsymbol{v}_k$ is assumed white, zero-mean, with covariance matrix Q.

The odometry measurements $\boldsymbol{u}_k^R = [\delta \boldsymbol{r}_r^R(k)^T, \delta\theta_k^R]^T = [\delta x_k^R, \delta y_k^R, \delta\theta_k^R]^T$ are used to propagate the estimated state as:

$$\bar{\boldsymbol{r}}_r^G(k+1) = \hat{\boldsymbol{r}}_r^G(k) + \begin{bmatrix} T\big(\hat{\theta}_G^R(k)\big)^T \delta \boldsymbol{r}_r^R(k) \\ \delta\theta_k^R \end{bmatrix} \tag{4.18}$$

This equation is obtained linearizing all the errors and then taking the expected value. Starting from

$$T\big(\theta_G^R(k)\big) = T\big(e_\theta(k)\big) \, T\big(\hat{\theta}_G^R(k)\big) \tag{4.19}$$

where the heading angle estimation error is given by $e_\theta(k) = \theta_G^R(k) - \hat{\theta}_G^R(k)$ and taking the expected value of the right-hand side of Eq. (4.19) we obtain

$$E\Big\{ T\big(e_\theta(k)\big) \, T\big(\hat{\theta}_G^R(k)\big) \Big\} = E\Big\{ T\big(e_\theta(k)\big) \Big\} \, T\big(\hat{\theta}_G^R(k)\big) \tag{4.20}$$

$$E\Big\{ T\big(e_\theta(k)\big) \Big\} = E\left\{ \begin{bmatrix} \cos(e_\theta(k)) & \sin(e_\theta(k)) \\ -\sin(e_\theta(k)) & \cos(e_\theta(k)) \end{bmatrix} \right\}$$
$$\approx E\left\{ \begin{bmatrix} 1 & e_\theta(k) \\ -e_\theta(k) & 1 \end{bmatrix} \right\} = \begin{bmatrix} 1 & 0 \\ 0 & 1 \end{bmatrix} \tag{4.21}$$

105

this approximation leads to equation (4.18); so long as both $e_\theta(k)$ and $\delta r_r^R(k)$ are small, it produces satisfactory results.

Since the rover roto-translates, the robocentric coordinates of the j-th landmark feature roto-translate in the opposite direction

$$\bar{r}_{f_j}^R(k+1) = T(\delta\theta_k^R)\left(\hat{r}_{f_j}^R(k) - \delta r_r^R(k)\right) \tag{4.22}$$

Similar to the discussion above, Eq. (4.22) is accurate so long as the uncertainty associated with $e_\theta(k)$ and the value $r_{f_j}^R(k) + \delta r_r^R(k)$ are small. In our analysis we found this not to be always true which leads to filter divergence. Our proposed approach is to include key second order terms:

$$E\left\{T\left(e_\theta(k)\right)\right\} \approx E\left\{\begin{bmatrix} 1 - e_\theta(k)^2/2 & e_\theta(k) \\ -e_\theta(k) & 1 - e_\theta(k)^2/2 \end{bmatrix}\right\}$$
$$= \begin{bmatrix} 1 - Q(3,3)/2 & 0 \\ 0 & 1 - Q(3,3)/2 \end{bmatrix} \tag{4.23}$$

where $Q(3,3)$ is the variance of $\delta\theta_k^R$. By adding the second order terms, Eq. (4.22) is replaced by

$$\bar{r}_{f_j}^R(k+1) = T(\delta\theta_k^R)\left(\hat{r}_{f_j}^R(k) - \delta r_r^R(k)\right) - \frac{1}{2}T(\delta\theta_k^R)\left(\hat{r}_{f_j}^R(k) - \delta r_r^R(k)\right)Q(3,3) \tag{4.24}$$

For the covariance time propagation, we define the matrices

$$F = \begin{bmatrix} F_{xx} & 0_{3\times2} & \dots & 0_{3\times2} \\ 0_{2\times3} & T\left(\delta\theta_k^R\right) & \dots & 0_{2\times2} \\ \vdots & \ddots & \vdots & \vdots \\ & \dots & & T\left(\delta\theta_k^R\right) \end{bmatrix} \tag{4.25}$$

where

$$F_{xx} = \begin{bmatrix} I_{2\times2} & dT\left(\hat{\theta}_G^R(k)\right)^T \delta r_r^R(k) \\ 0_{1\times2} & 1 \end{bmatrix} \tag{4.26}$$

106

and

$$B = \begin{bmatrix} T\big(\hat{\theta}_G^R(k)\big)^T & & 0 \\ & & 0 \\ 0 & 0 & 1 \\ T(\delta\theta_k^R) & dT(\delta\theta_k^R)\,\big(\hat{\boldsymbol{r}}_{f_1}^R(k) - \delta\boldsymbol{r}_r^R(k)\big) \\ T(\delta\theta_k^R) & dT(\delta\theta_k^R)\,\big(\hat{\boldsymbol{r}}_{f_2}^R(k) - \delta\boldsymbol{r}_r^R(k)\big) \\ \vdots & \vdots & \vdots \end{bmatrix} \tag{4.27}$$

where

$$dT(\alpha) = \begin{bmatrix} -\sin(\alpha) & \cos(\alpha) \\ -\cos(\alpha) & -\sin(\alpha) \end{bmatrix} \tag{4.28}$$

The classic EKF first order covariance propagation is given by

$$\bar{P}_{k+1} = F P_k F^T + B Q B^T \tag{4.29}$$

The covariance of the landmark features is further increased to include the second order terms

$$\bar{P}_{f_i,f_j}(k+1) \Leftarrow \bar{P}_{f_i,f_j}(k+1) + \frac{1}{2} T(\delta\theta_k^R) A_{ij} T(\delta\theta_k^R)^T Q(3,3)^2 \tag{4.30}$$

for all i and j, where P_{f_i,f_j} are the 2×2 components of the covariance matrix whose row corresponds to the i-th landmark and whose column corresponds to the j-th landmark, and where

$$A_{ij} = \big(\hat{\boldsymbol{r}}_{f_i}^R(k) - \delta\boldsymbol{r}_r^R(k)\big)\big(\hat{\boldsymbol{r}}_{f_j}^R(k) - \delta\boldsymbol{r}_r^R(k)\big)^T \tag{4.31}$$

Two unique features about our algorithm are worth mentioning. First, this propagation step converts the features coordinates from robocentric frame at time t_k to the robocentric frame at time t_{k+1} fully accounting for the common process noise terms corrupting the propagation of both the robot position

and the features positions. Second, we include selected second order terms to aid the consistency of the filter. While the second order terms we chose to include are sufficient to insure consistency in all of the test performed, it is possible that different scenarios might necessitate additional second order terms, or perhaps even higher than second order terms. The extreme conditions that might require the extra terms however, seem unlikely for practical situations.

In all examples and experiments performed, the second order components associated with the term $T\big(\theta_G^R(k)\big)^T \delta r_r^R(k)$ in the robot's position propagation were negligible because the odometry term $\delta r_r^R(k)$ is small. It is plausible, however, that long propagation steps due to measurement blackouts would cause this term to be needed.

4.2.2   Update

The predicted measurement for the ith landmark is given by

$$\bar{z}_i = \begin{bmatrix} \sqrt{(\bar{x}_{f_i}^R)^2 + (\bar{y}_{f_i}^R)^2} \\ \tan^{-1}\big(\bar{y}_{f_i}^R / \bar{x}_{f_i}^R\big) \end{bmatrix} \tag{4.32}$$

while the measurement Jacobian is given by

$$H^R = \begin{bmatrix} 0_{2\times 3} & \cdots & H_{f_i}^R & \cdots \end{bmatrix} \tag{4.33}$$

where

$$H_{f_i}^R = \begin{bmatrix} \dfrac{\bar{x}_{f_i}^R}{\bar{z}_i(1)} & \dfrac{\bar{y}_{f_i}^R}{\bar{z}_i(1)} \\ \dfrac{-\bar{y}_{f_i}^R}{\bar{z}_i(1)^2} & \dfrac{\bar{x}_{f_i}^R}{\bar{z}_i(1)^2} \end{bmatrix} \tag{4.34}$$

Matrix H^R above is linearized along the estimated relative position between the robot and the features. The global position or heading of the robot are not used in evaluating this derivative and hence their uncertainties do not contribute to errors in the Jacobian's evaluation. The update equations follow the conventional Kalman filter approach shown in Eqs. 4.11 - 4.15.

4.2.3   New Features

When a feature that is not yet part of the state is detected by the LIDAR, the new measurement is used to initialize the feature's estimate rather than to update the state. Moreover, the state covariance matrix is also augmented to include the uncertainty in the position of the feature as seen by the robot's current frame. If the measurements received for this new feature are given by the range and heading $[r_i, \phi_i]^T$, the state is augmented as:

$$\bar{\boldsymbol{x}}_{k+1} \Leftarrow \left[\bar{\boldsymbol{x}}_{k+1}^T, r_i \cos \phi_i, r_i \sin \phi_i\right]^T \tag{4.35}$$

and covariance as:

$$\bar{P}_{k+1} \Leftarrow \begin{bmatrix} \bar{P}_{k+1} & 0 \\ 0 & H_{z_i} R H_{z_i}^T \end{bmatrix} \tag{4.36}$$

where R is the measurement noise covariance matrix and

$$H_{z_i} = \begin{bmatrix} \cos \phi_i & -r \sin \phi_i \\ \sin \phi_i & r \cos \phi_i \end{bmatrix} \tag{4.37}$$

Once again, the global position of the robot does not play a role in the addition of new features to the state, since all position estimates for the filter are stored in the robocentric frame of reference.

4.3   Observability Analysis

It is well known that the global frame and azimuth are unobservable for terrestrial SLAM problems. The classical EKF-SLAM parameterizes the state with the global position of both the robot and the features, and with this parameterization the difference between the two is observable, while a global roto-translation of both is unobservable. With the proposed robocentric formulation, the state vector is naturally divided into its observable and unobservable components: the robocentric features are observable and the global robot position is not. That is to say, the initial global uncertainty of the robot's location and heading cannot be improved upon using odometry and lidar measurements only. This is one of the reasons many SLAM algorithms define an arbitrary global frame to coincide with the robot's initial pose, hence the initial covariance associated with the robot's state is set to zero.

Perfect odometry (or zero process noise) would keep the robot's and the features' uncertainty completely uncorrelated. Under this hypothetical scenario the robot's azimuth uncertainty would remain constant, and it's location uncertainty will grow linearly with slope determined by the initial azimuth uncertainty. In the absence of process noise, the robocentric feature's uncertainty will monotonically decrease to zero while they are observed. The counter example from Ref. [2] is a stationary robot problem observing a single feature and showed that EKF-SLAM is inevitably doomed to diverge. The divergence is due to the combined effect of the non-linearity of the system which is also unobservable. The robocentric approach however does not suffer from

this divergence, because the observable and unobservable states are separated and hence the filter "knows" where to apply the measurement update.

Adding process noise (odometry uncertainty) correlates the robot's global position to the features robocentric position. This allows for some of the uncertainty added to the robot's position from process noise to be scaled back with a lidar measurement update. The robot's pose is still unobservable (only uncertainty added during propagation can be removed with measurement updates, the initial uncertainty of the global frame remains).

When adding process noise to the counter example in Ref. [2] the robocentric approach diverges when the second order components are omitted. The proposed addition of the second order components (Eqs. 4.22 and 4.30) compensate for the nonlinearities that cause this divergence and the proposed solution is able to handle this very challenging scenario. The process noise enters the system nonlinearly and causes the correlation between robot states and landmark features. The feature's uncertainty and this correlation are then "used" by the filter to distribute the measurement update between the robot states and the feature. Adding the second order contributions allows for correctly accounting for the uncertainty and hence correctly distributing the measurement update and avoiding divergence.

4.4   Experiments

The performance of the proposed algorithm is tested in simulation in a 2D SLAM environment as well as on the dataset from Ref. [4]. A ground

robot equipped with an odometer and a lidar is considered. We assume the odometry data provides distance moved by the robot in the forward direction (X axis in the robot frame) and the change in heading angle of the robot (angular velocity). The Lidar can recognize features in the environment at up to a distance of 100m from the robot and at an angle of within 15 degrees in either direction of the robot's heading. The odometer measurement error has standard deviation of 2cm/sec in linear velocity and 0.1 deg/sec in angular velocity, uncorrelated with each other. The range and bearing measurement are assumed to also be uncorrelated, with an error standard deviation of 1cm in range and 0.05 degrees in bearing for each measurement.

The counterexample from Ref. [2] consists of a static robot (which knows it is static, hence odometry is not needed) observing a single feature. From Ref. [2] it is known that the classic EKF-SLAM diverges in this scenario while both our proposed approach and the robocentric SLAM from Ref. [3] perform well. The first test case shown is a variation of the counterexample from Ref. [2] in which the robot is stationary but it does not know it is. Hence, odometry is used by the robot and the odometry error corrupts the estimate. Figs. 4.1 and 4.2 show the performance of both our proposed algorithm and the robocentric SLAM from Ref. [3]. It can be seen that while our algorithm performs correctly the robocentric approach from Ref. [3] diverges.

In the second test case the robot follows the circular path surrounded by features, shown in Fig. 4.3. Figs. 4.4 and 4.5 shows the performance of the proposed algorithm while Figs. 4.6 and 4.7 shows the performance of the

robocentric algorithm from Ref.[3]. The results show that our algorithm is able to estimate both the robot's position and the features locations, while the algorithm from Ref. [3] is only able to correctly estimate the features. Monte Carlo simulation runs(zoomed in on the time scale for better visibility) for the second test case are shown in Figs. 4.8, 4.9, 4.10 and 4.11.

The third test case shown is the real-world data-set from Ref. [4]. The data-set was collected using a set of robots equipped with wheel odometry which provides forward translational and angular velocity, a camera providing range and bearing measurements to features which are barcodes in the environment and the true locations of the robot and the features using a motion capture system. The noise characteristics of the odometer and camera system are provided in the paper [4]. Figs. 4.12 and 4.13 shows the performance of the proposed algorithm for this data-set which can be seen to perform correctly in estimating both the robot's state and the features' location.

The fourth and last test case is on a real 4-wheeled robot with linear and angular odometry and a camera detecting QR codes for features (Fig. 4.14) providing range and bearing measurements. The setup and robot are shown in Fig. 4.15. Figs. 4.17 and 4.18 shows the performance of the proposed algorithm for the experimental setup with the robot following the trajectory shown in Fig. 4.16. The odometer error standard deviation is 2cm/sec in linear velocity and 0.01 deg/sec in angular velocity, while the LIDAR measurements have 5 cm in range and 5 degrees in bearing.

4.5   Conclusions

The problem of planetary exploration by a ground rover performing Simultaneous Localization and Mapping (SLAM) was considered in this chapter. A novel robocentric Extended Kalman Filter (EKF) based SLAM algorithm was proposed which uses a second order linearization for the propagation function and transforms the full feature state to a frame with its origin at the robots position before every update step. This idea improves upon existing robocentric EKF-SLAM algorithms in the literature and prevents divergence in challenging scenarios where existing methodologies failed. The proposed algorithm also performed consistently in the stationary robot with process noise scenario which was previously not possible. The algorithm is tested in simulation, with a real world data-set, and on a physical robot; and performed successfully in all the scenarios including those where existing EKF-SLAM algorithms failed.
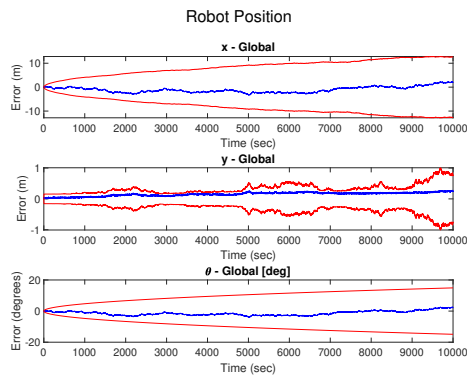
(a) Robot Position in Global Frame
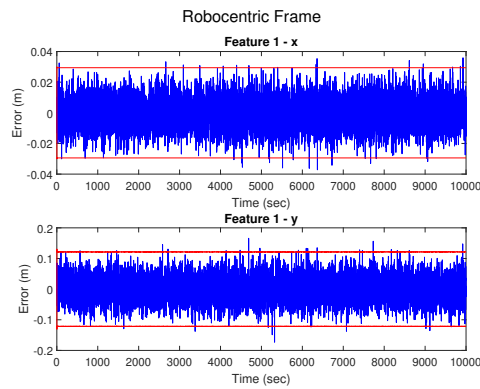
(b) Feature in Local Frame
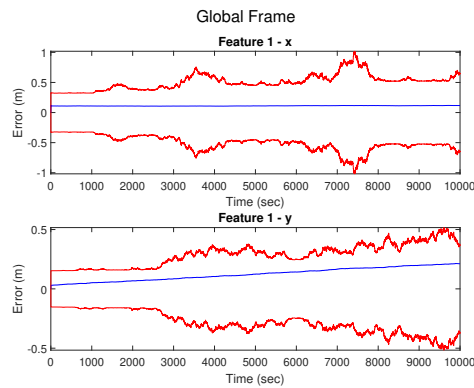
(c) Global Features

Figure 4.1: Robot and Feature position from the proposed algorithm for the stationary robot case from Ref. [2]
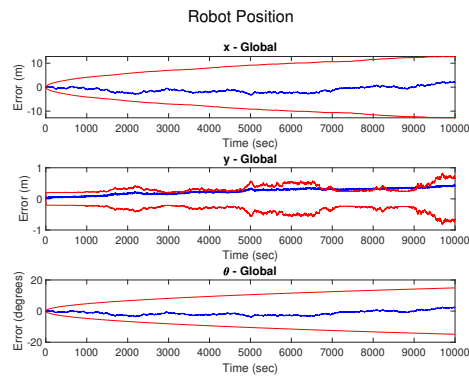
(a) Robot Position in Global Frame
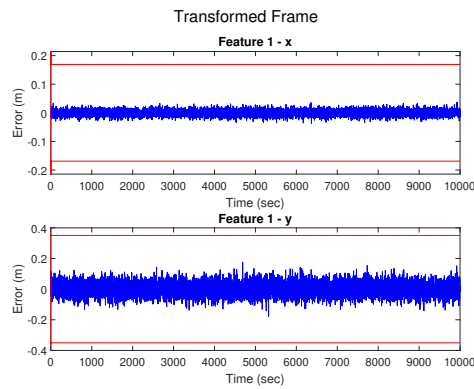
(b) Feature in Local Frame
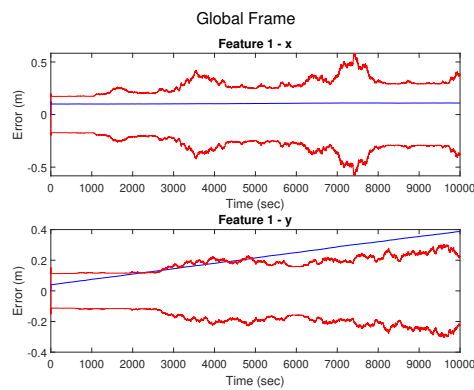
(c) Global Features

Figure 4.2: Robot and Feature position from Ref. [3] for the stationary robot case from Ref. [2]
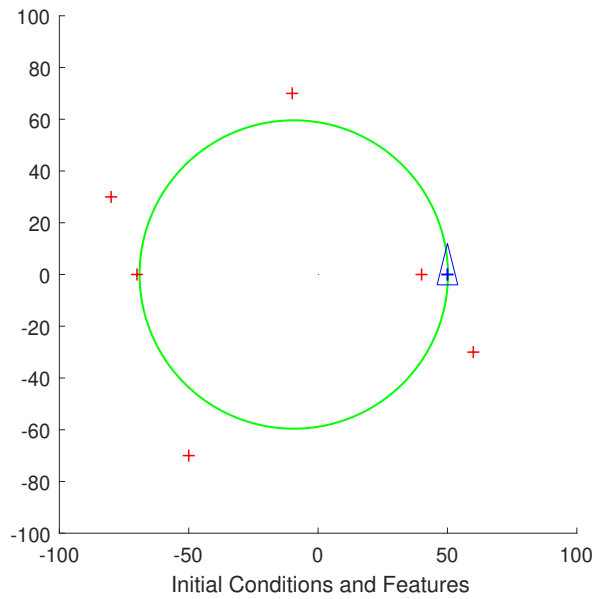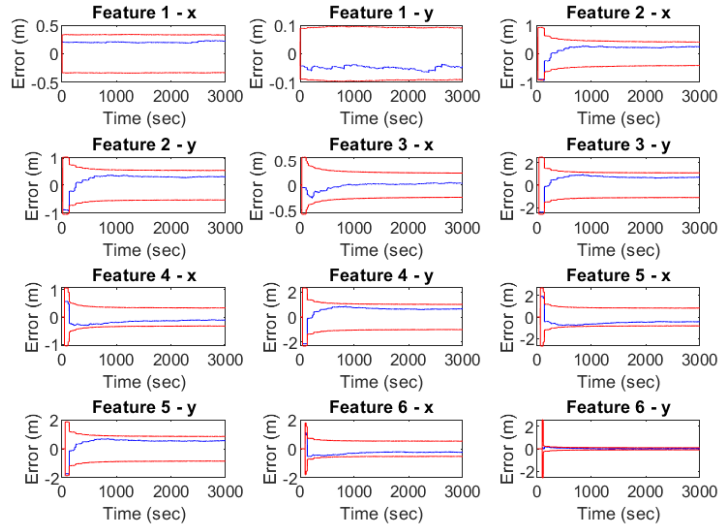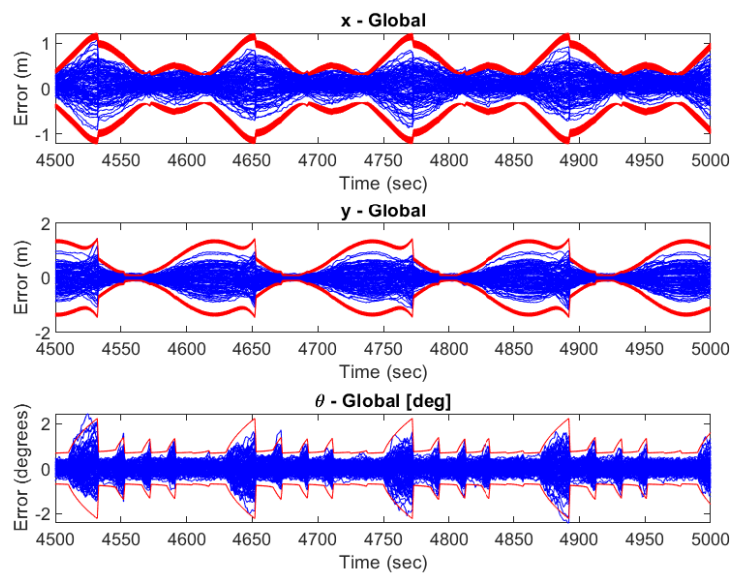
Figure 4.3: Simulation test case 2
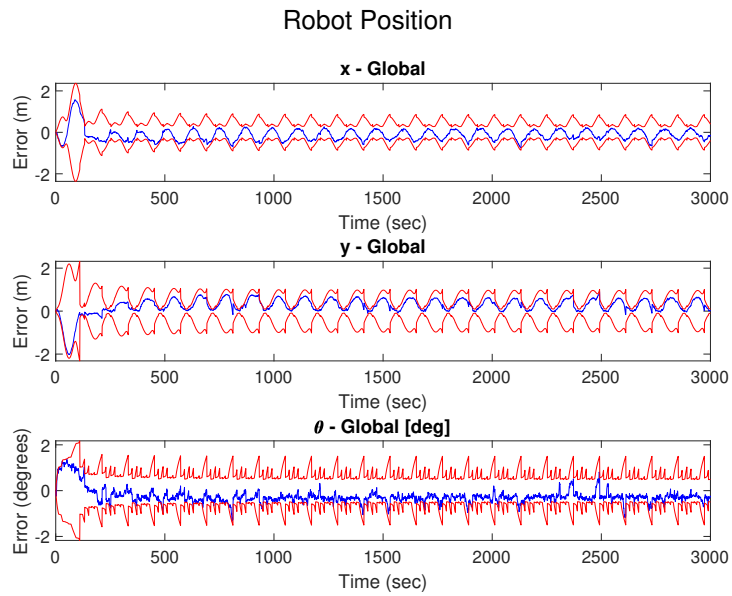
Robot Position

Figure 4.4: Global Robot Position of the proposed algorithm in test case 2

Robocentric Frame
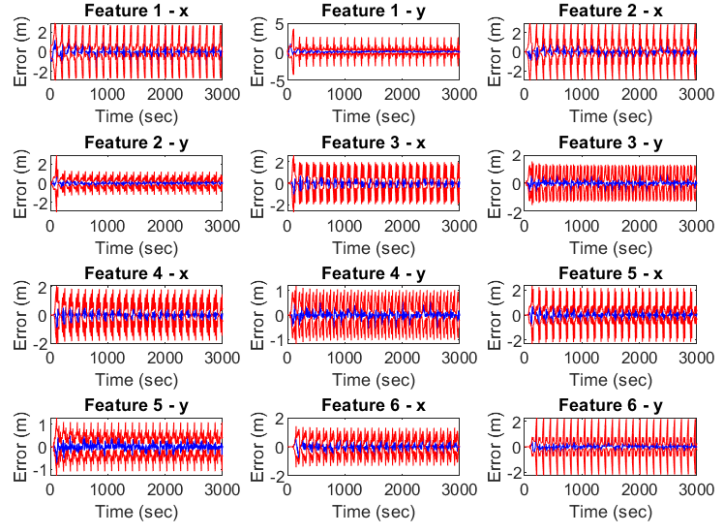
(a) Local Features

Global Frame

(b) Global Features

Figure 4.5: Performance of the proposed algorithm in test case 2
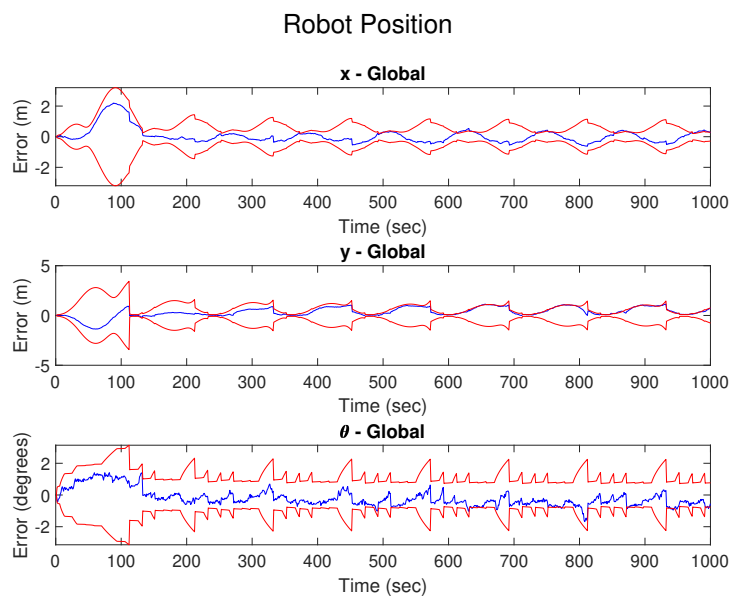
Figure 4.6: Robot Position in Global Frame for Ref. [3] in test case 2

(a) Local Features for Ref. [3]
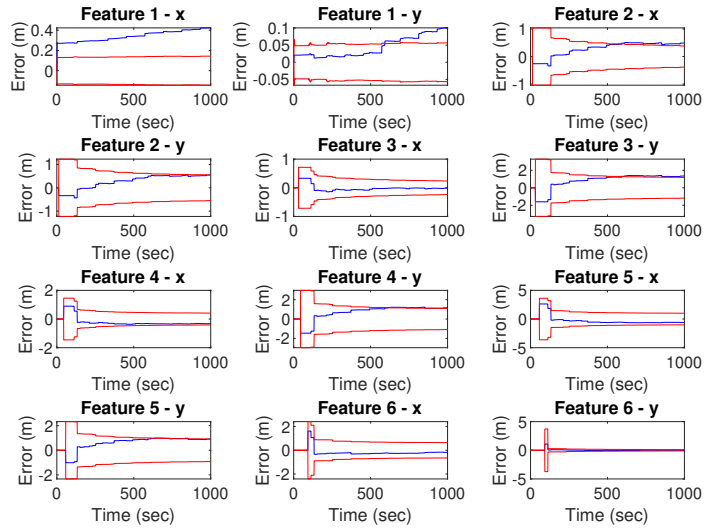
(b) Global Features for Ref. [3]

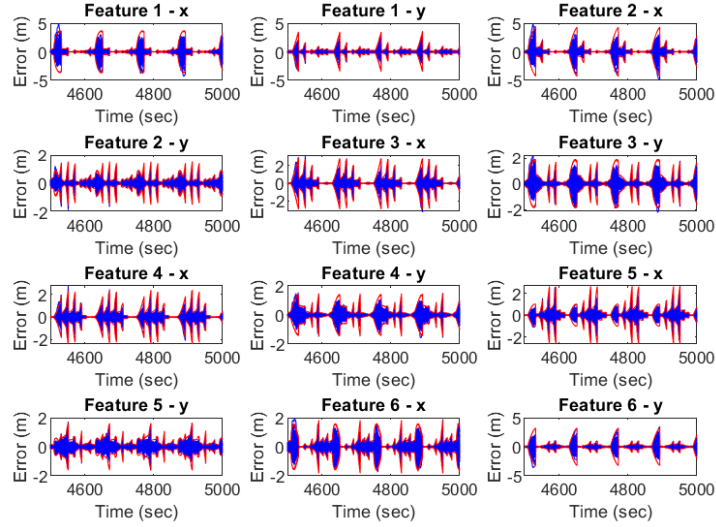Figure 4.7: Performance of the robocentric algorithm from Ref. [3] in test case 2

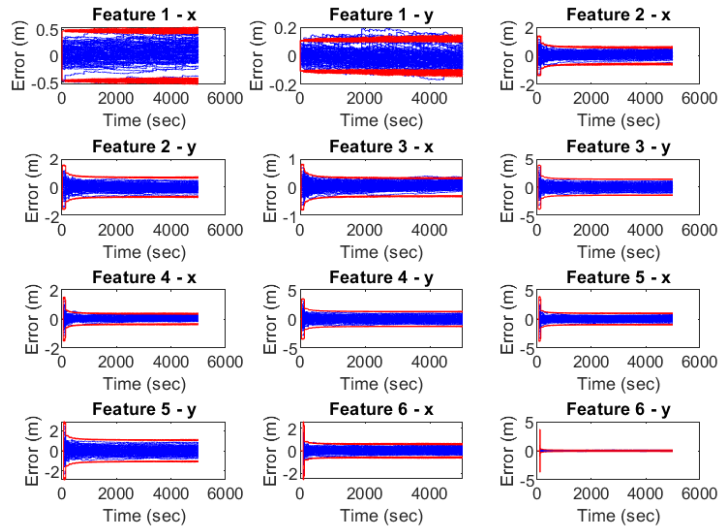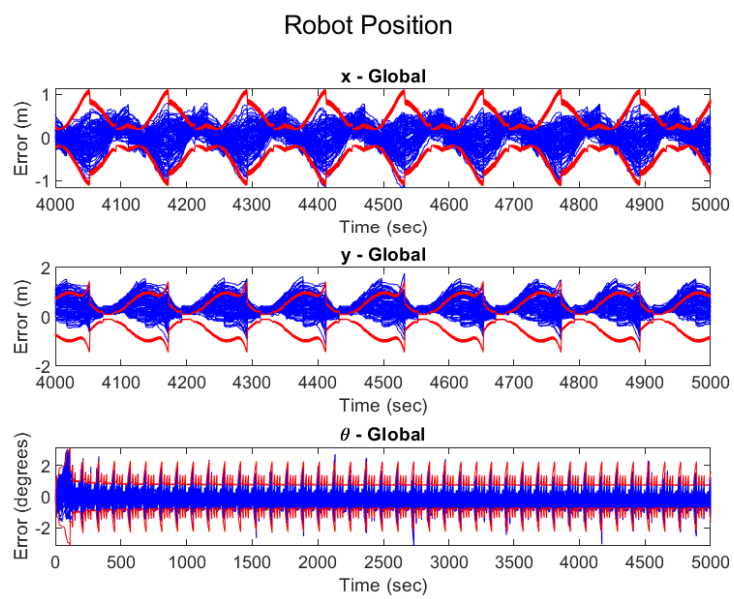Figure 4.8: Monte Carlo Robot Position for the proposed algorithm in test case 2

(a) Local Features

(b) Global Features
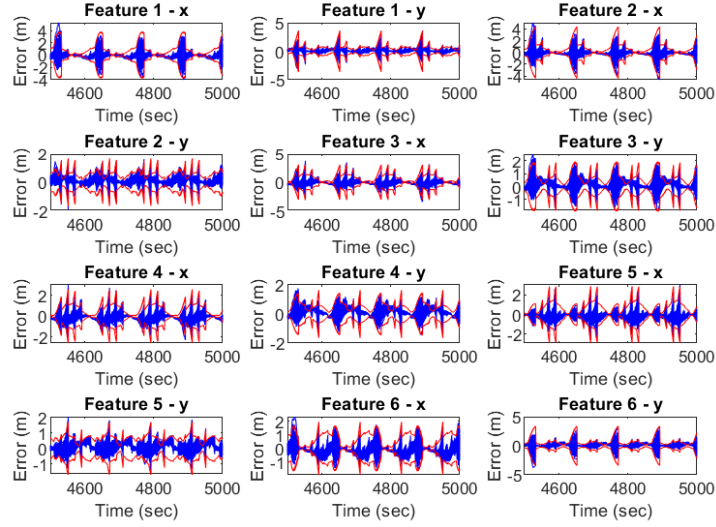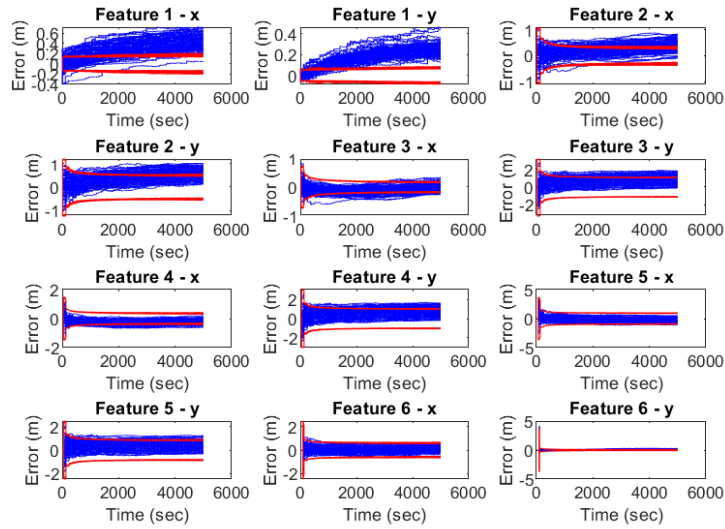
Figure 4.9: Monte Carlo Performance of the proposed algorithm in test case 2

Figure 4.10: Monte Carlo Global Robot Position Frame for Ref. [3] in test case 2

(a) Local Features for Ref. [3]

(b) Global Features for Ref. [3]

Figure 4.11: Monte Carlo Performance of the robocentric algorithm from Ref. [3] in test case 2

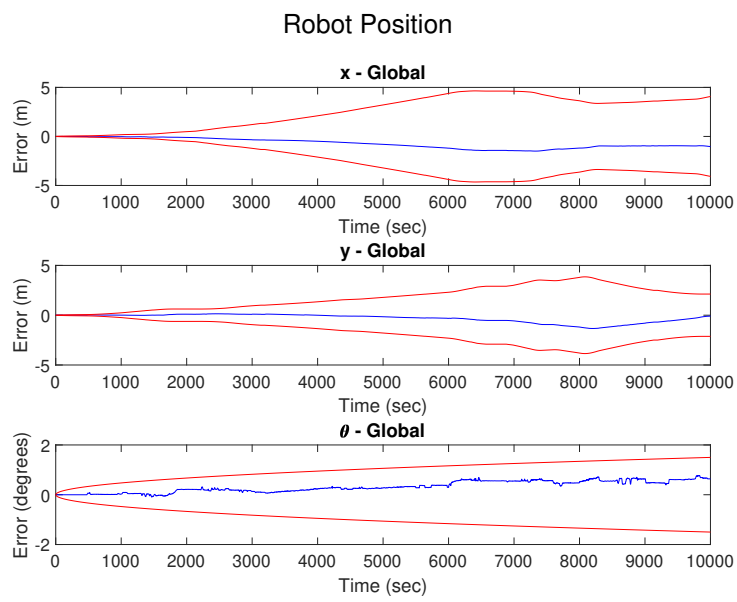Figure 4.12: Global Robot Position of the proposed algorithm using the dataset from Ref [4]

(a) Local Features

(b) Global Features

Figure 4.13: Performance of the proposed algorithm using the data-set from Ref [4]

Figure 4.14: Features used in the experiments

Figure 4.15: Robot used for experiments

Figure 4.16: Trajectory followed in the Experimental Setup

Figure 4.17: Global Robot Position of the proposed algorithm (test case 4)

Figure 4.18: Experimental performance of the proposed algorithm (test case 4)

Chapter 5

Conclusions

Onboard control, tracking and navigation is a crucial part of the development of autonomous systems for safe and efficient transportatio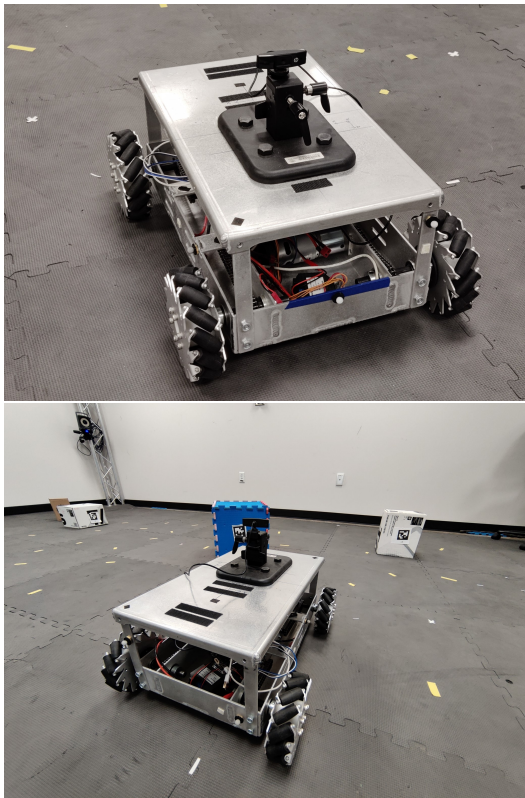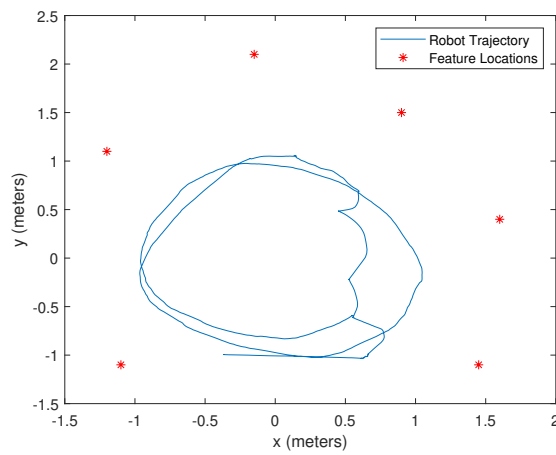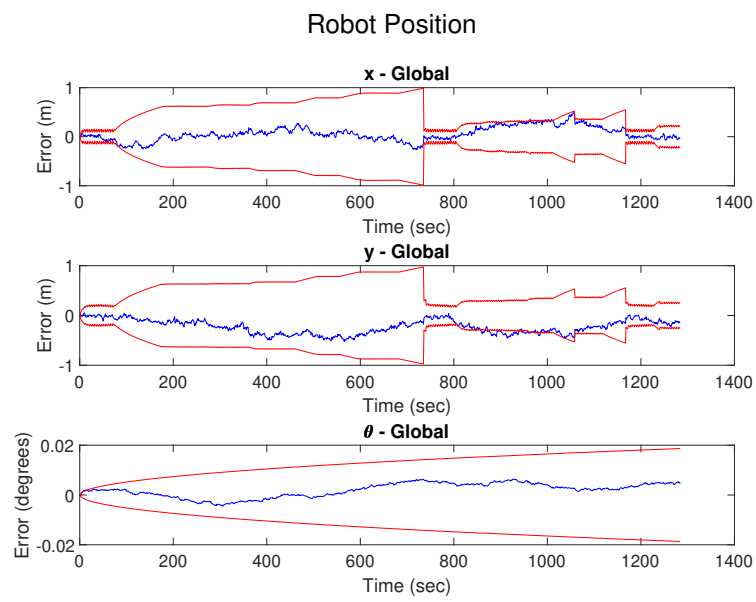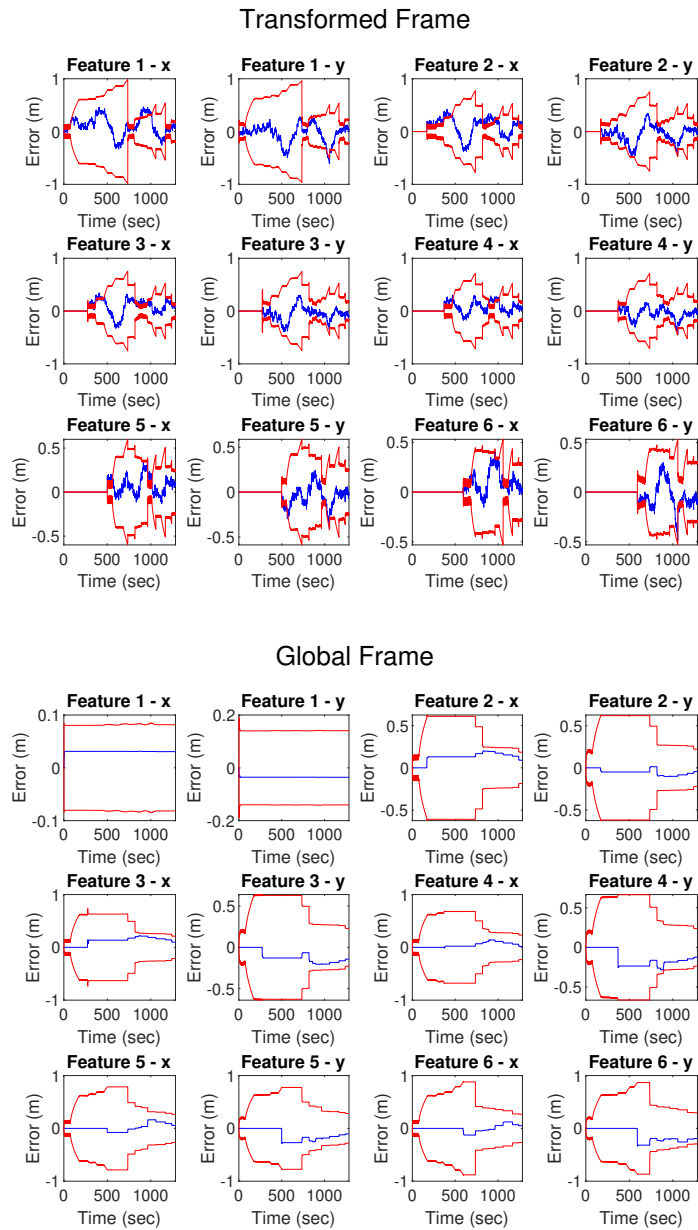n and space exploration. While mission planning and high level decisions on system behavior can be made beforehand or remotely, low level control and state estimation for most vehicles has to be performed onboard, requiring more efficient and better performing algorithms for these tasks. This dissertation presents novel methods of precise control, estimation and mapping for space systems and autonomous robots. When a trajectory is given to a spacecraft, a low level controller is required for tracking the attitude suggested by the trajectory. The first contribution of this dissertation provides such a controller for attitude tracking of a spacecraft with inertia uncertainties. The idea of using dynamic gains can be further applied to different systems with a wide class of system dynamics, which can be the focus of future works. A limitation of this adaptive controller is that it assumes the inertia of the system is constant and non-rigid spacecrafts with time varying inertia matrices were not considered.

The estimation and state tracking part of the dissertation focuses on angular velocity estimation using measurements from Rate-Integrating Gyro-

scopes (RIGs). While Kalman filters are often used to estimate the velocity states, unlike the proposed observer they require knowledge of the characteristics of the noise affecting the system. An in-depth study comparing the proposed observer with Kalman filters can prove useful in understanding the applicability of the observer in different scenarios. Moreover, the observer was designed in a continuous time setting but would need to be implemented in discrete time. The discretization process and its impact on the observer convergence properties as well as its response to measurement noise are scope for future work. The adaptive observer once again assumes constant inertia and knowledge of the upper and lower bounds on the norm of the inertia matrix.

The final part of this dissertation considers Simultaneous Localization and Mapping (SLAM) for robots and spacecraft required in planetary exploration, close-proximity operations, rendezvous and docking operations. This modified robocentric SLAM algorithm could contribute to the success of future autonomous space navigation and planetary exploration missions by providing long term consistent localization and map estimates, especially if further developed for the 3-dimensional scenario. The transformation of the features to the robocentric frame after every propagation step could be computationally expensive for some platforms, especially when the number of features increases, making the state space and covariance matrices too large. The focus of this work is limited to estimation and does not consider different sensing modalities, feature extraction methods and data association. Moreover, a study of the time and memory complexity of this algorithm when compared with

other Kalman filter based methods as well as optimization based methods can provide a compelling argument for the adoption of the proposed method. Applicability of the algorithm to different system and measurement models as well as their impact on the consistency of the filter need to be studied. Applying the solutions from this dissertation to more complex dynamical systems as well as improvements in all the modules along the estimation and control pipeline for autonomous systems provide necessary and interesting avenues for future work leading to a more autonomous world of the future.

Appendices

Appendix A

Nonlinear Stability Analysis

We review the following classical definitions [55, section 4] here:

1. Exponential Stability: The equilibrium point $\boldsymbol{x} = 0$ of $\dot{\boldsymbol{x}} = f(t, \boldsymbol{x})$ is exponentially stable if there exist finite positive constants c, k, and λ such that for all $t \geq t_0$, we have

$$\|\boldsymbol{x}(t)\| \leq k \|\boldsymbol{x}(t_0)\| \exp^{-\lambda(t-t_0)}, \ \forall \|\boldsymbol{x}(t_0)\| < c$$

and globally exponentially stable if this condition is satisfied for any initial state $x(t_0)$. The result is said to be uniform exponentially stable (UES) if the preceding condition holds for any initial time $t_0 \in \Re$.

2. Asymptotic Stability: The equilibrium point $\boldsymbol{x} = 0$ of $\dot{\boldsymbol{x}} = f(t, \boldsymbol{x})$ is asymptotically stable if there exist finite positive constant c such that we have

$$\lim_{t \to \infty} \|\boldsymbol{x}(t)\| = 0, \ \forall \|\boldsymbol{x}(t_0)\| < c$$

and globally asymptotically stable if this condition is satisfied for any initial state $\boldsymbol{x}(t_0)$.

3. Class $\mathcal{K}$ function: A continuous function $\phi \colon [0, \infty) \to \Re^+$ with $\phi(0) = 0$ and strictly increasing on $[0, \infty)$

4. Class $\mathcal{KR}$ function: $\phi \in \mathcal{K}$ with $\lim_{r \to \infty} \phi(r) = \infty$

5. Same order of magnitude: Two functions $\phi_1, \phi_2 \in \mathcal{K}$ on $[0, \infty)$ are said to be of same order of magnitude if $\exists$ positive constants k_1 and k_2 such that $k_1 \phi_1(r_1) \leq \phi_2(r_2) \leq k_2 \phi_1(r_1) \ \forall r_1 \in [0, \infty)$

6. Positive Definite function: A function $V(t, \boldsymbol{x}) \colon \Re^+ \times B_r \to \Re$ with $B_r = \{\boldsymbol{x} \in \Re^n \ni \|\boldsymbol{x}\| < r\}$ for some $r > 0$ and $V(t, 0) = 0 \ \forall t \in \Re^+$ is said to be positive definite if there exists a continuous function $\phi \in \mathcal{K}$ such that $V(t, \boldsymbol{x}) \geq \phi(\|\boldsymbol{x}\|) \ \forall t \in \Re^+, \boldsymbol{x} \in B_R$

7. Decrescent function: A function $V(t, \boldsymbol{x}) \colon \Re^+ \times B_r \to \Re$ with $B_r = \{\boldsymbol{x} \in \Re^n \ni \|\boldsymbol{x}\| < r\}$ for some $r > 0$ and $V(t, 0) = 0 \ \forall t \in \Re^+$ is said to be decrescent if $\exists$ a function $\phi \in \mathcal{K}$ such that $|V(t, \boldsymbol{x})| \leq \phi(\|\boldsymbol{x}\|) \ \forall t \in \Re^+$ and $\forall \boldsymbol{x} \in B_r$.

8. Radially unbounded function: A function $V(t, \boldsymbol{x}) \colon \Re^+ \times \Re^n \to \Re$ with $V(t, 0) = 0 \ \forall t \in \Re^+$ is said to be radially unbounded if $\exists$ a function $\phi \in \mathcal{KR}$ such that $|V(t, \boldsymbol{x})| \geq \phi(\|\boldsymbol{x}\|) \ \forall t \in \Re^+$ and $\forall \boldsymbol{x} \in \Re^n$.

9. Lyapunov stability theorem [55, pp. 154]: Suppose there exists a decrescent and radially unbounded function $V(t, \boldsymbol{x}) \colon \Re^+ \times \Re^n \to \Re^+$ with continuous first order partial derivatives with respect to t and $\boldsymbol{x}$ and $V(t, 0) = 0 \ \forall t \in \Re^+$. If there exist $\phi_1, \phi_2, \phi_3 \in \mathcal{KR}$ of the same order of magnitude such that $\phi_1(\|\boldsymbol{x}\|) \leq V(t, \boldsymbol{x}) \leq \phi_2(\|\boldsymbol{x}\|)$ and $\dot{V}(t, \boldsymbol{x}) \leq -\phi_3(\|\boldsymbol{x}\|)$ then the equilibrium point $\boldsymbol{x} = 0$ of $\dot{\boldsymbol{x}} = f(t, \boldsymbol{x})$ is global UES.

10. Positively Invariant set: A set $\mathbb{M}$ is said to be an invariant set for a system $\dot{\boldsymbol{x}} = f(\boldsymbol{x})$ if

$$\boldsymbol{x}(0) \in \mathbb{M} \implies \boldsymbol{x}(t) \in \mathbb{M}, \forall t \geq 0$$

11. LaSalle's Invariance Principle: Let $\Omega \subset \mathbb{D}$ be a compact set that is positively invariant with respect to $\dot{\boldsymbol{x}} = f(\boldsymbol{x})$. Let $V : \mathbb{D} \to \mathbb{R}$ be a continuously differentiable function such that $\dot{V}(\boldsymbol{x}) \leq 0$ in Ω. Let E be the set of all points in Ω where $\dot{V}(\boldsymbol{x}) = 0$. Let $\mathbb{M}$ be the largest invariant set in E. Then every solution starting in Ω approaches $\mathbb{M}$ as $t \to \infty$.

12. Barbalat's Lemma: If $f(t)$ has a finite limit as $t \to \infty$ and $\dot{f}(t)$ is a uniformly continuous function, then

$$\lim_{t \to \infty} \dot{f}(t) = 0$$

Appendix B

Rate Integrating Gyroscope Observer

B.1   Regressor Matrix $\boldsymbol{\theta}^*$

Consider the dynamics from Eq.3.1 rearranged as Eq.3.86

$$\dot{\boldsymbol{\omega}} = -J^{-1}\boldsymbol{\omega}^* J\boldsymbol{\omega} + J^{-1}\boldsymbol{\tau} \tag{B.1}$$

Let the symmetric inertia matrix have components

$$J = \begin{bmatrix} J_{11} & J_{12} & J_{13} \\ J_{12} & J_{22} & J_{23} \\ J_{13} & J_{23} & J_{33} \end{bmatrix} \tag{B.2}$$

Using the eigenvectors v_1, v_2 and v_3 of J, there exists an orthogonal matrix R:

$$R = \begin{bmatrix} \uparrow & \uparrow & \uparrow \\ v_1 & v_2 & v_3 \\ \downarrow & \downarrow & \downarrow \end{bmatrix} \tag{B.3}$$

which converts the inertia to the principal axis frame as matrix D which has all its off-diagonal terms to be zero such that:

$$J = RDR^T \tag{B.4}$$

and

$$J^{-1} = RD^{-1}R^T \tag{B.5}$$

where $D = \text{diag}[D_1, D_2, D_3]$, and $R^T R = I_{3\times3}$. However, since J is now known, we do not know the matrices D or R, which are functions of the terms of the inertia matrix.

Now consider the term $J^{-1}\boldsymbol{\omega}^* J\boldsymbol{\omega}$. Substituting for the value of J,

$$
\begin{aligned}
J^{-1}\boldsymbol{\omega}^* J\boldsymbol{\omega} &= RD^{-1}R^T\boldsymbol{\omega}^* RDR^T\boldsymbol{\omega} \\
&= RD^{-1}\left(R^T\boldsymbol{\omega}\right)^* R^T RDR^T\boldsymbol{\omega} \\
&= RD^{-1}\boldsymbol{\eta}^* D\boldsymbol{\eta}
\end{aligned}
\tag{B.6}
$$

where $\boldsymbol{\eta} = [\eta_1, \eta_2, \eta_3]^T = R^T\boldsymbol{\omega}$.

Since D is a diagonal matrix, we also have

$$
\boldsymbol{\eta}^* D\boldsymbol{\eta} = \begin{bmatrix} D_2 - D_3 & 0 & 0 \\ 0 & D_3 - D_1 & 0 \\ 0 & 0 & D_1 - D_2 \end{bmatrix} \begin{bmatrix} \eta_2\eta_3 \\ \eta_3\eta_1 \\ \eta_1\eta_2 \end{bmatrix} = S \begin{bmatrix} \eta_2\eta_3 \\ \eta_3\eta_1 \\ \eta_1\eta_2 \end{bmatrix}
\tag{B.7}
$$

Using the vector Kronecker product,

$$
\boldsymbol{\eta} \otimes \boldsymbol{\eta} = \left[\eta_1^2, \eta_1\eta_2, \eta_1\eta_3, \eta_2\eta_1, \eta_2^2, \eta_2\eta_3, \eta_3\eta_1, \eta_3\eta_2, \eta_3^2\right]^T
\tag{B.8}
$$

we have

$$
\begin{bmatrix} \eta_2\eta_3 \\ \eta_3\eta_1 \\ \eta_1\eta_2 \end{bmatrix} = \begin{bmatrix} 0 & 0 & 0 & 0 & 0 & 1 & 0 & 0 & 0 \\ 0 & 0 & 1 & 0 & 0 & 0 & 0 & 0 & 0 \\ 0 & 1 & 0 & 0 & 0 & 0 & 0 & 0 & 0 \end{bmatrix} \boldsymbol{\eta} \otimes \boldsymbol{\eta} = M(\boldsymbol{\eta} \otimes \boldsymbol{\eta})
\tag{B.9}
$$

Also

$$
\boldsymbol{\eta} \otimes \boldsymbol{\eta} = R^T\boldsymbol{\omega} \otimes R^T\boldsymbol{\omega} = (R^T \otimes R^T)(\boldsymbol{\omega} \otimes \boldsymbol{\omega})
\tag{B.10}
$$

Thus

$$
J^{-1}\boldsymbol{\omega}^* J\boldsymbol{\omega} = RD^{-1}SM(R^T \otimes R^T)(\boldsymbol{\omega} \otimes \boldsymbol{\omega})
\tag{B.11}
$$

Since $\boldsymbol{\omega} \otimes \boldsymbol{\omega}$ has duplicate entries, we can reduce redundancies by using

$$
\boldsymbol{\omega} \otimes \boldsymbol{\omega} = \begin{bmatrix} \omega_1^2 \\ \omega_1\omega_2 \\ \omega_1\omega_3 \\ \omega_2\omega_1 \\ \omega_2^2 \\ \omega_2\omega_3 \\ \omega_3\omega_1 \\ \omega_3\omega_2 \\ \omega_3^2 \end{bmatrix} = \begin{bmatrix} 1 & 0 & 0 & 0 & 0 & 0 \\ 0 & 1 & 0 & 0 & 0 & 0 \\ 0 & 0 & 1 & 0 & 0 & 0 \\ 0 & 1 & 0 & 0 & 0 & 0 \\ 0 & 0 & 0 & 1 & 0 & 0 \\ 0 & 0 & 0 & 0 & 1 & 0 \\ 0 & 0 & 1 & 0 & 0 & 0 \\ 0 & 0 & 0 & 0 & 1 & 0 \\ 0 & 0 & 0 & 0 & 0 & 1 \end{bmatrix} \begin{bmatrix} \omega_1^2 \\ \omega_1\omega_2 \\ \omega_1\omega_3 \\ \omega_2^2 \\ \omega_2\omega_3 \\ \omega_3^2 \end{bmatrix} \triangleq N\boldsymbol{\Omega} \tag{B.12}
$$

Hence

$$
J^{-1}\boldsymbol{\omega}^* J\boldsymbol{\omega} = RD^{-1}SM(R^T \otimes R^T)N\boldsymbol{\Omega}
$$

$$
= \Lambda(\boldsymbol{\omega})\mathrm{vec}\left(RD^{-1}SM(R^T \otimes R^T)N\right)
$$

$$
= \Lambda(\boldsymbol{\omega})\boldsymbol{\theta}^* \tag{B.13}
$$

where vec is the vectorization operation along the row and using $\boldsymbol{\Omega}$ from Eq.B.12,

$$
\Lambda(\boldsymbol{\omega}) = \begin{bmatrix} \boldsymbol{\Omega}^T & 0 & 0 \\ 0 & \boldsymbol{\Omega}^T & 0 \\ 0 & 0 & \boldsymbol{\Omega}^T \end{bmatrix} \tag{B.14}
$$

and

$$
\boldsymbol{\theta}^* = \mathrm{vec}\left(RD^{-1}SM(R^T \otimes R^T)N\right) \tag{B.15}
$$

Thus we have managed to separate the components of $\boldsymbol{\omega}$ from the cross product term and consolidated all the unknown inertia component into one vector which can be estimated using the adaptive control method proposed in this paper.

For the time derivative of $\Lambda(\boldsymbol{\omega})$ which is required in Eq.3.99, we can first differentiate Ω:

$$\dot{\Omega} = \begin{bmatrix} 2\omega_1\dot{\omega}_1 \\ \omega_1\dot{\omega}_2 + \omega_2\dot{\omega}_1 \\ \omega_1\dot{\omega}_3 + \omega_3\dot{\omega}_1 \\ 2\omega_2\dot{\omega}_2 \\ \omega_2\dot{\omega}_3 + \omega_3\dot{\omega}_2 \\ 2\omega_3\dot{\omega}_3 \end{bmatrix} \tag{B.16}$$

which leads to

$$\frac{d\Lambda(\omega)}{dt} = \frac{\partial\Lambda}{\partial\omega}\frac{d\boldsymbol{\omega}}{dt} = \begin{bmatrix} \dot{\boldsymbol{\Omega}}^T & 0 & 0 \\ 0 & \dot{\boldsymbol{\Omega}}^T & 0 \\ 0 & 0 & \dot{\boldsymbol{\Omega}}^T \end{bmatrix} \tag{B.17}$$

B.2 Regressor Matrix ϕ^*

Similar to the previous section, consider next the term $J^{-1}\boldsymbol{\tau}$. By performing symbolic multiplication and then partial differentiation with respect to the torque terms, we have

$$J^{-1}\boldsymbol{\tau} = \begin{bmatrix} \tau_1 & 0 & 0 & \tau_2 & -\tau_3 & 0 \\ 0 & \tau_2 & 0 & \tau_1 & 0 & \tau_3 \\ 0 & 0 & \tau_3 & 0 & -\tau_1 & \tau_2 \end{bmatrix} \begin{bmatrix} J_{22}J_{33} - J_{23}^2 \\ J_{11}J_{33} - J_{13}^2 \\ J_{11}J_{22} - J_{12}^2 \\ J_{13}J_{23} - J_{12}J_{33} \\ J_{22}J_{13} - J_{12}J_{23} \\ J_{12}J_{13} - J_{11}J_{23} \end{bmatrix} /\det(J) = W(\boldsymbol{\tau})\phi^* \tag{B.18}$$

where det is the determinant of the matrix and ϕ^* has all the inertia terms.

Moreover, the time derivative of W as required in Eq.3.100 can be

computed as

$$\frac{dW}{dt} = \frac{\partial W}{\partial \tau} \frac{d\boldsymbol{\tau}}{dt} = \begin{bmatrix} \dot{\tau}_1 & 0 & 0 & \dot{\tau}_2 & -\dot{\tau}_3 & 0 \\ 0 & \dot{\tau}_2 & 0 & \dot{\tau}_1 & 0 & \dot{\tau}_3 \\ 0 & 0 & \dot{\tau}_3 & 0 & -\dot{\tau}_1 & \dot{\tau}_2 \end{bmatrix} = W(\dot{\boldsymbol{\tau}}) \qquad \text{(B.19)}$$

Bibliography

[1] J. T. . Wen and K. Kreutz-Delgado. The attitude control problem. *IEEE Transactions on Automatic Control*, 36(10):1148–1162, 1991.

[2] Simon J Julier and Jeffrey K Uhlmann. A counter example to the theory of simultaneous localization and map building. In *Proceedings 2001 ICRA. IEEE International Conference on Robotics and Automation (Cat. No. 01CH37164)*, volume 4, pages 4238–4243. IEEE, 2001.

[3] José A Castellanos, Ruben Martinez-Cantin, Juan D Tardós, and José Neira. Robocentric map joining: Improving the consistency of ekf-slam. *Robotics and autonomous systems*, 55(1):21–29, 2007.

[4] Keith YK Leung, Yoni Halpern, Timothy D Barfoot, and Hugh HT Liu. The utias multi-robot cooperative localization and mapping dataset. *The International Journal of Robotics Research*, 30(8):969–974, 2011.

[5] Panagiotis Tsiotras. Stabilization and optimality results for the attitude control problem. *Journal of Guidance, Control, and Dynamics*, 19(4):772–779, 1996.

[6] S. P. Arjun Ram and Maruthi R. Akella. Uniform exponential stability result for the rigid-body attitude tracking control problem. *Journal of Guidance, Control, and Dynamics*, 43(1):39–45, 2020.

[7] SP Arjun Ram and Maruthi R Akella. Adaptive attitude tracking control preserving the self-reduction property. *Journal of Guidance, Control, and Dynamics*, 45(8):1538–1545, 2022.

[8] Shankar Sastry, Marc Bodson, and James F Bartram. *Adaptive control: Stability, convergence, and robustness*. Acoustical Society of America, 1990.

[9] Dongeun Seo and Maruthi R. Akella. High-performance spacecraft adaptive attitude-tracking control through attracting-manifold design. *Journal of Guidance, Control, and Dynamics*, 31(4):884–891, 2008.

[10] Jasim Ahmed, Vincent T. Coppola, and Dennis S. Bernstein. Adaptive asymptotic tracking of spacecraft attitude motion with inertia matrix identification. *Journal of Guidance, Control, and Dynamics*, 21(5):684–691, 1998.

[11] Hanspeter Schaub, Maruthi R. Akella, and John L. Junkins. Adaptive control of nonlinear attitude motions realizing linear closed loop dynamics. *Journal of Guidance, Control, and Dynamics*, 24(1):95–100, 2001.

[12] O. Egeland and J. . Godhavn. Passivity-based adaptive attitude control of a rigid spacecraft. *IEEE Transactions on Automatic Control*, 39(4):842–846, 1994.

[13] S. N. Singh. Nonlinear adaptive attitude control of spacecraft. *IEEE Transactions on Aerospace and Electronic Systems*, 23(3):371–379, 1987.

[14] A. Tayebi. Unit quaternion-based output feedback for the attitude tracking problem. *IEEE Transactions on Automatic Control*, 53(6):1516–1520, 2008.

[15] BT Costic, DM Dawson, MS De Queiroz, and Vikram Kapila. Quaternion-based adaptive attitude tracking controller without velocity measurements. *Journal of Guidance, Control, and Dynamics*, 24(6):1214–1222, 2001.

[16] Panagiotis Tsiotras. Stabilization and optimality results for the attitude control problem. *Journal of Guidance, Control, and Dynamics*, 19(4):772–779, 1996.

[17] D. E. Zlotnik and J. R. Forbes. Rotation-matrix-based attitude control without angular velocity measurements. In *2014 American Control Conference*, pages 4931–4936, 2014.

[18] Shankar Sastry and Marc Bodson. *Adaptive control: stability, convergence and robustness*. Courier Corporation, 2011.

[19] Allan Y. Lee and Julie A. Wertz. In-flight estimation of the cassini spacecraft's inertia tensor. *Journal of Spcaecraft and Rockets*, 39(1):153–155, 2002.

[20] Jing Sun and Petros A. Ioannou. *Robust Adaptive Control*. Dover Publications Incorporated, 2012.

[21] SP Arjun Ram, Renato Zanetti, and Maruthi R Akella. Angular velocity estimation using rate-integrating gyro measurements. *Journal of Guidance, Control, and Dynamics*, 2023.

[22] Paul G Savage. Strapdown inertial navigation integration algorithm design part 2: Velocity and position algorithms. *Journal of Guidance, Control, and Dynamics*, 21(2):208–221, 1998.

[23] John L. Crassidis, F. Landis Markley, and Yang Cheng. Survey of nonlinear attitude estimation methods. *Journal of Guidance, Control, and Dynamics*, 30(1):12–28, 2007.

[24] James C Kinsey, Ryan M Eustice, and Louis L Whitcomb. A survey of underwater vehicle navigation: Recent advances and new challenges. In *IFAC Conference of Manoeuvring and Control of Marine Craft*, volume 88, pages 1–12. Lisbon, 2006.

[25] Navid Fallah, Ilias Apostolopoulos, Kostas Bekris, and Eelke Folmer. Indoor human navigation systems: A survey. *Interacting with Computers*, 25(1):21–33, 2013.

[26] Billur Barshan and Hugh F Durrant-Whyte. Inertial navigation systems for mobile robots. *IEEE Transactions on Robotics and Automation*, 11(3):328–342, 1995.

[27] F Landis Markley and John L Crassidis. *Fundamentals of spacecraft attitude determination and control*, volume 33. Springer, 2014.

[28] D Senkal, EJ Ng, V Hong, Y Yang, CH Ahn, TW Kenny, and AM Shkel. Parametric drive of a toroidal mems rate integrating gyroscope demonstrating¡ 20 ppm scale factor stability. In *2015 28th IEEE International Conference on Micro Electro Mechanical Systems (MEMS)*, pages 29–32. IEEE, 2015.

[29] Pradeep Pai, Hoorad Pourzand, and Massood Tabib-Azar. Magnetically coupled resonators for rate integrating gyroscopes. In *Sensors*, pages 1173–1176. IEEE, 2014.

[30] John L Crassidis and F Landis Markley. Three-axis attitude estimation using rate-integrating gyroscopes. *Journal of Guidance, Control, and Dynamics*, 39(7):1513–1526, 2016.

[31] B. Friedkand. Estimating angular velocity from output of rate-integrating gyro. *IEEE Transactions on Aerospace and Electronic Systems*, AES-11(4):551–555, 1975.

[32] Håvard Fjær Grip, Thor I. Fossen, Tor A. Johansen, and Ali Saberi. Globally exponentially stable attitude and gyro bias estimation with application to gnss/ins integration. *Automatica*, 51:158 – 166, 2015.

[33] S. Berkane, A. Abdessameud, and A. Tayebi. A globally exponentially stable hybrid attitude and gyro-bias observer. In *2016 IEEE 55th Conference on Decision and Control (CDC)*, pages 308–313, 2016.

[34] Murat Arcak and Dragan Nešić. A framework for nonlinear sampled-data observer design via approximate discrete-time models and emulation. *Automatica*, 40(11):1931–1938, 2004.

[35] Ahmed M Dabroom and Hassan K Khalil. Discrete-time implementation of high-gain observers for numerical differentiation. *International Journal of Control*, 72(17):1523–1537, 1999.

[36] Ahmed Mohamed Dabroom and Hassan K Khalil. Output feedback sampled-data control of nonlinear systems using high-gain observers. *IEEE Transactions on Automatic Control*, 46(11):1712–1725, 2001.

[37] A. Astolfi and R. Ortega. Immersion and invariance: a new tool for stabilization and adaptive control of nonlinear systems. *IEEE Transactions on Automatic Control*, 48(4):590–606, 2003.

[38] Young Man Cho and Rajesh Rajamani. A systematic approach to adaptive observer synthesis for nonlinear systems. *IEEE Transactions on Automatic Control*, 42(4):534–537, 1997.

[39] Riccardo Marino and Patrizio Tomei. Adaptive observers with arbitrary exponential rate of convergence for nonlinear systems. *IEEE Transactions on Automatic Control*, 40(7):1300–1304, 1995.

[40] Gildas Besançon. Remarks on nonlinear adaptive observer design. *Systems & Control letters*, 41(4):271–280, 2000.

[41] Hassan K Khalil. *Nonlinear systems*, volume 3. Prentice Hall Upper Saddle River, NJ, 2002.

[42] Cuebong Wong, Erfu Yang, Xiu-Tian Yan, and Dongbing Gu. Adaptive and intelligent navigation of autonomous planetary rovers — a survey. In *2017 NASA/ESA Conference on Adaptive Hardware and Systems (AHS)*, pages 237–244, 2017.

[43] P Cheeseman, R Smith, and M Self. A stochastic map for uncertain spatial relationships. In *4th International Symposium on Robotic Research*, pages 467–474. MIT Press Cambridge, 1987.

[44] John J Leonard and Hugh F Durrant-Whyte. Simultaneous map building and localization for an autonomous mobile robot. In *IROS*, volume 3, pages 1442–1447, 1991.

[45] Dimitrios Geromichalos, Martin Azkarate, Emmanouil Tsardoulias, Levin Gerdes, Loukas Petrou, and Carlos Perez Del Pulgar. Slam for autonomous planetary rovers with global localization. *Journal of Field Robotics*, 37(5):830–847, 2020.

[46] Raul Mur-Artal and Juan D Tardós. Orb-slam2: An open-source slam system for monocular, stereo, and rgb-d cameras. *IEEE transactions on robotics*, 33(5):1255–1262, 2017.

[47] Jakob Engel, Thomas Schöps, and Daniel Cremers. Lsd-slam: Large-scale direct monocular slam. In *European conference on computer vision*,

pages 834–849. Springer, 2014.

[48] Michael Montemerlo, Sebastian Thrun, Daphne Koller, Ben Wegbreit, et al. Fastslam 2.0: An improved particle filtering algorithm for simultaneous localization and mapping that provably converges. In *IJCAI*, volume 3, pages 1151–1156, 2003.

[49] Tim Bailey, Juan Nieto, Jose Guivant, Michael Stevens, and Eduardo Nebot. Consistency of the ekf-slam algorithm. In *2006 IEEE/RSJ International Conference on Intelligent Robots and Systems*, pages 3562–3568. IEEE, 2006.

[50] José A Castellanos, José Neira, and Juan D Tardós. Limits to the consistency of ekf-based slam. *IFAC Proceedings Volumes*, 37(8):716–721, 2004.

[51] Shoudong Huang and Gamini Dissanayake. Convergence analysis for extended kalman filter based slam. In *Proceedings 2006 IEEE International Conference on Robotics and Automation, 2006. ICRA 2006.*, pages 412–417. IEEE, 2006.

[52] Guoquan P Huang, Anastasios I Mourikis, and Stergios I Roumeliotis. Observability-based rules for designing consistent ekf slam estimators. *The International Journal of Robotics Research*, 29(5):502–528, 2010.

[53] Zheng Huai and Guoquan Huang. Robocentric visual-inertial odometry. In *2018 IEEE/RSJ International Conference on Intelligent Robots and*

Systems (IROS), pages 6319–6326. IEEE, 2018.

[54] Anastasios I Mourikis and Stergios I Roumeliotis. A multi-state constraint kalman filter for vision-aided inertial navigation. In *Proceedings 2007 IEEE International Conference on Robotics and Automation*, pages 3565–3572. IEEE, 2007.

[55] H.K. Khalil. *Nonlinear Control Systems*. Prentice Hall, 2nd edition, 1996.

[56] Panagiotis Tsiotras. New control laws for the attitude stabilization of rigid bodies. *IFAC Proceedings Volumes*, 27(13):321 – 326, 1994. IFAC Symposium on Automatic Control in Aerospace 1994, Palo Alto, CA, USA, 12-16 September 1994.

[57] S.R. Marandi and V.J. Modi. A preferred coordinate system and the associated orientation representation in attitude dynamics. *Acta Astronautica*, 15(11):833 – 843, 1987.

[58] Hanspeter Schaub and John L. Junkins. Aas 95-137 stereographic orientation parameters for attitude dynamics: A generalization of the rodrigues parameters. *Journal of the Astronautical Sciences*, 44:13–15, 1996.

[59] Hanspeter Schaub and John L. Junkins. *Analytical Mechanics of Space Systems*. AIAA Education Series, 3rd edition, 2014.

[60] Ziyang Meng, Wei Ren, and Zheng You. Distributed finite-time attitude containment control for multiple rigid bodies. *Automatica*, 46(12):2092 – 2099, 2010.

[61] Maruthi R. Akella. Rigid body attitude tracking without angular velocity feedback. *Systems and Control Letters*, 42(4):321 – 326, 2001.

[62] J. T. . Wen and K. Kreutz-Delgado. The attitude control problem. *IEEE Transactions on Automatic Control*, 36(10):1148–1162, Oct 1991.

[63] John L Junkins, Maruthi R Akella, and Rush D Robinett. Nonlinear adaptive control of spacecraft maneuvers. *Journal of Guidance, Control, and Dynamics*, 20(6):1104–1110, 1997.

[64] Hanspeter Schaub, Maruthi R Akella, and John L Junkins. Adaptive control of nonlinear attitude motions realizing linear closed loop dynamics. *Journal of Guidance, Control, and Dynamics*, 24(1):95–100, 2001.

[65] Kunfeng Lu and Yuanqing Xia. Adaptive attitude tracking control for rigid spacecraft with finite-time convergence. *Automatica*, 49(12):3591 – 3599, 2013.

[66] D. E. Zlotnik and J. R. Forbes. Rotation-matrix-based attitude control without angular velocity measurements. In *2014 American Control Conference*, pages 4931–4936, June 2014.

[67] Fjellstad and Fossen. Quaternion feedback regulation of underwater vehicles. In *1994 Proceedings of IEEE International Conference on Control and Applications*, pages 857–862 vol.2, Aug 1994.

[68] Ken Shoemake. Iii.6 - uniform random rotations. In DAVID KIRK, editor, *Graphics Gems III (IBM Version)*, pages 124 – 132. Morgan Kaufmann, San Francisco, 1992.

[69] Maruthi R. Akella. Rigid body attitude tracking without angular velocity feedback. *Systems and Control Letters*, 42(4):321 – 326, 2001.

[70] John L. Junkins, Maruthi R. Akella, and Rush D. Robinett. Nonlinear adaptive control of spacecraft maneuvers. *Journal of Guidance, Control, and Dynamics*, 20(6):1104–1110, 1997.

[71] Romeo Ortega and Elena Panteley. Overcoming the detectability obstacle in certainty equivalence adaptive control. *IFAC Proceedings Volumes*, 34(14):455 – 460, 2001. IFAC Workshop on Adaptation and Learning in Control and Signal Processing (ALCOSP 2001), Cernobbio-Como, Italy, 29-31 August 2001.

[72] SP Arjun Ram, Maruthi Akella, and Renato Zanetti. Angular velocity estimation using rate-integrating gyro measurements. In *AAS/AIAA Astrodynamics Specialist Conference*. Big Sky, Montana, 2021.

[73] SP Arjun Ram and Maruthi Akella. Adaptive observers for angular velocity estimation using rate-integrating gyro measurements. In *AAS/AIAA*

Astrodynamics Specialist Conference. Charlotte, NC, 2022.

[74] M. Ekramian, F. Sheikholeslam, S. Hosseinnia, and M.J. Yazdanpanah. Adaptive state observer for lipschitz nonlinear systems. *Systems & Control Letters*, 62(4):319 – 323, 2013.

Vita

S P Arjun Ram was born in Coimbatore and raised in Bangalore, India. He graduated from National Public School Indiranagar before attending the Birla Institute of Technology and Science, Pilani to pursue Electronics and Instrumentation Engineering. During that time, Arjun worked as a research assistant at the Indian Institute of Science, Bangalore. Upon graduation in 2016, he worked as an Embedded Software Engineer at Intel Labs designing coordination and coverage algorithms for search and rescue swarms. Motivated by his interest in robotics and autonomous systems, Arjun started his doctoral studies in 2017 at The Department of Aerospace Engineering and Engineering Mechanics, UT Austin under the guidance of Dr. Maruthi Akella and Dr. Renato Zanetti. He graduated with a masters degree in 2020 and interned with Pensa systems in 2021, working on sensor fusion for localization of drones. His research interests are in autonomous systems, control, estimation and coordination.

Permanent address: arjun.ram@utexas.edu

This dissertation was typeset with LATEX[†] by the author.

[†]LATEX is a document preparation system developed by Leslie Lamport as a special version of Donald Knuth's TEX Program.